# Studies on New Narrow-Bandgap Polymers Composed of Aromatic-Donor and *o*-Quinoid-Acceptor Segments

Chitoshi Kitamura

DOCTOR OF PHILOSOPHY

Department of Structural and Molecular Science
School of Mathematical and Physical Science
The Graduate University for Advanced Studies

1995

## Contents


Chapter 1 Introduction ..... 1

1.1 General Introduction ..... 1

1.2 Historic Background of Narrow-Bandgap Polymers ..... 5

1.3 Purpose and Constitution of Present Thesis ..... 12

1.4 References ..... 16

Chapter 2 Syntheses and Properties of Triheterocyclic Monomers Composed of Aromatic-Donor and *o*-Quinoid-Acceptor Segments ..... 20

2.1 Introduction ..... 21

2.2 Results and Discussion ..... 23

2.2.1 Syntheses of Triheterocyclic Monomers ..... 23

2.2.2 Molecular Orbital Calculations ..... 28

2.2.3 Properties and Structures of Monomers ..... 34

2.3 Experimental ..... 45

2.4 References and Notes ..... 58

2.5 Supplementary Materials ..... 60

Chapter 3 Syntheses and Properties of Polymers Composed of Aromatic-Donor and *o*-Quinoid-Acceptor Segments ..... 69

3.1 Introduction ..... 70

3.2 Results and Discussion ..... 71

3.2.1 Electrochemical Polymerization ..... 71

3.2.2 Electrochemistry and Electronic Spectra of Polymers ..... 78

3.3 Experimental ..... 113

3.4 References and Notes ..... 114

Conclusions ..... 115

Acknowledgments ..... 117

List of Publications ..... 118

# Chapter 1 Introduction

## 1.1 General Introduction

Over two decades, organic π-conjugated polymers have been increasingly investigated as a new class of materials because of their interesting electrical and electronic properties. Their practical and potential applications include electric conductors, rechargeable battery electrodes, electrochromic devices, light-emitting diodes, and nonlinear optical materials.[1] Therefore, the field of conjugated polymers has been attracting organic synthetic chemists, physicists, and technologists, and has grown into a wide scientific boundary area. Researchers in other fields have cooperated each other to make new ideas leading to the development of the field of conjugated polymers.

The synthesis of poly(acetylene) (**1**) by Shirakawa *et al.*[2] and the discovery of a 12 order of magnitude increase of conductivity of the polymer on charge-transfer oxidative doping by Heeger *et al.*[3] in the 1970s made one epoch. While poly(acetylene) is a one-dimensional extended conjugated system regularly built from repeated ethylene units, the energy gap occurs in the electronic structure due to the Peierls transition[4] (even if the conjugation length is infinitely long, the gap does not become zero). The gap is called bandgap, the energy between valence and conduction band on the basis of band theory, and corresponds to HOMO-LUMO gap on the basis of molecular orbital (MO) theory (Figure 1). Usually the value is estimated from the edge of an absorption spectrum. *trans*-Poly(acetylene) displayed a bandgap of 1.4 eV,[5] suggesting a semiconductor. These studies introduced new important ideas concerning conjugated polymers such as soliton, polaron, and bipolaron. The reason for the increase of conductivity by doping was explained with these terms.

Another important development of conjugated polymers occurred in 1979. The formation of excellent free-standing films of poly(pyrrole) (**2**) by electrochemically oxidative polymerization of pyrrole was discovered by Diaz *et al.* (Figure 2).[6] After the work, electrochemical polymerization of other aromatic and heteroaromatic compounds such as

azulene[7], fluorene[8], pyrene[8], thiophene[9], indole[10], and carbazole[7] were attempted to succeed in the synthesis of the corresponding conjugated polymers (**3-8**).

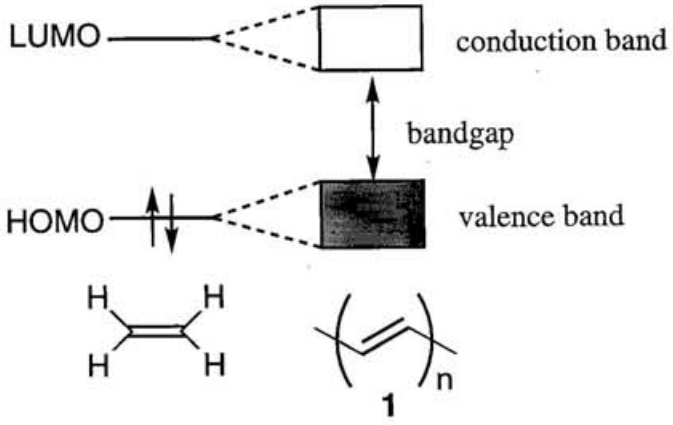


**Figure 1**. Bandgap.

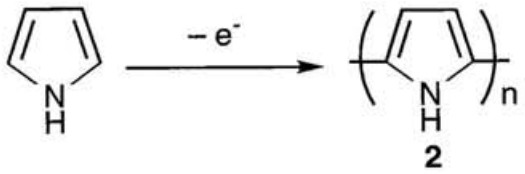


**Figure 2.** Electrochemical polymerization.

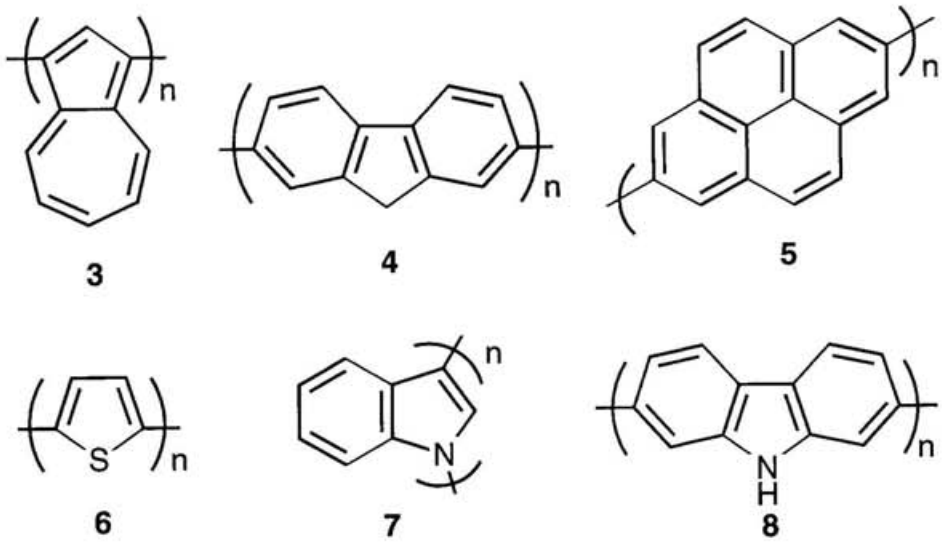

This electrochemical method has the following favorable features: (*i*) the operation of polymerization is easy, meaning that the polymer can be deposited directly onto the surface of an electrode from the monomer solution containing a supporting electrolyte, (*ii*) the polymerization and doping reactions take place at the same time, (*iii*) the degree of doping can be adjusted by applied potentials. Owing to the above merits, the electrochemical polymerization has been widely used to date. The resulting polymers that consisted of aromatic cyclic compounds have been found to have an advantage of high stability against common surroundings compared with poly(acetylene).

However, insolubility and infusibility of the conjugated polymers described above often rendered their treatment intractable and made their characterization difficult. In order to overcome these drawbacks, the molecular design for an improvement in solubility was incorporated into the polymers. That is, the introduction of long alkyl chains to the polymers was undertaken, especially for poly(thiophene) (Figure 3).[11] It produced soluble polymers in organic solvents and enabled measurement of NMR spectra and determination of molecular weights by gel permeation chromatography (GPC).

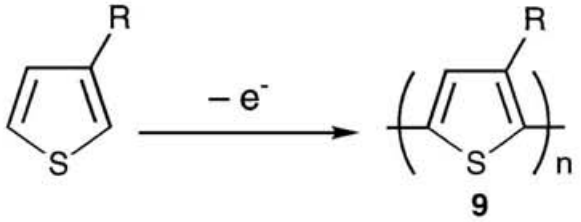


**9**

**Figure 3.** Solubilization of poly(thiophene).

As another synthetic method, the chemical coupling reaction is well known. The oxidative polymerization using an oxidizing agent such as $FeCl_3$[12] has been used similarly to electropolymerization. The chemical polymerization utilizing a cross-coupling reaction with a transition metal catalyst has also been widely used. In recent years, the latter method has been remarkably advanced. Rieke[13] and McCullough[14] individually succeeded in the synthesis of highly regioselective poly(3-alkylthiophene) (**9**) using reactive zinc and nickel catalysts, respectively. Yamamoto *et al.* were successful in the preparation of various conjugated polymers by dehalogenation with zelovalent nickel complexes (Figure 4).[15] The

catalytic preparation has a feature that the polymers without structural defects can be obtained.

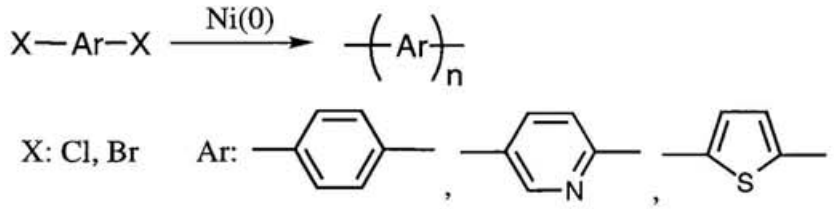


**Figure 4.** Yamamoto coupling.

As the physical properties of various conjugated polymers were elucidated, theoretical studies progressed. Brédas *et al.* established the *ab initio* Valence Effective Hamiltonian (VEH) technique to explore the band structure of conjugated polymers.[16] It provided an excellent qualitative correlation between the parameters obtained theoretically (e.g., bandgap, bandwidth, ionization potential, and electron affinity) and the experimental data. The prominent result served to design new polymers for synthetic researchers at the early stage. Table 1 shows the band parameters[1b] of representative conjugated polymers. There is a direct correlation between the bandgap and the difference in onset potentials between p- and n-doping. The bandwidth is associated with the degree of delocalization of electrons in the polymer chains. The ionization potential and electron affinity are related to the measure of susceptibility for p- and n-doping, respectively.

**Table 1.** The band parameters[a] of reperesentative conjugated polymers.

| polymer | bandgap $E_g$ / eV | bandwidth $B_w$ / eV | ionization potential $I_p$ / eV | electron affinity $E_A$ / eV |
|---|---|---|---|---|
| poly(acetylene) | 1.4 | 6.5 | 4.7 | 3.3 |
| poly(*p*-phenylene) | 3.5 | 3.5 | 5.6 | 2.1 |
| poly(thiophene) | 2.0 | 3.3 | 5.6 | 3.6 |
| poly(pyrrole) | 3.6 | 3.8 | 3.9 | 0.3 |

[a] reference 1b.

The bandgap ($E_g$) is particularly significant among the band parameters because it is one of the most important factors that controls electrical and optical properties. For example, the concentration of charge carriers $n$ is expressed by $n = n_O \exp(-E_g / 2kT)$, where $n_O$, $k$, and $T$ mean the concentration of carriers in molecular units in the solid state, the Boltzmann constant, and temperature, respectively.[17] The equation indicates that the electrical conductivity can increase with decreasing the bandgap down to near zero. The nonlinear optical responses are also dependent upon the bandgap. The relationship between the bandgap and the third-order nonlinear susceptibility $\chi^{(3)}$ is represented by $\chi^{(3)} \propto (1 / E_g)^6$,[18] showing that the small value of the bandgap will lead to the large optical nonlinearity. On the other hand, the polymers with large bandgap have also attracted much attention because the blue light emission is expected from the light-emitting diode.[19]

On the grounds described above, "band structure engineering" has become important. While the research for conjugated polymers was, so far, mainly undertaken for collecting information on the relation between properties and structures, the coming object will be the control of the band structure at our will and the occurrence of function at our desire. Therefore, it is necessary to clarify the molecular design controlling the band structure and to further understand the narrow-bandgap polymer. In particular, pursuing narrower-bandgap polymers is significant from scientific and practical points of view as described above.

## 1.2 Historic Background of Narrow-Bandgap Polymers

In order to show the activity in this research field and make the location and orientation of this thesis clear, the research background is stated as follows.

In 1984, poly(benzo[*c*]thiophene) (**10**) was prepared by Wudl *et al.* as the first narrow-bandgap polymer and showed a bandgap of 1.1 eV.[20] It was remarkably noteworthy that the condensation of benzene ring to poly(thiophene) succeeded in the reduction of about 1 eV bandgap compared with poly(thiophene). That showed a possibility of tuning the bandgap by structural modification, and many groups started to enter into this

field. The polymer also displayed a characteristic electrochromic feature that its color was blue-black in the undoped state and became transparent yellow on p-doping.

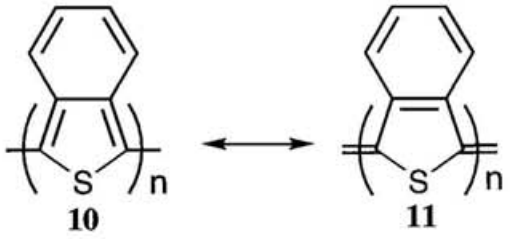


**10** **11**

The reason for the bandgap reduction was investigated with much interest. Brédas performed the VEH calculations on poly(thiophene) by varying the geometry to elucidate the relationship between bandgap and bond-length alternation (the difference between carbon–carbon single and double bond lengths along the polymer backbone). Thus, as the V-shape line is seen in Figure 5, the bandgaps decrease linearly as a function of increasing quinoid character.[21,22] Therefore, the contribution of the *o*-quinoid resonance structure (**11**) in the ground state due to benzene-ring annelation proved to be effective for the bandgap reduction in the case of poly(benzo[*c*]thiophene). Poly(thiophene) lacks such contribution. NMR and

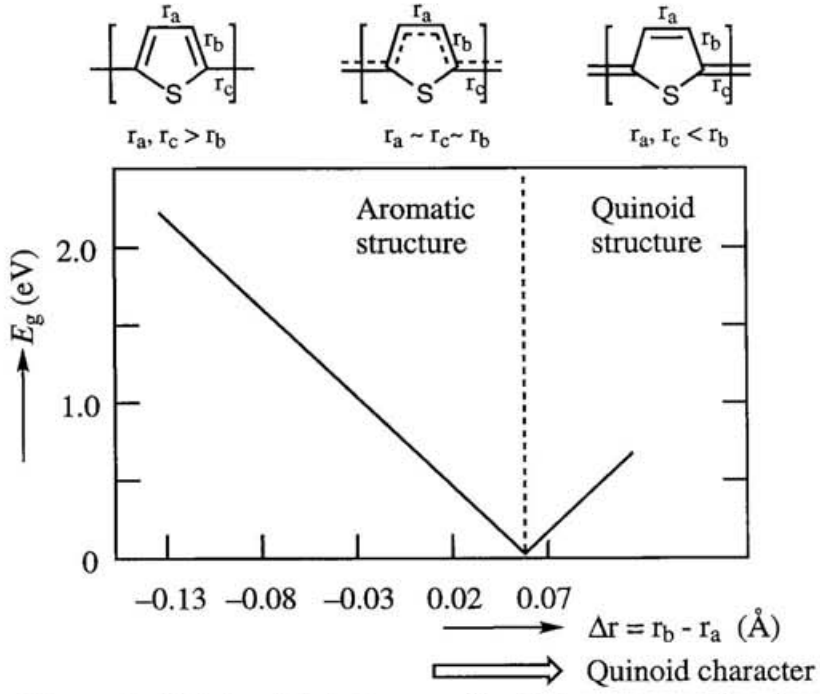


**Figure 5.** Relationship between quinoid character and bandgap.

Raman measurements also supported this finding.[23,24] Thus, the introduction of quinoid character into the main chain has become one important strategy.

Taking the quinoid character into a molecular design, other conjugated polymers were released. As an extension of poly(benzo[*c*]thiophene), poly(naphtho[2,3-*c*]thiophene) (**12**) was prepared by Ikenoue in 1990. Although the bandgap was expected to be near zero from theoretical calculations,[21] it was, in practice, 1.5 eV.[25] This fact indicates that the factor determining bandgaps is not always limited to the quinoid character. Poly(dioxymethylenebenzo[*c*]thiophene) (**13**) was synthesized in 1991 in order to improve the oxidation stability of poly(benzo[*c*]thiophene) and showed a bandgap of 1 eV.[26] Recently, the poly(benzo[*c*]thiophene) derivatives substituted with halogen (e.g., **14**) were prepared by Higgins *et al.* to gain the stable n-doped form, that is inaccessible in the case of general conjugated polymers.[27] Those polymers also exhibited bandgaps of about 1 eV. Very recently, Tour *et al.* synthesized zwitterionic pyrrole-derived conjugated polymers (**15**) from iodide-substituted monomers by Ullman coupling using copper-bronze and succeeded in the transformation of them with a base to their quinoid forms (**16**), which were reverted to **15** by the addition of an acid.[28] The *o*-quinoid forms showed bandgaps of 1.1 eV.

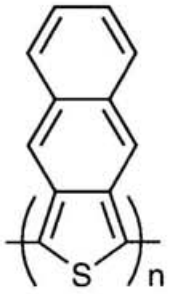


**12**

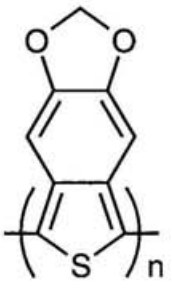


**13**

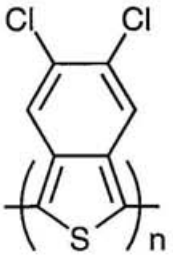


**14**

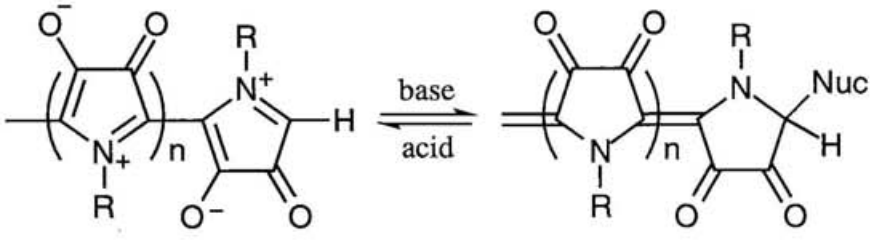


**15** **16**

The methine-bridged conjugated polymers are also known. Recently, Jeneke resynthesized the conjugated polymer containing alternating aromatic and quinoid segments (**17**), whose bandgap exhibited 1.1-1.4 eV.[29] Hanack *et al.* recently prepared a series of extended poly(arenemethylne) derivatives (**18**),[30] whose bandgaps were in a range of 1.8-2.1 eV. These values were higher than the predicted values of 1-1.5 eV.[31,32] The difference was attributed to some structural effects.[30]

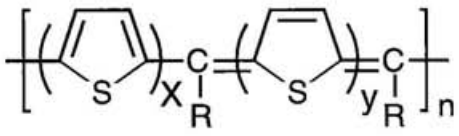

**17**

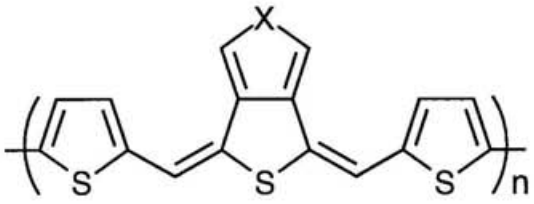

X = S, CH=CH, benzo

**18**

On the basis of other unique ideas, some narrow-bandgap polymers were prepared. Poly(dithieno[3,4-*b*:3',4'-*d*]thiophene) (**19**) was prepared by Taliani *et al.* in 1989.[33] The monomer had a feature that two thiophene sub-units can undergo polymerization. Therefore, in that case, a two-dimensional network of the conjugated polymer would be formed. The polymer exhibited a bandgap of 1.1 eV. In the other place, Ferraris *et al.* adopted an approach using monomers whose HOMO-LUMO gap are small, that might lead to the

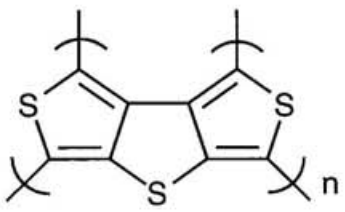

**19**

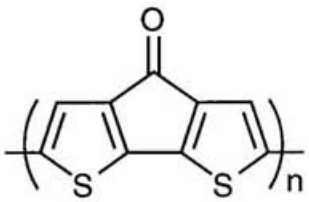

**20**

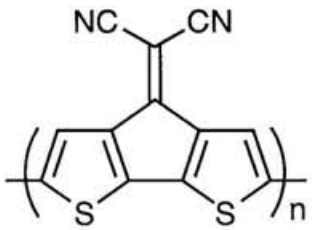

**21**

reduction of bandgaps over their polymers. Two polymers of 4*H*-cyclopenta[2,1-*b*;3,4-*b*']dithiophene derivatives (**20,21**) were prepared in 1991 and showed bandgaps of 1.2 and 0.8 eV, respectively.[34]

While many narrow-bandgap polymers have been prepared, a theoretical study proposed an influential molecular design to obtain narrow-bandgap polymers. In 1991, Kertesz *et al.* reported that mixing the alternating units of polymers with significantly different band structures can lower the bandgap through the relaxation of the bond alternation along the polymer backbone.[35] For example, they indicated that although the experimental bandgaps of aromatic poly(thiophene) (**6**) and *o*-quinoid poly(naphtho[2,3-*c*]thiophene) (**12**) were 2.1 and 1.5 eV, respectively, the alternating copolymer composed of thiophene and naphtho[2,3-*c*]thiophene (**22**) is expected to have a smaller bandgap of 0.54 eV (Figure 6).

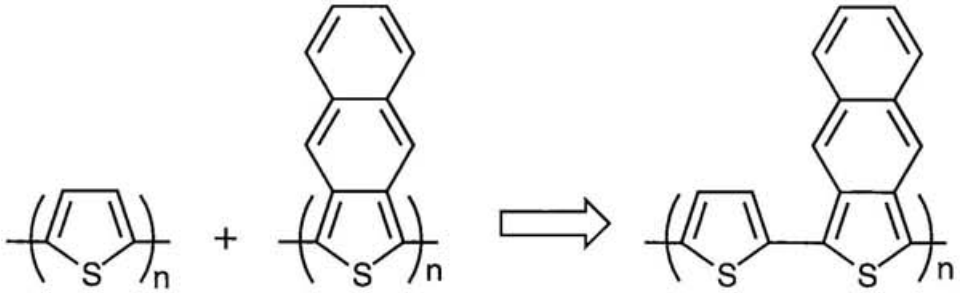


**6** **12** **22**

$E_g$ = 2.1 eV(exp) $E_g$ = 1.5 eV(exp) $E_g$ = 0.54 eV(calc)

**Figure 6.** Copolymerization of different band structures.

According to this strategy, some copolymers were recently synthesized by Ferraris and Cava's groups.[36,37] The copolymer composed of thiophene and benzo[*c*]thiophene units (**23**) exhibited a bandgap of 1.7 eV, whose value was large beyond expectation. On the other hand, the bandgap of the copolymer composed of thiophene and naphtho[2,3-*c*]thiophene units (**24**) was 0.6 eV though the author thinks that the way to measure it is in question. There seems to be still great room for improvement in this molecular design. Very recently, Ferraris reported that the polymer (**25**) which replaced the benzene ring in **23** with pyridine exhibited a bandgap of 1.4 eV, indicating the importance of steric interaction within the polymer backbone.[38]

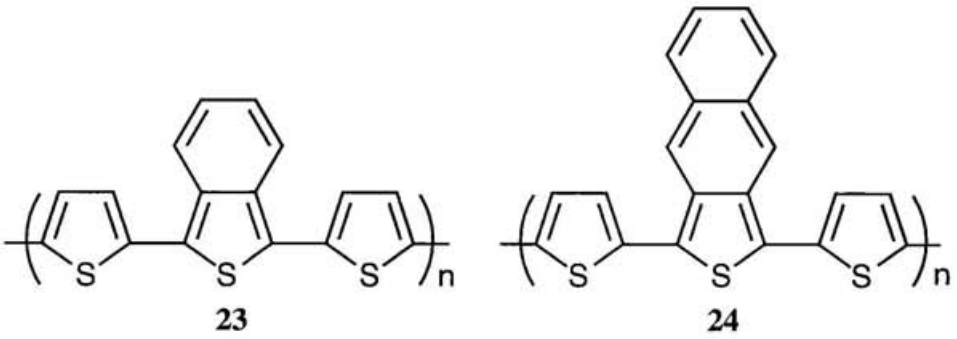

**23** **24**

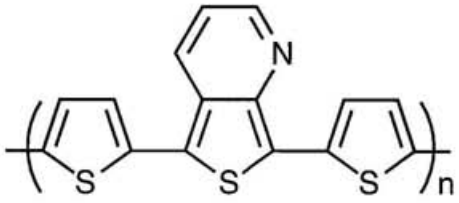

**25**

Concerning the copolymer, another powerful molecular design was demonstrated. Havinga *et al.* proposed a concept of the regular alternation of strong electron-donating and electron-accepting segments. When π-electron delocalization is extended over the polymer backbone, a small HOMO-LUMO gap that consisted of the high HOMO and the low LUMO levels is expected. In 1992, they succeeded in the synthesis of the narrowest-bandgap polymer (**26**) composed of benzobisthiazole as a donor unit and croconic acid as an acceptor unit, whose bandgap was 0.5 eV.[39] Yamamoto *et al.* also have already prepared the copolymer composed of aromatic donor and acceptor segments (**27**) in 1991.[40] The bandgap was, however, estimated to be 1.8 eV. This result may suggest that the combination of units having similar electronic structures is unfavorable.

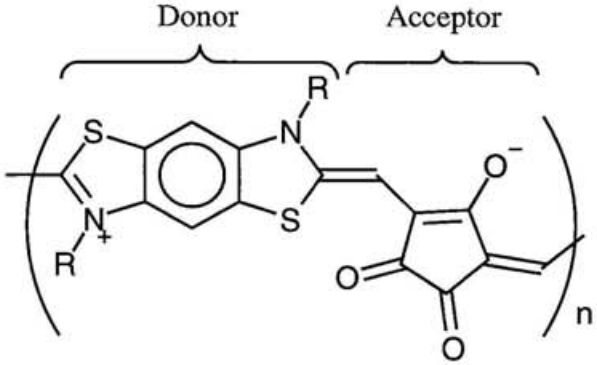


**26**

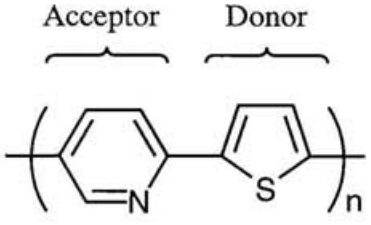


**27**

Though the hitherto introduced investigation of narrow-bandgap polymers was mainly based on polymer frameworks, attention should be directed to other factors. For example, steric factors cannot be neglected. Deviation of experimental data from theoretical predictions would be largely due to the lack of discussion about the coplanarity to maximize the effective conjugation length. In 1990, Marynick *et al.* pointed out that poly(benzo[*c*]thiophene) (**10**) is a nonplanar polymer even in the transoid form because of steric interactions between the peripheral hydrogen atoms of benzene rings and the sulfur atoms of adjacent thiophene units by conformational analysis (Figure 7a) and suggested that the coplanarity would be achieved by the substitution of pyrazine for benzene (Figure 7b).[41] Based on this suggestion, poly(thieno[3,4-*b*]pyrazine) (**28**) was synthesized by Pomerantz *et al.* in 1992 and showed a bandgap of about 1 eV.[42]

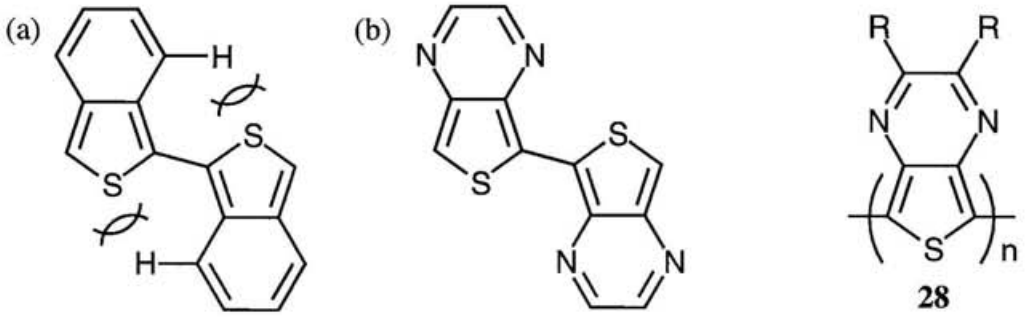


**Figure 7.** Steric interactions between adjacent units.

Recently, Roncali *et al.* have accomplished the coplanarity by another method. The origin resulting in torsional conformations is free rotation of the single C–C bonds between adjacent segments in the polymer. Therefore, they used the thiophene oligomers rigidified by one methylene chain to suppress the free rotation as monomers.[43] The polymers

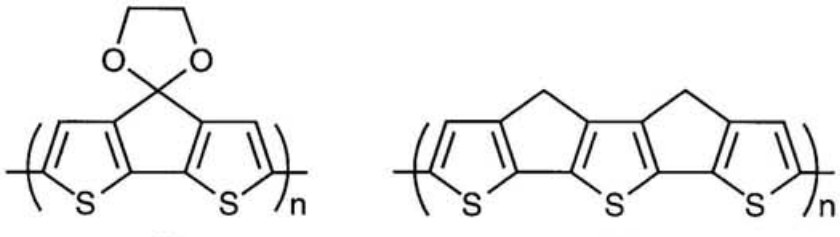

(**29,30**) exhibited bandgaps of around 1.2 eV, which were about 1 eV lower than that of poly(thiophene).

## 1.3 Purpose and Constitution of Present Thesis

Many studies on narrow-bandgap polymers were modifications of known simple aromatic compounds due to synthetic difficulties and now appear to encounter the limitation of application of the strategy. A systematic study of functionalized derivatives that is based on new molecular designs is anticipated in order to gain narrower bandgap polymers, to elucidate the relationship between structure and properties of polymers, and to clarify the factor reducing the bandgap. Therefore, the author has designed new narrow-bandgap systems on the basis of (*i*) the alternating copolymerization of aromatic and *o*-quinoid units and (*ii*) the alternation of strong electron-donating and electron-accepting segments as described above. The systems are expressed by $[–A–Q–A–]_n$, where A is a kind of aromatic-donor unit and Q is a kind of *o*-quinoid-acceptor unit (**31-39** in Figure 8). As the same system, copolymers **40**[44] and **41**[45] have been recently reported by the author's group, which showed bandgaps of 0.9 and 0.5 eV, respectively. Since the properties of polymers are considered to correlate straightforwardly to those of structurally defined monomers [A–Q–A], it is important to examine the latter in detail. In this thesis, synthesis of a series of monomers (**31-39**) and their polymerization are attempted. The monomers **31-37** consist of thiophene as 6π-aromatic-donor unit and 10π- or 14π-heterocycles as *o*-quinoid-acceptor unit (thieno[3,4-*b*]pyrazine for **31**, quinoxaline for **32**, 2,1,3-benzothiadiazole for **33**, [1,2,5]thiadiazolo[3,4-*g*]quinoxaline for **34**, benzo[1,2-*c*;4,5-*c*']bis[1,2,5]thiadiazole for **35**, pyrazino[2,3-*g*]quinoxaline for **36**, pyrazino[2,3-*b*]quinoxaline for **37**). The monomers among **31-33** and among **34-36** share an isoelectronic structure, respectively. The monomers **36** and **37** are geometrical isomers, meaning that the position of pyrazine based on quinoxaline is different. It is interesting to know to what extent the various *o*-quinoid-acceptor segments module physical properties of

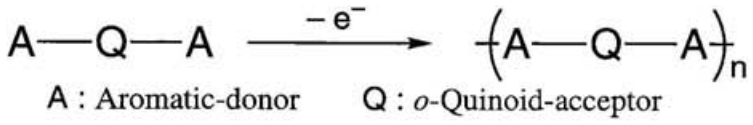


**Figure 8.** New molecular design.

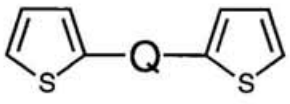


Q:

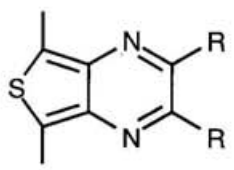


**31**

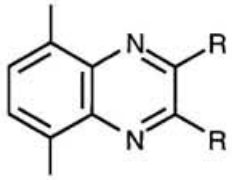


**32**

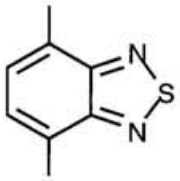


**33**

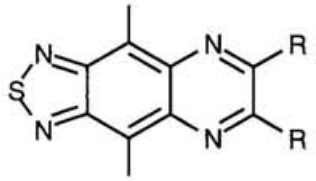


**34**

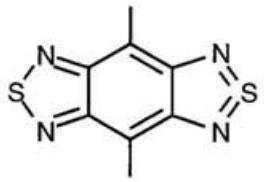


**35**

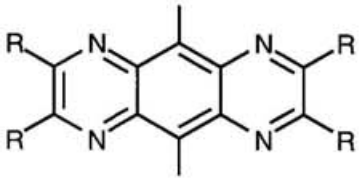


**36**

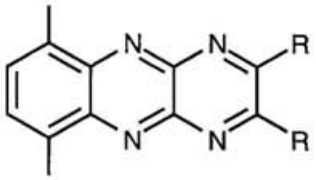


**37**

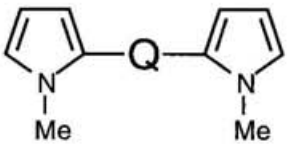


Q:

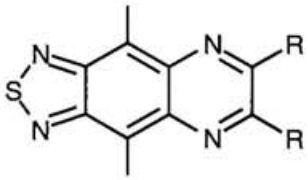


**38**

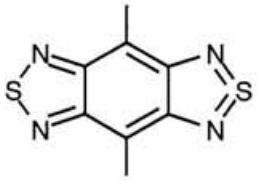


**39**

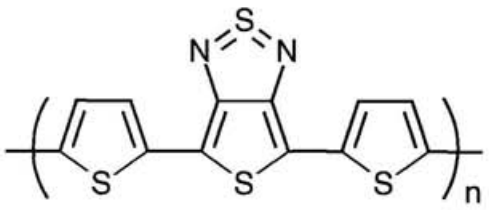

**40**

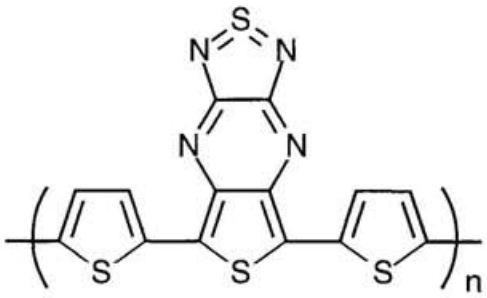

**41**

the monomers and the corresponding polymers. Those *o*-quinoid-acceptor units also have a feature that there is no hydrogen atom at the peripheral positions, which will lead to no or less steric interactions between adjacent rings. The monomers **38** and **39** share the same *o*-quinoid-acceptor units as **34** and **35**, respectively, and differ from only aromatic-donor parts, indicating the different HOMO levels. With the above molecular designs in mind, the investigation of properties of a series of the monomers and the polymers is undertaken to explore the structure-property correlation.

The present thesis consists of three chapters including this chapter.

Chapter 2 deals with a series of monomers **31-39** characterized by composition of aromatic-donor and *o*-quinoid-acceptor segments. The monomers are of interest as novel heterocyclic oligomers because few synthetic studies are reported. Preparation of the monomers was carried out through a cross-coupling reaction of dihalo-substituted compounds with stannane compounds in the presence of a palladium catalyst[46] as a main reaction. As to some monomers with pyrazine (**31**, **32**, **34**, and **38**), long alkyl chains were introduced in expectation of improving processability of their polymers. HOMO and LUMO energy levels of each segment and atomic orbital coefficients are discussed from the MO calculations to estimate physical properties, and the results are related to the absorption spectra and redox behaviors of the monomers. The coplanarity between the adjacent segments is argued from X-ray structural analysis and conformational analysis, and are associated with the physical properties of the monomers.

Chapter 3 is concerned with polymerization of the monomers and properties of the resulting polymers. The polymers were prepared directly onto Pt disk and indium tin oxide

(ITO) coated glass electrodes by electrochemical oxidation with a cyclic potential sweep technique. Unique p- and n-doping processes of the polymers on a Pt electrode are examined by cyclic voltammetry measurements. Electrochemical bandgaps of the polymers were determined from the cyclic voltammograms. Electronic spectra of the polymers on an ITO-coated glass electrode were measured *ex situ* under control of potentials in order to explore electrochromic properties and to estimate optical bandgaps. The correlation between the bandgaps and structures of the polymers is discussed.

## 1.4 References


(1) For reviews, see: (a) Skotheim, T. A., Ed. *Handbook of Conducting Polymers*; Marcel Dekker: New York, 1986. (b) Yoshimura, S. *Dodensei Polymer*; Kyoritsu Shuppan: Tokyo, 1987. (c) Patil, A. O.; Heeger, A. J.; Wudl, F. *Chem. Rev.* **1988**, *88*, 183. (d) Yoshino, K. In *Bunshi To Electronics*; Sangyo Tosho: Tokyo, 1991. (d) Scherf, U.; Müllen, K. *Synthesis* **1992**, 23. (e) Brédas, J.-L.; Silbey, R., Eds. *Conjugated Polymers*; Kluwer Academic Publishers: Dordrecht, 1991. (f) Roncali, J. *Chem. Rev.* **1992**, *92*, 711. (g) Brédas, J.-L. *Adv. Mater.* **1995**, *7*, 263.

(2) Ito, T.; Shirakawa, H.; Ikeda, S. *J. Polym. Sci., Polym. Chem. Ed.* **1974**, *12*, 11.

(3) Chiang, C. K.; Fincher, C. R., Jr.; Park, Y. W.; Heeger, A. J.; Shirakawa, H.; Louis, E. J.; Gau, S. C.; MacDiarmid, A. G. *Phys. Rev. Lett.* **1977**, *39*, 1098.

(4) Peierls, R. E. In *Quantum Theory of Solids*; Oxford Univ. Press, Oxford, 1955, p. 108.

(5) Fincher, C. R., Jr.; Ozaki, M.; Tanaka, M.; Peebles, D.; Lauchlan, L.; Heeger, A. J.; MacDiarmid, A. G. *Phys. Rev. B* **1979**, *20*, 1589.

(6) Diaz, A. F.; Kanazawa, K. K.; Gardini, G. P. *J. Chem. Soc., Chem. Commun.* **1979**, 635.

(7) Bargon, J.; Mohmand, S.; Waltman, *R. J. IBM J. Res. Dev.* **1983**, *27*, 330.

(8) Waltman, R. J.; Diaz, A. F.; Bargon, J. *J. Electrochem. Soc.* **1985**, *132*, 632.

(9) Diaz, A. F. *Chem. Scr.* **1981**, *17*, 145.

(10) Waltman, R. J.; Diaz, A. F.; Bargon, J. *J. Phys. Chem.* **1984**, *88*, 4343.

(11) (a) Sato, M.; Tanaka, S.; Kaeriyama, K. *J. Chem. Soc., Chem. Commun.* **1986**, 873. (b) Jen, K.-Y.; Miller, G. G.; Elsenbaumer, R. L. *J. Chem. Soc., Chem. Commun.* **1986**, 1346.

(12) Sugimoto, R.; Takeda, S.; Gu, H. B.; Yoshino, K. *Chem. Express* **1986**, *1*, 635.

(13) (a) Chen, T.-A.; Rieke, R. D. *J. Am Chem. Soc.* **1992**, *114*, 10087. (b) Chen, T.-A.; Rieke, R. D. *Synth. Met.* **1993**, *60*, 175. (c) Chen, T.-A.; Wu, X.; Rieke, R.

D. *J. Org. Chem.* **1995**, *117*, 233.

(14) (a) McCullough, R. D.; Lowe, R. D. *J. Chem. Soc., Chem. Commun.* **1992**, 70. (b) McCullough, R. D.; Lowe, R. D.; Jayaraman, M.; Anderson, D. L. *J. Org. Chem.* **1993**, *58*, 904.

(15) (a) Yamamoto, T.; Morita, A.; Miyazaki, Y.; Maruyama, T.; Wakayama, H.; Zhou, Z.; Nakamura, Y.; Kanbara, T. *Macromolecules* **1992**, *25*, 1214. (b) Yamamoto, T.; Maruyama, T.; Zhou, Z.; Ito, T.; Fukuda, T.; Yoneda, Y.; Begum, F.; Ikeda, T.; Sasaki, S.; Takezoe, H.; Fukuda, A.; Kubota, K. *J. Am. Chem. Soc.* **1994**, *116*, 4832.

(16) Brédas, J. L.; Elsenbaumer, R. L.; Chance, R. R.; Silbey, R. *J. Chem. Phys.* **1983**, *78*, 5656.

(17) Simon, J. In *Nanostructures Based on Molecular Materials*; Göpel, W., Ziegler, Ch., Eds; VCH: Weinheim, 1992, p267.

(18) Nalwa, H. S. *Adv. Mater.* **1993**, *5*, 341.

(19) Yoshino, K.; Tada, K.; Onoda, M. *Jpn. J. Appl. Phys., Pt. 2* **1994**, *33*, L1785.

(20) (a) Wudl, F.; Kobayashi, M.; Heeger, A. J. *J. Org. Chem.* **1984**, *49*, 3382. (b) Kobayashi, M.; Colaneri, N.; Boysel, M.; Wudl, F.; Heeger, A. J. *J. Chem. Phys.* **1985**, *82*, 5717.

(21) (a) Brédas, J.-L. *J. Chem. Phys.* **1985**, *82*, 3808. (b) Brédas, J.-L. *Synth. Met.* **1987**, 17, 115.

(22) Brédas, J.-L.; Heeger, A. J.; Wudl, F. *J. Chem. Phys.* **1986**, *85*, 4673.

(23) (a) Hoogmartens, I.; Vanderzande, H.; Martens, H.; Gelan, J. *Synth. Met.* **1991**, *41-43*, 513. (b) Hoogmartens, I.; Adriaensens, P.; Vanderzande, H.; Gelan, J.; Quattrocchi, C.; Lazzaroni, R.; Brédas, J.-L. *Macromolecules* **1992**, *25*, 7347.

(24) Kastner, J.; Kuzmany, H.; Vegh, D.; Landl, M.; Cuff. L.; Kertesz, M. *Macromolecules* **1995**, *28*, 2922.

(25) Ikenoue, Y. *Synth. Met.* **1990**, *35*, 263.

(26) Ikenoue, Y.; Wudl, F.; Heeger, A. J. *Synth. Met.* **1991**, *40*, 1.

(27) (a) King, G.; Higgins, S. J. *J. Chem. Soc., Chem. Commun.* **1994**, 825. (b) King,

G.; Higgins, S. J.; Garner, S. E.; Hillmann, A. R. *Synth. Met.* **1994**, *67*, 241. (c) King, G.; Higgins, S. J. *J. Mater. Chem.* **1995**, *5*, 447.

(28) (a) Brockmann, T. W.; Tour, J. M. *J. Am. Chem. Soc.* **1994**, *116*, 7435. (b) Brockmann, T. W.; Tour, J. M. *J. Am. Chem. Soc.* **1995**, *117*, 4437.

(29) Chen, W.-C.; Jenekhe, S. A. *Macromolecules* **1995**, *28*, 465.

(30) (a) Hieber, G.; Hanack, M.; Wurst, K.; Strähle, J. *Chem. Ber.* **1991**, *124*, 1597. (b) Hanack, M.; Schmid, U.; Echinger, S.; Teichert, F.; Hieber, J. *Synthesis* **1993**, 634. (c) Hanack, M.; Schmid, U.; Röhrig, U.; Adant, C.; Brédas, J.-L. *Chem. Ber.* **1993**, *126*, 1487. (d) Ritter, H.; Mangold, K.-M.; Röhrig, U.; Schmid, U.; Hanack, M. *Synth. Met.* **1993**, *55-57*, 1193. (e) Hanack, M.; Mangold, K.-M.; Röhrig, U.; Maichle-Mössmer, C. *Synth. Met.* **1993**, *60*, 199.

(31) Lee, Y.-S.; Kertesz, M. *J. Chem. Phys.* **1988**, *88*, 2609.

(32) Toussaint, J.-M.; Thémans, B.; André, J.-M.; Brédas, J.-L. *Synth. Met.* **1989**, *28*, C205.

(33) Taliani, C.; Ruani, G.; Zamboni, R.; Bonognesi, A.; Catellani, M.; Destri, S.; Porzio, W.; Ostoja, P. *Synth. Met.* **1989**, *28*, C507.

(34) (a) Lambert, T. L.; Ferraris, J. P. *J. Chem. Soc., Chem. Commun.* **1991**, 752. (b) Ferraris, J. P.; Lambert, T. L. *J. Chem. Soc., Chem. Commun.* **1991**, 1268.

(35) Kürti, J.; Surján, P. R.; Kertesz, M. *J. Am. Chem. Soc.* **1991**, *113*, 9865.

(36) Musmanni, S.; Ferraris, J. P. *J. Chem. Soc., Chem. Commun.* **1993**, 172.

(37) Lakshmikantham, M. V.; Lorcy, D.; Scordilis-Kelley, C.; Wu, X.-L.; Parakka, J. P.; Metzger, R. M.; Cava, M. P. *Adv. Mater.* **1993**, *5*, 723.

(38) Ferraris, J. P.; Bravo, A.; Kim, W.; Hrncir, D. C. *J. Chem. Soc., Chem. Commun.* **1994**, 991.

(39) (a) Havinga, E. E.; ten Hoeve, W.; Wynberg, H. *Polym. Bull.* **1992**, *29*, 119. (b) Havinga, E. E.; ten Hoeve, W.; Wynberg, H. *Synth. Met.* **1993**, *55-57*, 299.

(40) Zhou, Z.; Maruyama, T.; Kanbara, T.; Ikeda, T.; Ichimura, K.; Yamamoto, T; Tokuda, K. *J. Chem. Soc., Chem. Commun.* **1991**, 1210.

(41) Nayak, K.; Marynick, D. S. *Macromolecules* **1990**, *23*, 2237.

(42) (a) Pomerantz, M.; Chaloner-Gill, B.; Harding, L. O.; Tseng, J. J.; Pomerantz, W. J. *J. Chem. Soc., Chem. Commun.* **1992**, 1672. (b) Pomerantz, M.; Chaloner-Gill, B.; Harding, L. O.; Tseng, J. J.; Pomerantz, W. J. *Synth. Met.* **1993**, *55-57*, 960.

(43) (a) Brisset, H.; Thobie-Gautier, C.; Gorgues, A.; Jubault, M.; Roncali, J. *J. Chem. Soc., Chem. Commun.* **1994**, 1305. (b) Roncali, J.; Thobie-Gautier, C. *Adv. Mater.* **1994**, *6*, 846.

(44) Tanaka, S.; Yamashita, Y. *Synth. Met.* **1993**, *55-57*, 1251.

(45) Tanaka, S.; Yamashita, Y. *Synth. Met.* **1995**, *69*, 599.

(46) (a) Stille, J. K. *Angew. Chem., Int. Ed. Engl.* **1986**, *25*, 508. (b) Mitchell, T. N. *Synthesis* **1992**, 803.

# Chapter 2 Syntheses and Properties of Triheterocyclic Monomers Composed of Aromatic-Donor and *o*-Quinoid-Acceptor Segments.

Abstract: Triheterocyclic monomers composed of aromatic-donor (thiophene and *N*-methylpyrrole) and a series of *o*-quinoid-acceptor segments were synthesized through the coupling reaction of dihalo-substituted compounds with stannane compounds in the presence of a Pd(II) catalyst. MO calculations of each segment were carried out by the MNDO-PM3 method to estimate the properties of monomers roughly and to facilitate discussion later. Electronic spectra of the various monomers with thiophene as aromatic-donor moieties indicated a trend that the monomer with *o*-quinoid-acceptor whose LUMO is lower has a longer absorption maximum. On the other hand, the absorption bands of the monomers containing *N*-methylpyrrole displayed small blue shifts compared with the corresponding thiophene analogs against the expectation based on the MO calculations. From the results of X-ray analyses of some monomers with thiophene and conformational analyses of the other monomers, it was demonstrated that the molecules containing thiophene have almost coplanar conformations and the molecules containing *N*-methylpyrrole have torsional geometries. It was expected that the nonplanar conformations bring about the reduction of extensive delocalization. Cyclic voltammetry measurements of the monomers displayed an irreversible oxidation wave and a reversible or quasi-reversible reduction wave, indicating their amphoteric redox properties. The difference between anodic and cathodic peak potentials depended on the LUMO level of *o*-quinoid-acceptor heterocycle.

## 2.1 Introduction

Recently, narrow-bandgap polymers have attracted much interest because of their interesting properties and potential as promising materials.[1] To attain the polymers, the synthesis of the monomers has to be conducted firstly. The author designed a new series of monomers **1-9** on the basis of the alternating copolymer composed of aromatic-donor and the *o*-quinoid-acceptor segments as mentioned in Chapter 1. The monomers have two structural features. First, they are triheterocyclic oligomers possessing a sandwich structure where both sides of the *o*-quinoid-acceptor moiety are bonded to aromatic-donor rings, which enables anodic polymerization. Double blocking of *o*-quinoid-acceptor units would be also helpful to stabilize the molecules since *o*-quinoid compounds are usually unstable.[2] Secondly, the absence of hydrogen atoms at peripheral positions on *o*-quinoid-acceptor segments is advantageous for steric interaction between adjacent segments.[3] As to the monomers **1**, **2**, **4**, and **8**, long alkyl chains could be introduced to improve solubility of the corresponding polymers.

Recently, synthesis of triheterocyclic oligomers is of increasing interest from a synthetic standpoint because of their importance in many fields such as biological properties.[4] It is well known that cross-coupling reactions, such as Kumada,[5] Suzuki,[6] and Stille[7] couplings, are effective for the synthesis of the oligomers. Novel triheterocyclic oligomers **1-9** as monomers were prepared using the Pd(II)-catalyzed coupling reaction[8] of dihalo-substituted heterocyclic compounds with heterocyclic trialkyl stannane.

It is interesting to investigate how structural modification modulates the physical properties of the triheterocyclic monomers. As it is generally assumed that the preferred conformation of a monomer is maintained in the polymer,[9] it is important to examine coplanarity of the monomer. The structure-property relationship among the monomers is discussed in combination with the results of X-ray structural analyses, conformational analyses, and MO calculations.

In this chapter, syntheses and properties of triheterocyclic monomers **1-9** are described.

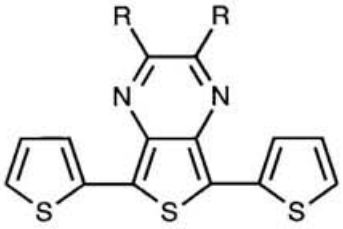

**1a** : R = H
**1b** : R = $CH_3$
**1c** : R = $C_6H_{13}$
**1d** : R = $C_{13}H_{27}$

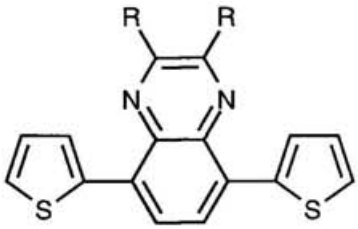

**2a** : R = $CH_3$
**2b** : R = $C_6H_{13}$

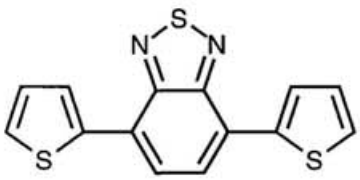

**3**

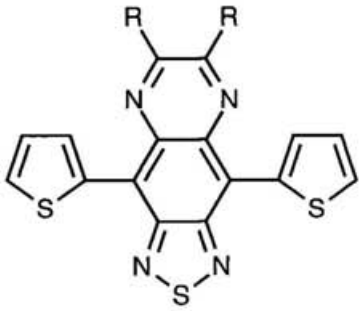

**4a** : R = H
**4b** : R = $CH_3$
**4c** : R = $C_6H_{13}$

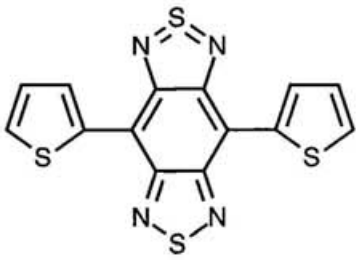

**5**

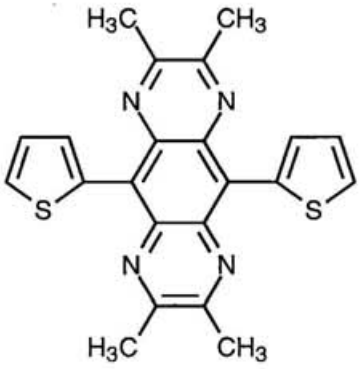

**6**

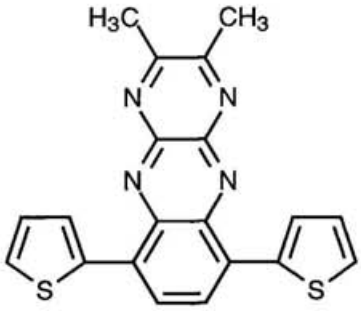

**7**

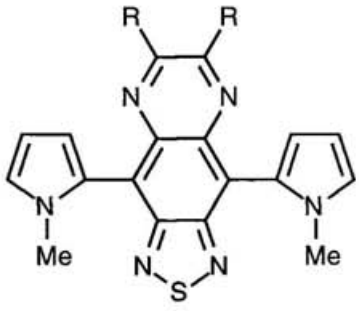

**8a** : R = $CH_3$
**8b** : R = $C_6H_{13}$

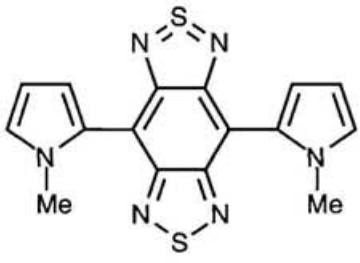

**9**

## 2.2 Results and Discussion

### 2.2.1 Syntheses of Triheterocyclic Monomers

The synthesis of the monomers **1a-d** is described in Scheme 1. The Stille coupling reaction of 2,5-dibromo-3,4-dinitrothiophene[10] (**10**) with tributyl(thien-2-yl)stannane[11] in the presence of catalytic bis(triphenylphosphine)dichloropalladium(II) $[PdCl_2(PPh_3)_2]$[8] gave dinitroterthiophene (**11**) in 60% yield. Reduction of **11** with $SnCl_2$ in ethanol-hydrochloric acid produced diaminoterthiophene **12** in 62% yield. Condensation of **12** with 1,2-diketones[12,13] (involving a synthetic equivalent of glyoxal)[14] produced thieno[3,4-*b*]pyrazine (**TP**) derivatives **1a-d** in 52-82% yield. The monomers **1a-d** showed good solubilities in common organic solvents, although **1c,d** were only slightly soluble in polar solvents such as acetonitrile and acetone.

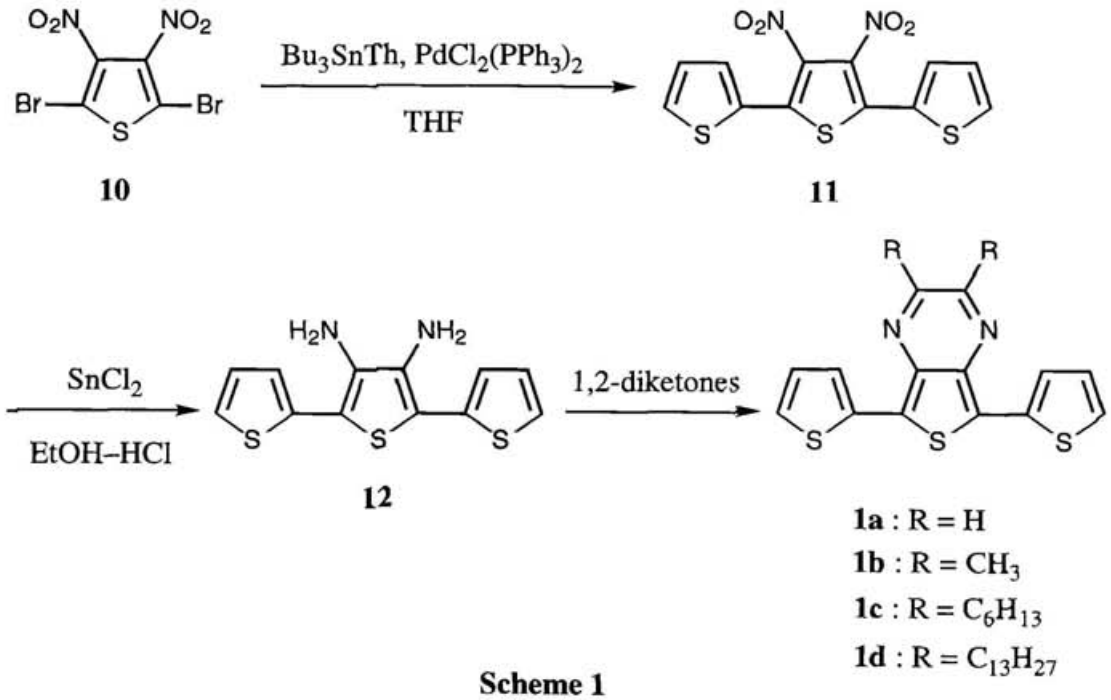


**Scheme 1**

Scheme 2 shows the syntheses of the monomers **2a,b** and **3**. The coupling reaction of 4,7-dibromo-2,1,3-benzothiadiazole[15] (**13**) with tributyl(thien-2-yl)stannane in the presence of $PdCl_2(PPh_3)_2$ afforded the 2,1,3-benzothiadiazole (**BT**) derivative **3** in 82%

yield. Reduction of **3** with zinc in acetic acid accompanied by opening of the [1,2,5]thiadiazole ring gave the diamino compound **14** in 60% yield. Quinoxaline (**QU**) derivatives **2a,b** were prepared by condensation of **14** with 1,2-diketones in 89-90% yields. The solubilities of **2a,b** and **3** were good, whereas **2b** had poor solubility in polar solvents such as acetonitrile.

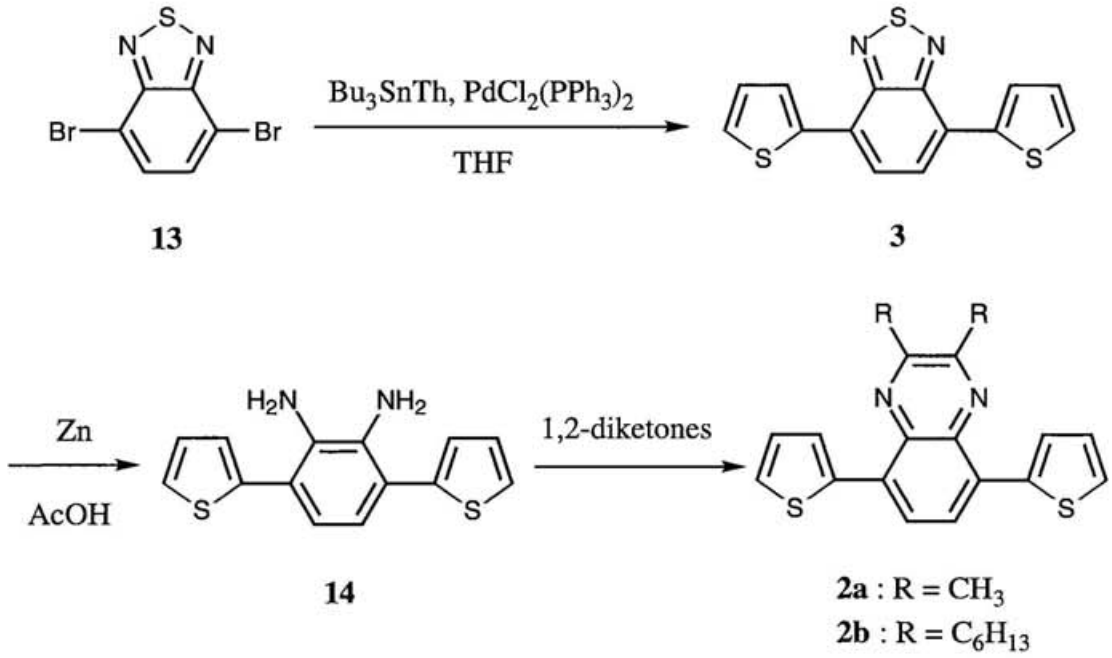


**Scheme 2**

In Scheme 3, the syntheses of the monomers **4a-c** and **5** are described. The coupling reaction of 4,7-dibromo-5,6-dinitro-2,1,3-benzothiadiazole[16] (**15**) with tributyl(thien-2-yl)stannane in the presence of $PdCl_2(PPh_3)_2$ gave a dinitro compound **16** in 47% yield. Reduction of **16** with iron in acetic acid yielded a diamino compound **17** in 58% yield. Condensation of **17** with 1,2-diketones gave [1,2,5]thiadiazolo[3,4-*g*]quinoxaline (**TQ**) derivatives **4a-c** in 50-82% yields. On the other hand, the reaction of **17** with *N*-sulfinylaniline and chlorotrimethylsilane in pyridine gave a benzo[1,2-*c*;4,5-*c*']bis[1,2,5]thiadiazole (**BBT**) derivative **5**, which was a stable nonclassical[17] 14π-electron system,[18] in 82% yield. The monomers **4a,b** and **5** were only slightly soluble in organic solvents, while **4c** was soluble except in polar solvents.

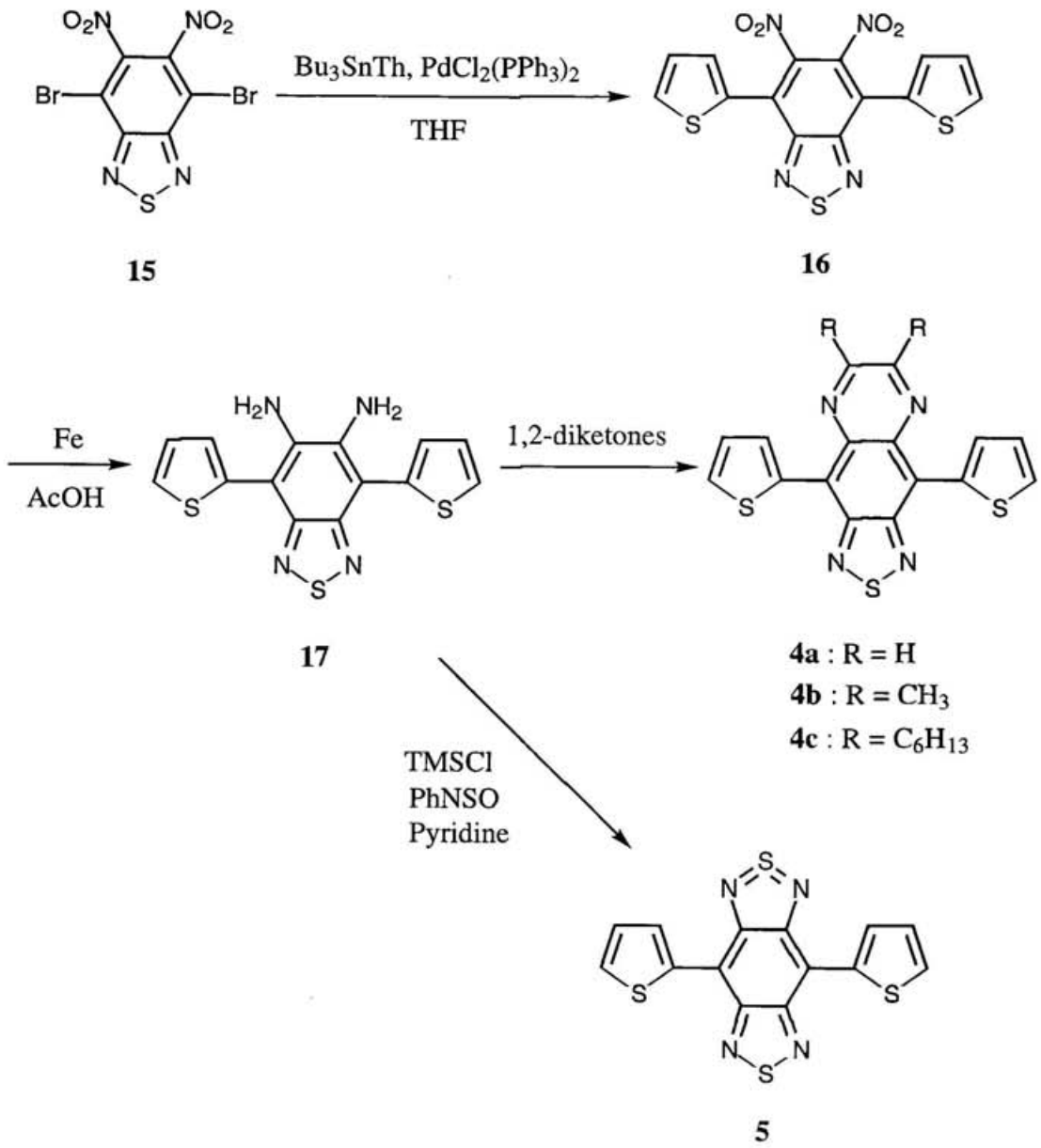


**Scheme 3**

The monomer **6** was synthesized as shown in Scheme 4. Reduction of **16** with a large excess of zinc in acetic acid followed by treatment with diacetyl in one pot afforded a pyrazino[2,3-*g*]quinoxaline (**GPQ**) derivative **6** in 53% yield. A tetra-amino intermediate **18** could not be isolated due to its instability on exposure to air. In spite of the substitution of four alkyl groups, **6** was sparingly soluble in organic solvents.

The preparation of the monomer **7** is represented in Scheme 5. Treatment of **14** with dimethyl oxaldiimidate[19] (**19**) gave a 2,3-diaminoquinoxaline derivative **20** in 58% yield. This reaction proceeded by addition of a small amount of acetic acid to the methanol solution

of the reaction mixture. Condensation of **20** with diacetyl in acetic acid afforded a pyrazino[2,3-*b*]quinoxaline (**BPQ**) derivative **7** in 86% yield. The monomer **7** also exhibited poor solubility in organic solvents.

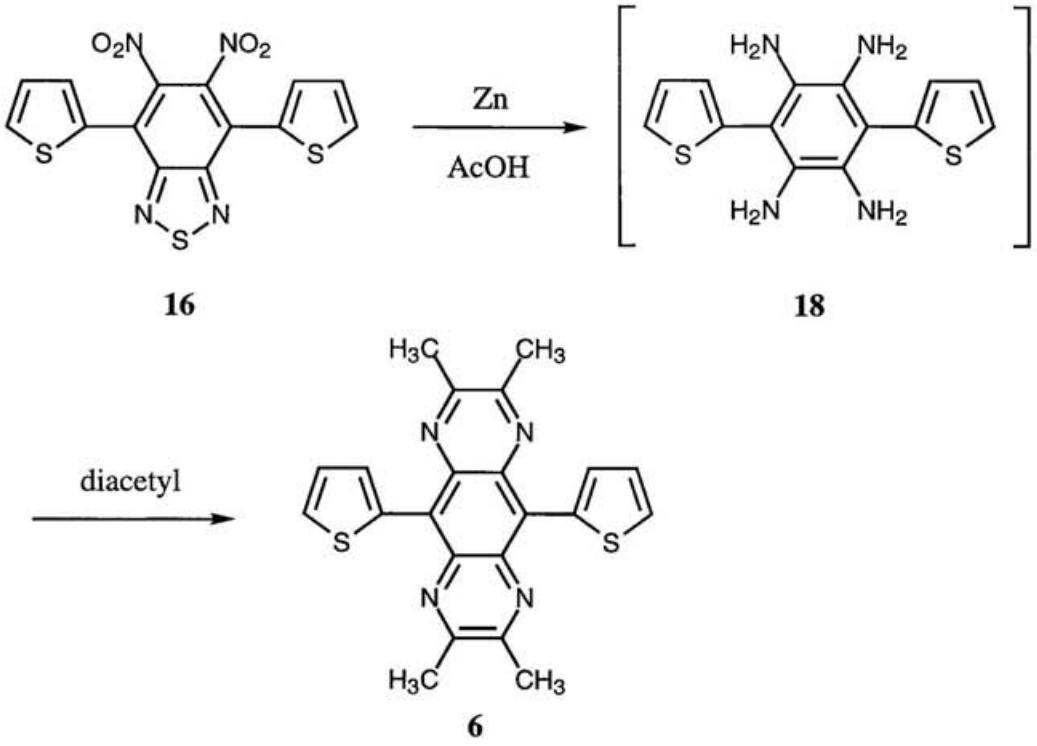


**Scheme 4**

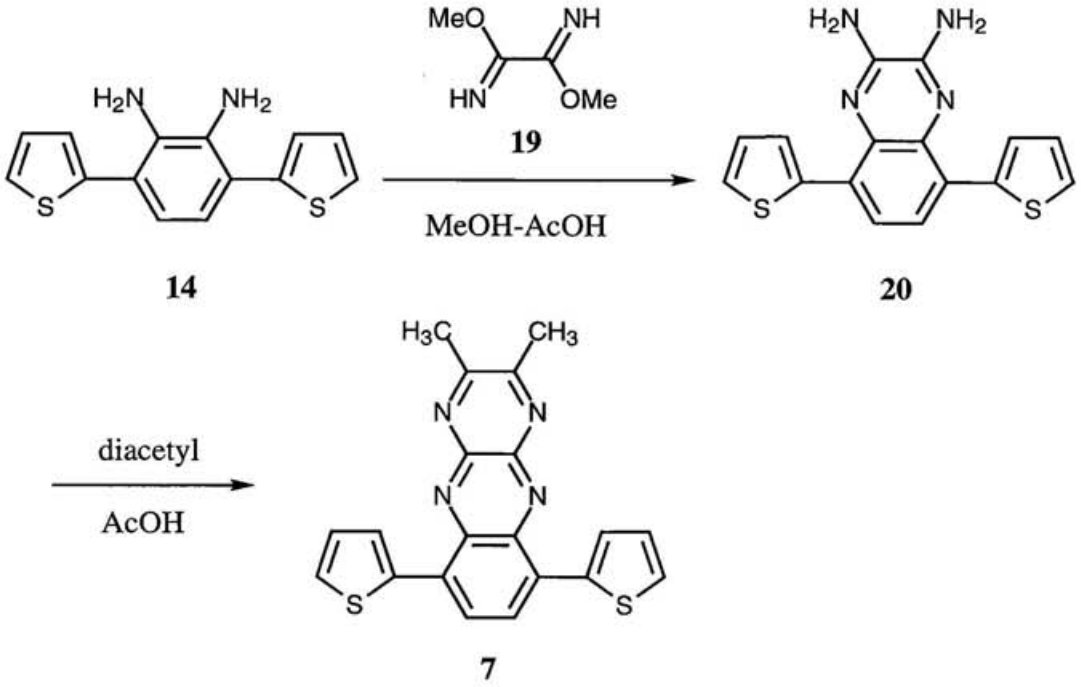


**Scheme 5**

The syntheses of the monomers **8a,b** and **9** are shown in Scheme 6 according to the procedure similar to that used in the syntheses of the monomers **4** and **5**, except for the purification of a dinitro compound **21**. The coupling reaction of **15** with tributyl(*N*-methylpyrrol-2-yl)stannane[20] in the presence of $PdCl_2(PPh_3)_2$ followed by reduction with iron in acetic acid gave a diamino compound **22** in 73% yield. Condensation of **22** with 1,2-diketones gave **TQ** derivatives **8a,b** in 62 and 59% yields, respectively, whereas the reaction of **22** with *N*-sulfinylaniline and chlorotrimethylsilane in pyridine gave a **BBT**

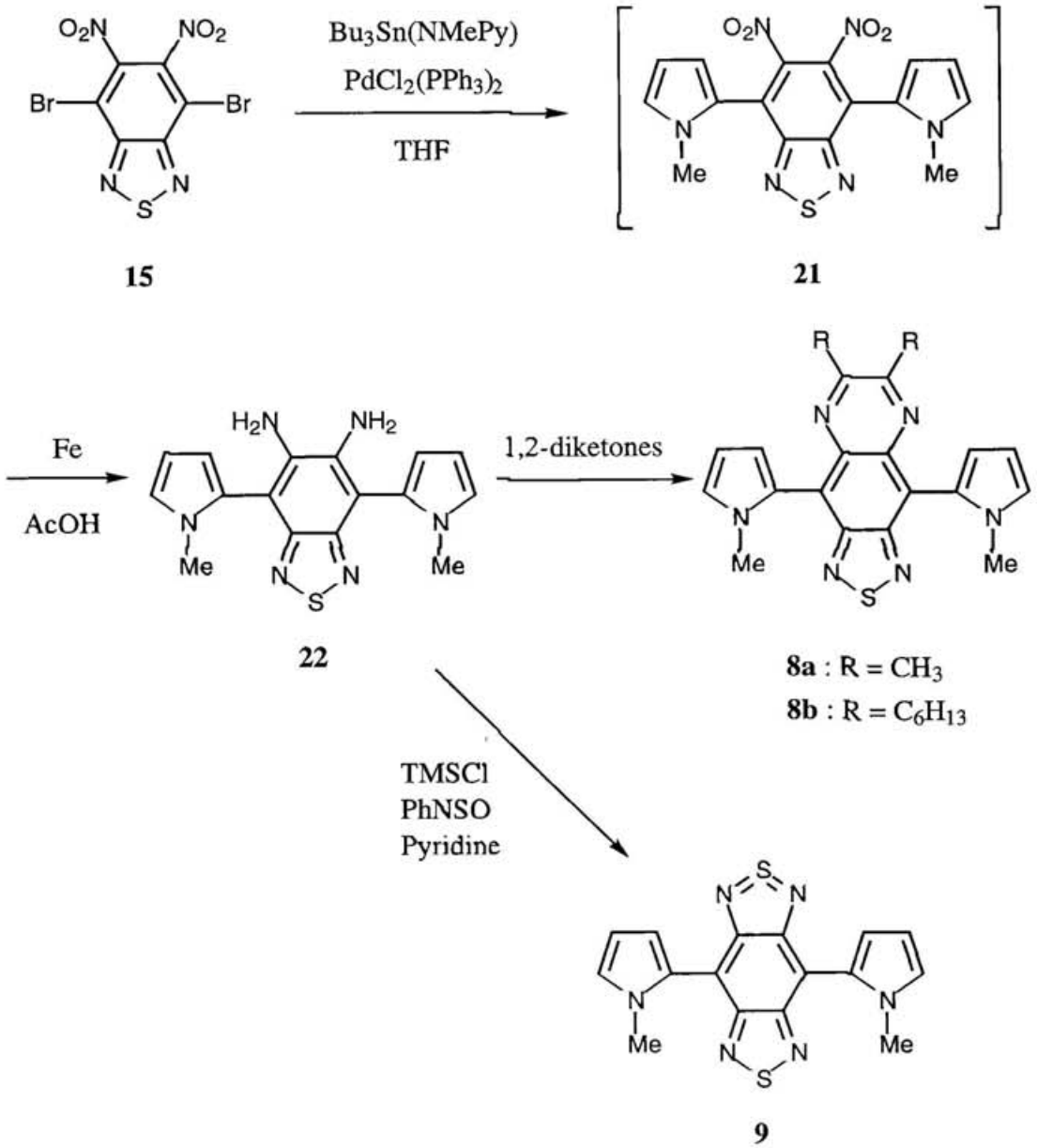


**15** **21** **22**

**8a** : R = $CH_3$
**8b** : R = $C_6H_{13}$

**9**

**Scheme 6**

derivative **9** in 28% yield. The monomers **8a,b** and **9** were much more soluble than the thiophene analogs **4a-c** and **5**. The solubilities of **8a,b** and **9** were good in organic solvents. In particular, **8b** were soluble even in polar solvents such as acetonitrile. In preparation of **2**, **6**, **7**, and **8**, treatment of amino compounds (**14**, **18**, **20**, and **22**) with 40% glyoxal or 1,4-dioxane-2,3-diol was unsuccessful in giving the parent pyrazine derivatives.

### 2.2.2 Molecular Orbital Calculations

The MNDO-PM3 calculations[21] were performed in order to estimate properties of the monomers and their polymers and facilitate discussion later. First, MO energies of the relating heterocyclic segments were compared with each other. Their HOMO and LUMO energies are shown in Table 1 and Figure 1. The HOMO energies of *o*-quinoid-acceptor heterocycles range from –8.73 to –9.45 eV, while their LUMO energies are in a wide range of –3.21 to –0.90 eV. Namely, the structures of *o*-quinoid-acceptor heterocycles affect primarily the LUMO levels. Among the *o*-quinoid-acceptor heterocycles, **BBT** has the lowest LUMO (–3.21 eV), showing the strongest electron-accepting ability, whereas **QU** has the highest LUMO (–0.90 eV), indicating the weakest electron-accepting ability. Additionally, **BBT** has the highest HOMO, therefore, the smallest HOMO-LUMO separation itself. Among the aromatic-donor heterocycles, the HOMO level of *N*-methylpyrrole (–8.87 eV) is higher than that of thiophene (–9.54 eV), indicating its stronger electron-donating ability.

It is necessary to examine the electronic interaction between adjacent segments, particularly, at the bonding positions of the monomers. To estimate it, atomic orbital (AO) coefficients were also evaluated (Figure 2). Five-membered-ring aromatic-donor heterocycles have a next HOMO level near the HOMO level. Thiophene has the largest AO coefficients at the 2- and 5-positions in both next HOMO and LUMO, and pyrroles also have the largest AO coefficients at the 2- and 5-positions in both HOMO and LUMO. These

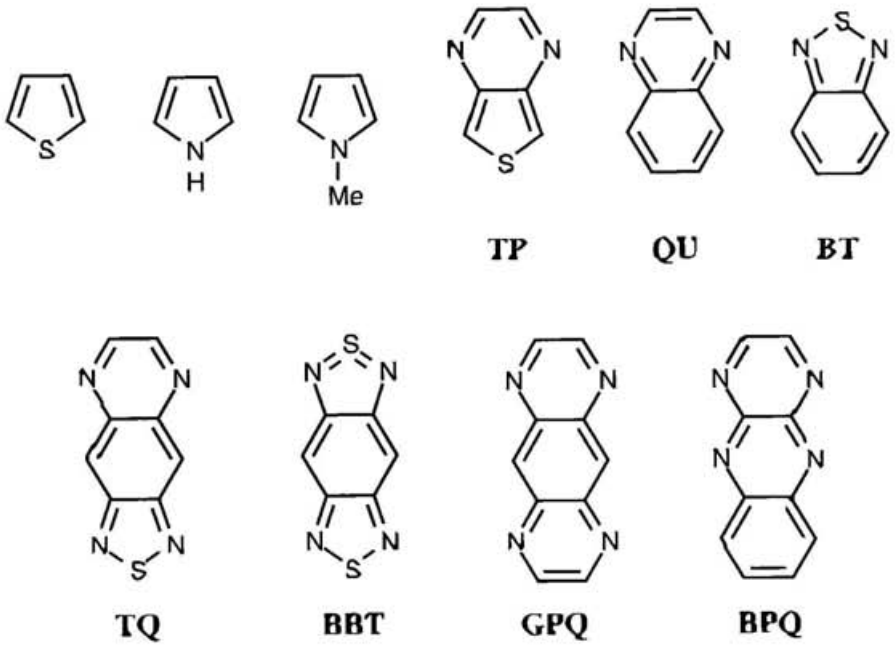


**Table 1.** HOMO and LUMO energies of constituent heterocycles calculated by the PM3 method.

| heterocycle | HOMO / eV | LUMO / eV |
|---|---|---|
| *thiophene* | –9.54 | –0.19 |
| pyrrole | –8.93 | 1.11 |
| *N*-methylpyrrole | –8.87 | 1.08 |
| **TP** | –9.45 | –1.41 |
| **QU** | –9.58 | –0.90 |
| **BT** | –9.63 | –1.81 |
| **TQ** | –9.27 | –2.39 |
| **BBT** | –8.73 | –3.21 |
| **GPQ** | –9.33 | –1.60 |
| **BPQ** | –9.49 | –1.81 |

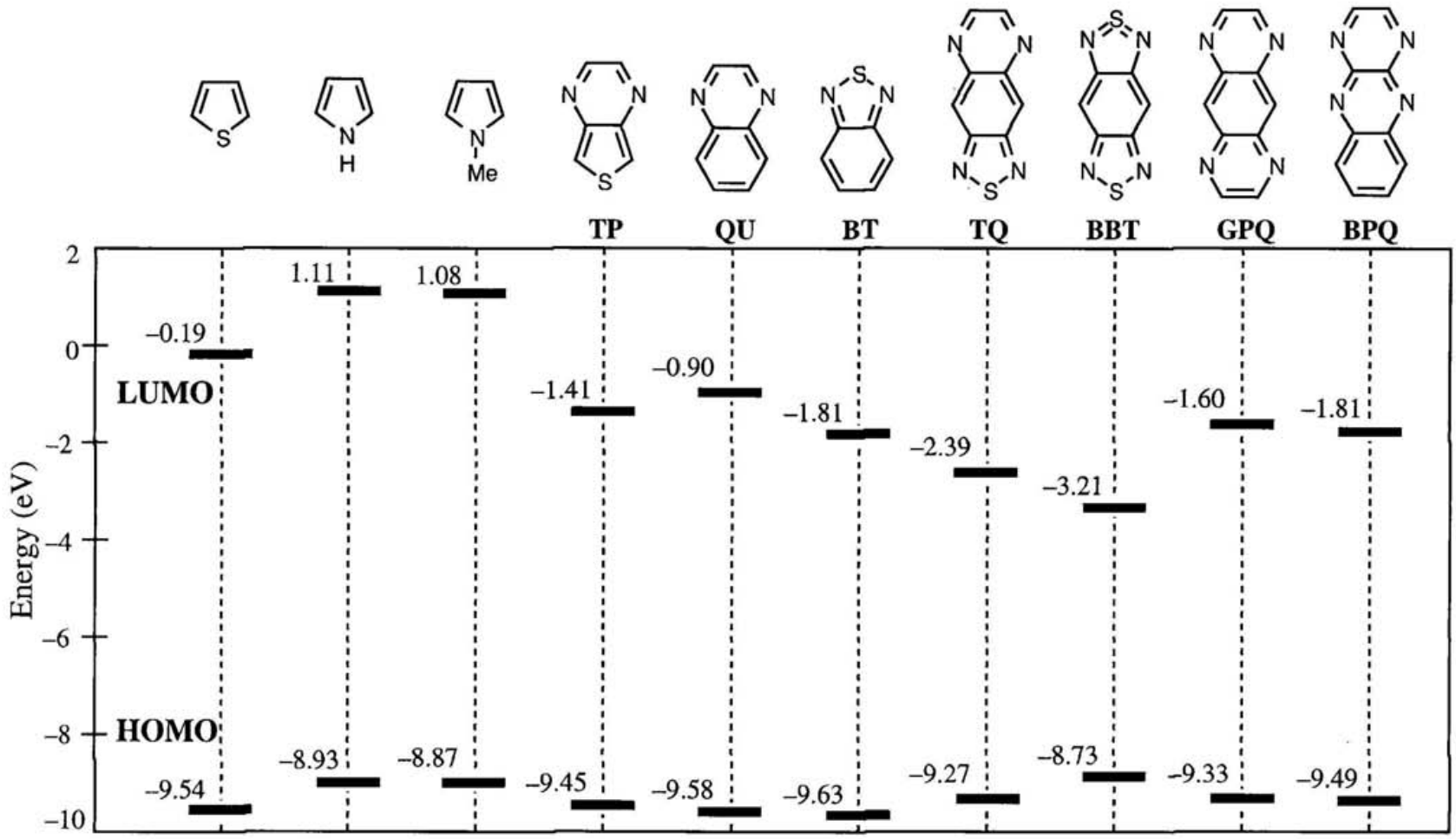


**Figure 1.** Energy diagram of the HOMOs and LUMOs of constituent heterocycles calculated by the PM3 method.

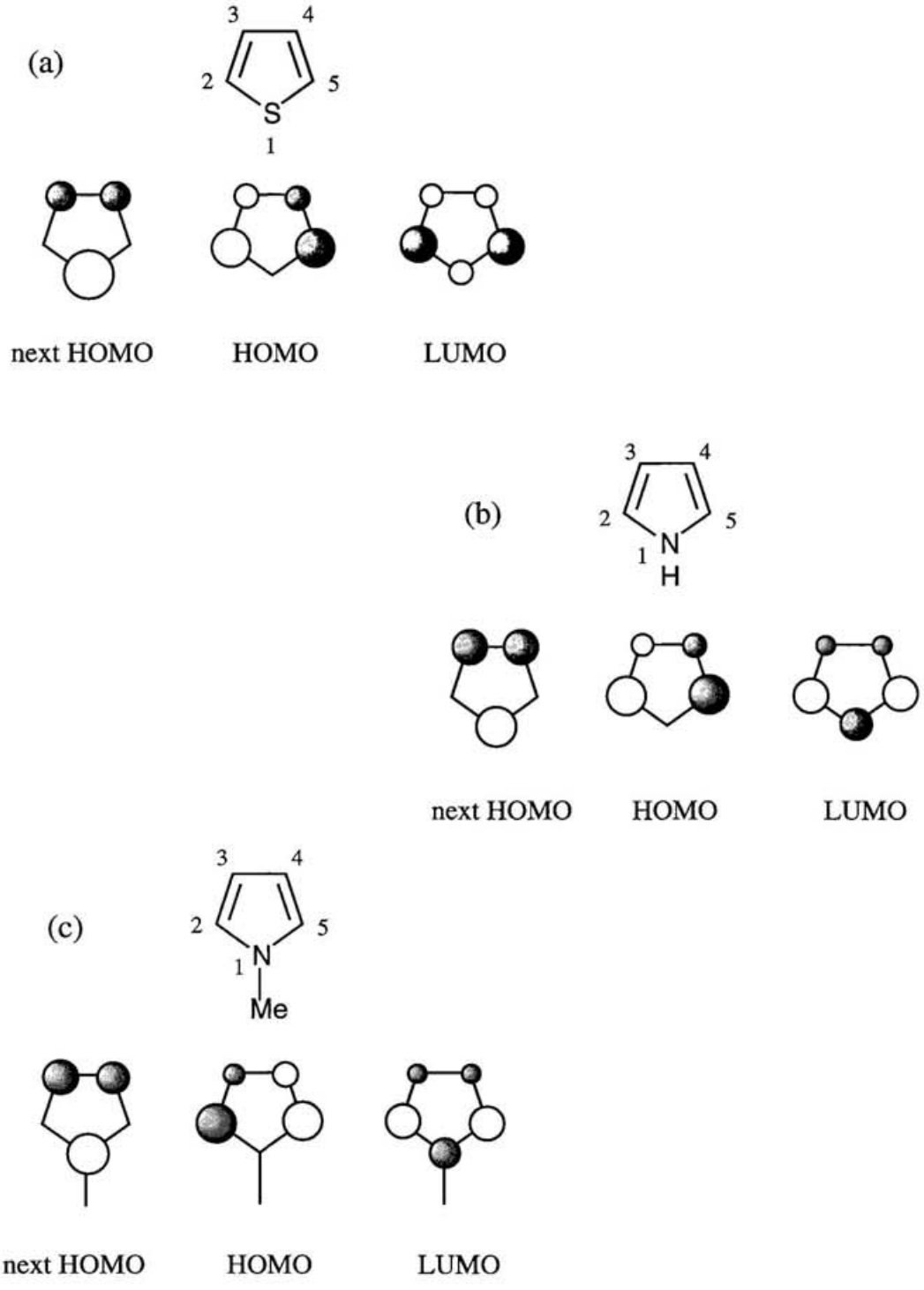


**Figure 2.** Energies and AO composition of the MOs of (a) thiophene, (b) pyrrole, (c) *N*-methylpyrrole, (d) **TP**, (e) **QU**, (f) **BT**, (g) **TQ**, (h) **BBT**, (i) **GPQ**, and (j) **BPQ**. The size of the AO coefficients shows their relative magnitude. Coefficients smaller than 0.15 are not indicated.

(d)

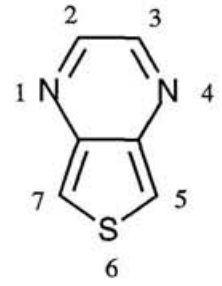


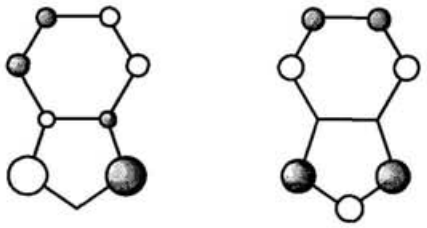

HOMO LUMO

(e)

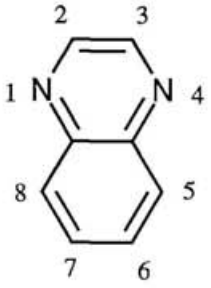


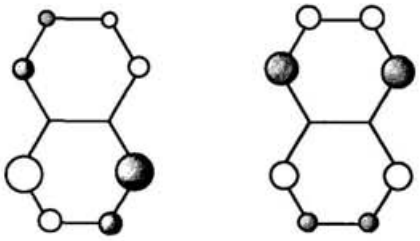

HOMO LUMO

(f)

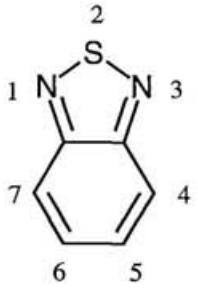


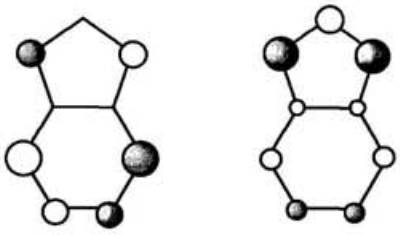

HOMO LUMO

(g)

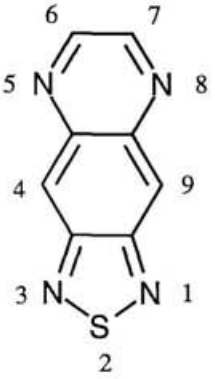


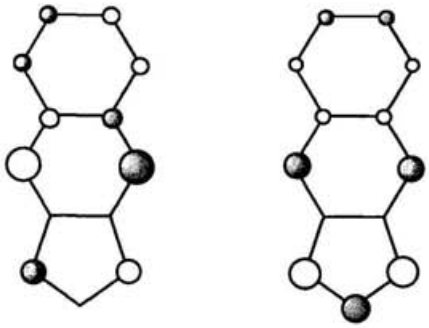

HOMO LUMO

(h)

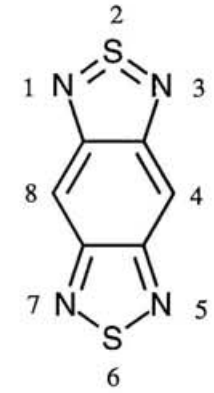


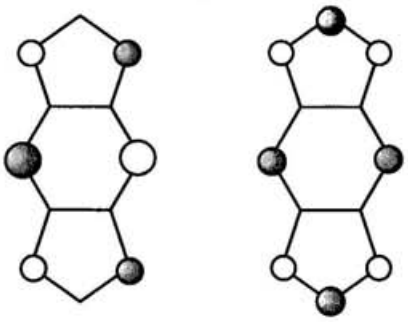

HOMO LUMO

(i)

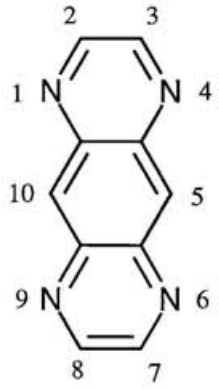


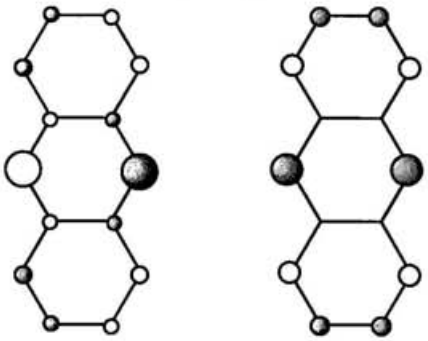

HOMO LUMO

(j)

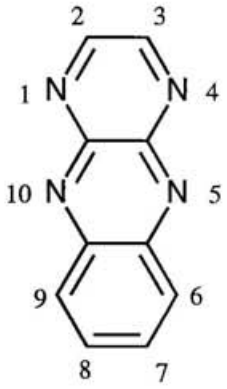


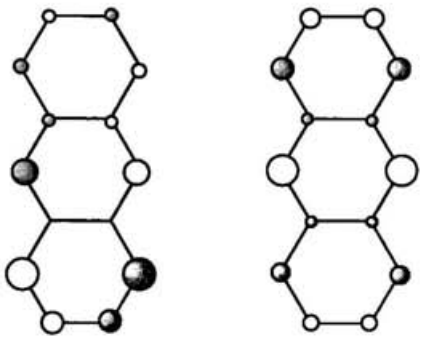

HOMO LUMO

would lead to an effective interaction between adjacent units. Among the *o*-quinoid-acceptor heterocycles, the largest AO coefficients in HOMO of the monomers are situated in the bonding positions (the 5- and 7-positions in **TP**, the 5- and 8-positions in **QU**, the 4- and 7-positions in **BT**, the 4- and 9-positions in **TQ**, the 4- and 8-positions in **BBT**, the 5- and 10-positions in **GPQ**, and the 6- and 9-positions in **BPQ**). On the other hand, the heterocycles with the largest AO coefficients in LUMO at the same positions as those in HOMO are **TP**, **TQ**, **BBT**, and **GPQ**. The bonding positions of **QU**, **BT**, and **BPQ** have the second or third largest AO coefficients, and the places with the largest AO coefficients are the 1- and 4-positions in **QU**, the 1- and 3-positions in **BT**, and the 5- and 9-positions in **BPQ**. This result may bring about the slightly weak interaction between adjacent units.

### 2.2.3 Properties and Structures of Monomers

Physical data of a series of triheterocyclic monomers are summarized in Table 2. The electronic spectra of the monomers **1-9** cover almost all visible regions: **1a-d**, red ($\lambda_{max}$, 500-529 nm); **2a,b**, fluorescent yellow (405-407 nm); **3**, orange (466 nm); **4a-c**, blue (591-604 nm); **5**, blue (702 nm); **6**, orange-red (491 nm); **7**, red (533 nm); **8a,b**, bluish violet (571-572 nm); and **9**, blue (694 nm). The monomer **5** has the longest absorption band among the monomers, indicating the smallest HOMO-LUMO separation, while the monomers **2a,b** has the shortest absorption band, showing the largest HOMO-LUMO separation. Among the monomers **1-7**, the order of decreasing absorption maxima in eV (**2** > **3** > **6** > **1** > **7** > **4** > **5**) corresponds roughly to that of decreasing LUMO energies of *o*-quinoid-acceptor segments in the monomers (**2** > **1** > **6** > **3** = **7** > **4** > **5**) as shown in Figure 3. The monomer **9** displays 8 nm blue shift compared to **BBT** analogue **5**, and the monomers **8** exhibit about 20-30 nm blue shifts compared with **TQ** analogues **4**. These results are contrary to the initial speculation that the more electron-donating pyrrole derivatives have smaller HOMO-LUMO separation than the corresponding thiophene ones. Here it is necessary to take into account the segment conformation in connection with the

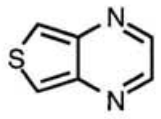

**TP**

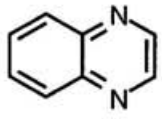

**QU**

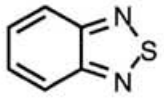

**BT**

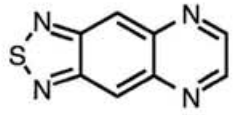

**TQ**

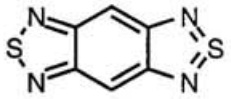

**BBT**

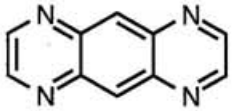

**GPQ**

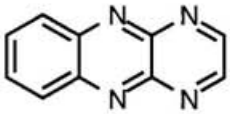

**BPQ**

**Table 2.** Absorption maxima and redox potentials of monomers (A–Q–A) **1-9**.

| monomer | A | Q | $\lambda_{max}$ / nm (eV)[a] | $E_{pa}$ / V[b] | $E_{pc}$ / V[b] | $\Delta E$ / V |
|---|---|---|---|---|---|---|
| **1a** | Th | **TP** | 529(2.35) | 0.97 | –1.05 | 2.02 |
| **1b** | Th | **TP** | 500(2.48) | 0.88 | –1.36 | 2.24 |
| **1c** | Th | **TP** | 502(2.48) | 0.91 | –1.37 | 2.28 |
| **1d** | Th | **TP** | 500(2.48) | 0.86 | –1.37 | 2.23 |
| **2a** | Th | **QU** | 405(3.06) | 1.15 | –1.51 | 2.66 |
| **2b** | Th | **QU** | 407(3.05) | 1.18 | –1.49 | 2.67 |
| **3** | Th | **BT** | 466(2.66) | 1.23 | –1.22 | 2.45 |
| **4a** | Th | **TQ** | 604(2.05) | 0.98 | –0.72 | 1.70 |
| **4b** | Th | **TQ** | 593(2.09) | 1.05 | –0.85 | 1.90 |
| **4c** | Th | **TQ** | 593(2.09) | 1.05 | –0.81 | 1.86 |
| **5** | Th | **BBT** | 702(1.77) | 0.95 | –0.53 | 1.48 |
| **6** | Th | **GPQ** | 491(2.53) | 1.02 | –1.17 | 2.19 |
| **7** | Th | **BPQ** | 533(2.32) | 1.27 | –0.84[c] | 2.11 |
| **8a** | Py | **TQ** | 572(2.17) | 0.86 | –1.03 | 1.89 |
| **8b** | Py | **TQ** | 571(2.17) | 0.88 | –0.99 | 1.87 |
| **9** | Py | **BBT** | 694(1.79) | 0.78 | –0.69 | 1.47 |

$\Delta E = E_{pa}–E_{pc}$, Th = thien-2-yl, Py = *N*-methylpyrrol-2-yl. [a] in $CHCl_3$. [b] 0.1 mol $dm^{-3}$ $Bu_4NClO_4$ in PhCN, Pt electrode, scan rate 100 mV $s^{-1}$, V *vs* SCE. [c] irreversible.

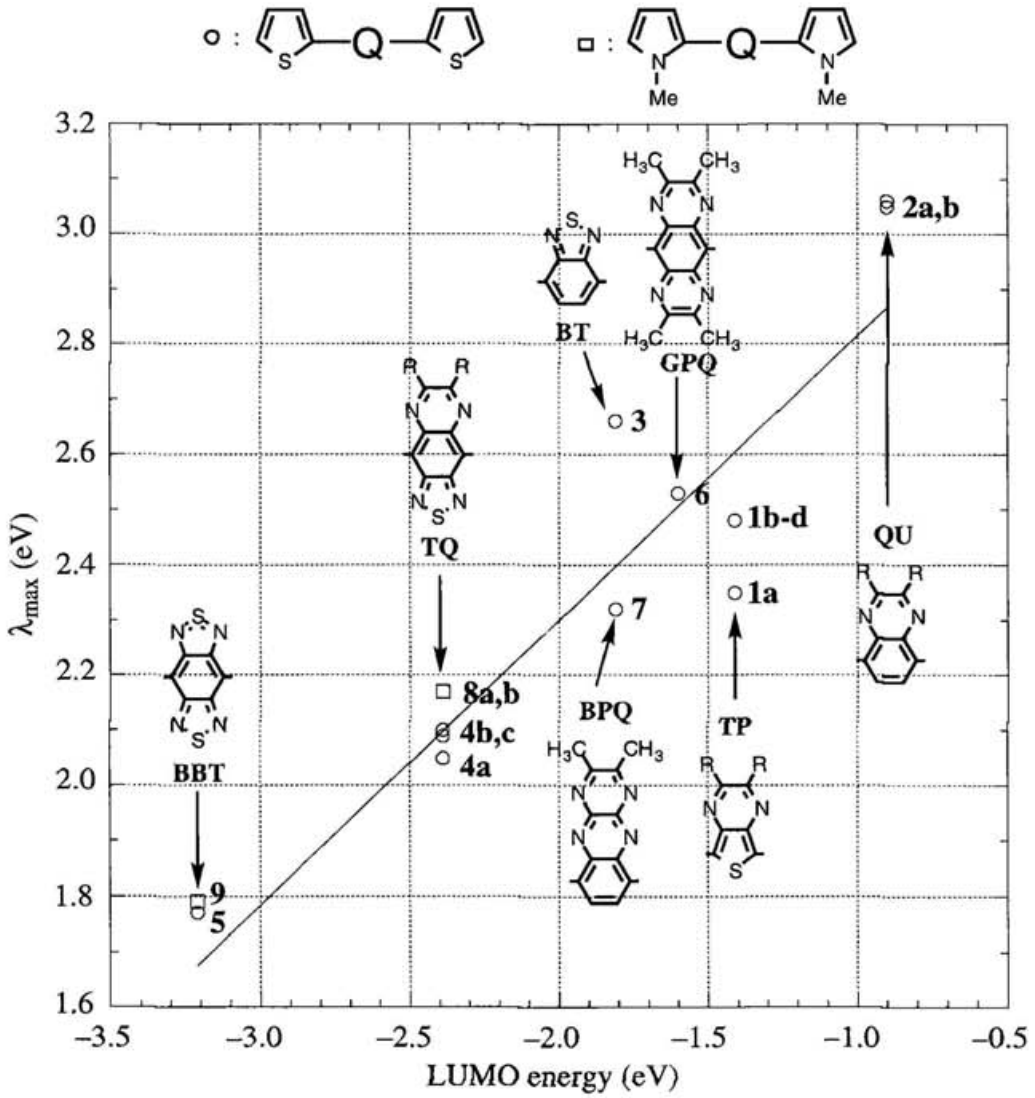


**Figure 3.** Absorption maxima in eV *vs* LUMO energies of *o*-quinoid-acceptor segments. Inserted line: $y = 0.515x + 3.330$, $r = 0.916$.

effective conjugation length.[22,23]

Therefore, the conformations of the monomers were investigated. Since single crystals of **1b**, **2a**, **4c**, and **5** (all thiophene derivatives) were obtained, X-ray crystallographic analyses of the monomers were carried out. The exact solution of the structure was impossible as the molecules crystallize in a statistically disordered way which results from the 180° rotation of thiophene rings.[24] It was observed in the course of the analyses that the bond lengths corresponding to the C–S bonds in thiophene are shorter than usual and those corresponding to the C=C bonds are than longer usual. Thus, the electron density between the S and C atoms in the thiophene rings is averaged. Therefore, the

refinement of the structures was performed in a simple approach with mixed atom scattering factors of the S and C atoms according to the procedure by Hanack.[24] The contribution of the S and C atoms were arbitrarily assigned to minimize *R* factors. For **1b**, one mixed atom with 50% S and 50% C was applied to one thiophene ring. For **2a**, two mixed atoms with 80% S and 20% C, and 20% S and 80% C, respectively, were applied to thiophene rings. For **4c**, as the degree of the disorder was estimated to be small (about 10%), an ordinary solving technique was used. For **5**, two mixed atoms with 75% S and 25% C, and 75% S and 25% C, respectively, were applied to thiophene rings. The results of these analyses afforded unreliable structural parameters such as bond length and bond angle, however, the information on conformation is certain. The molecular structures of **1b**, **2a**, **4c**, and **5** are shown in Figure 4. As can be seen from Figure 4, each molecule exhibits almost planar conformation owing to the absence of the steric hindrance on peripheral positions in *o*-quinoid acceptor rings described above. The dihedral angles of the molecules are 10.3 and 11.3° for **1b**, 11.7 and 3.2° for **2a**, and 8.6 and 1.7° for **4c**, respectively. The molecule **5** possesses perfect planarity. These results indicate that the combination of thiophene and *o*-quinoid-acceptor segments leads to the coplanar geometry, further, maximal extension of π-delocalization. Moreover, all the monomers have smaller intramolecular contacts than the sum of the van der Waals radii such as $D$(C•••N) = 3.25 Å or $D$(S•••N) = 3.50 Å.[25] This finding may be favorable for the coplanarity.

With respect to the other molecules which was not obtained as crystals, conformation analyses were carried out. The geometries of the molecules composed of *o*-quinoid-acceptor and aromatic-donor rings were fully optimized using the MNDO-PM3 method. Figures 5 and 6 display their structures with minima energies. As indicated in Figure 5, theoretical calculations predict that the molecules composed of thiophene and either **BT**, **GPQ**, or **BPQ** have a good planarity similarly to the results of X-ray analyses due to no steric repulsion. On the other hand, concerning the molecules composed of *N*-methylpyrrole and either **TQ** or **BBT**, non-coplanar geometries are inferred from Figure 6. The distortions of dihedral angles of 74.2° between *N*-methylpyrrole and **TQ**, and 58.0° between *N*-methylpyrrole and **BBT** seem to come from the steric interaction between the methyl group of *N*-methylpyrrole

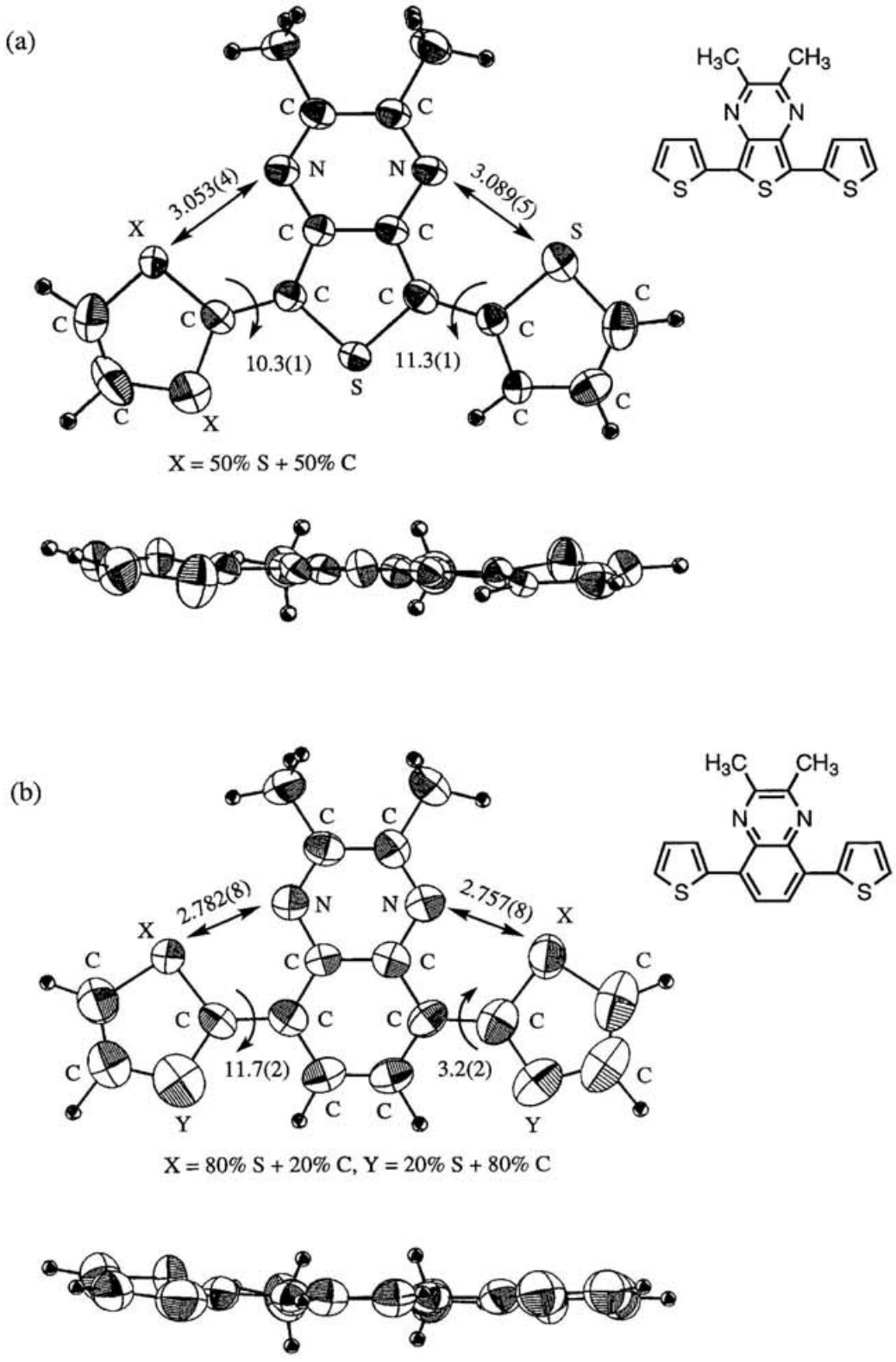


**Figure 4.** Molecular structures of the monomers (a) **1b**, (b) **2a**, (c) **4c**, and (d) **5**, showing top (upper) and side (lower) views.

(c)

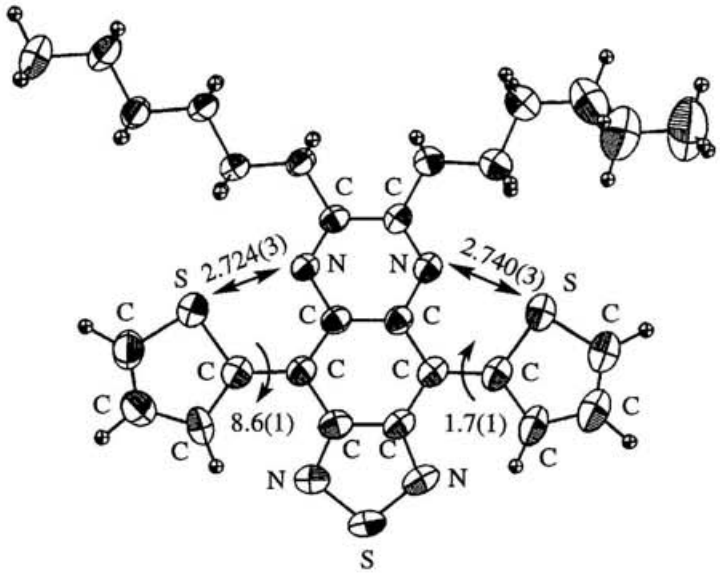


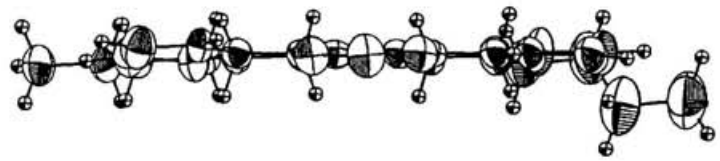

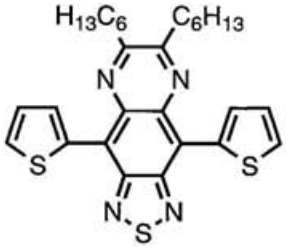


(d)

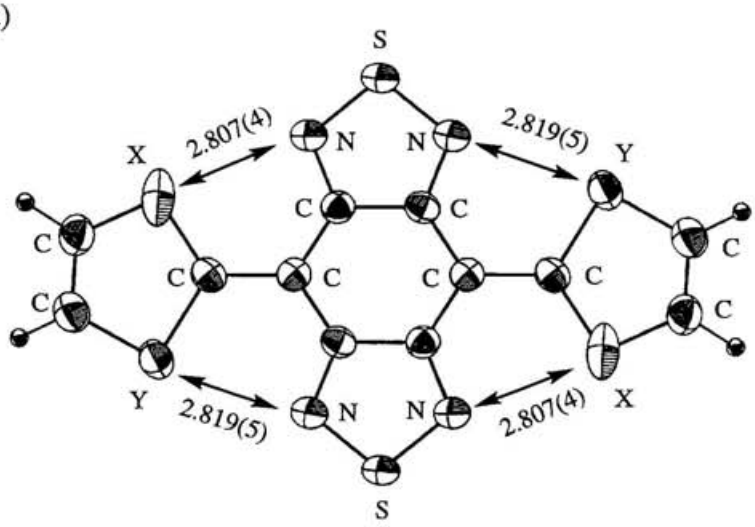


X = 75% S + 25% C, Y = 25% S + 75% C

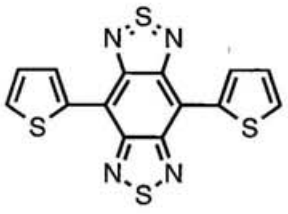

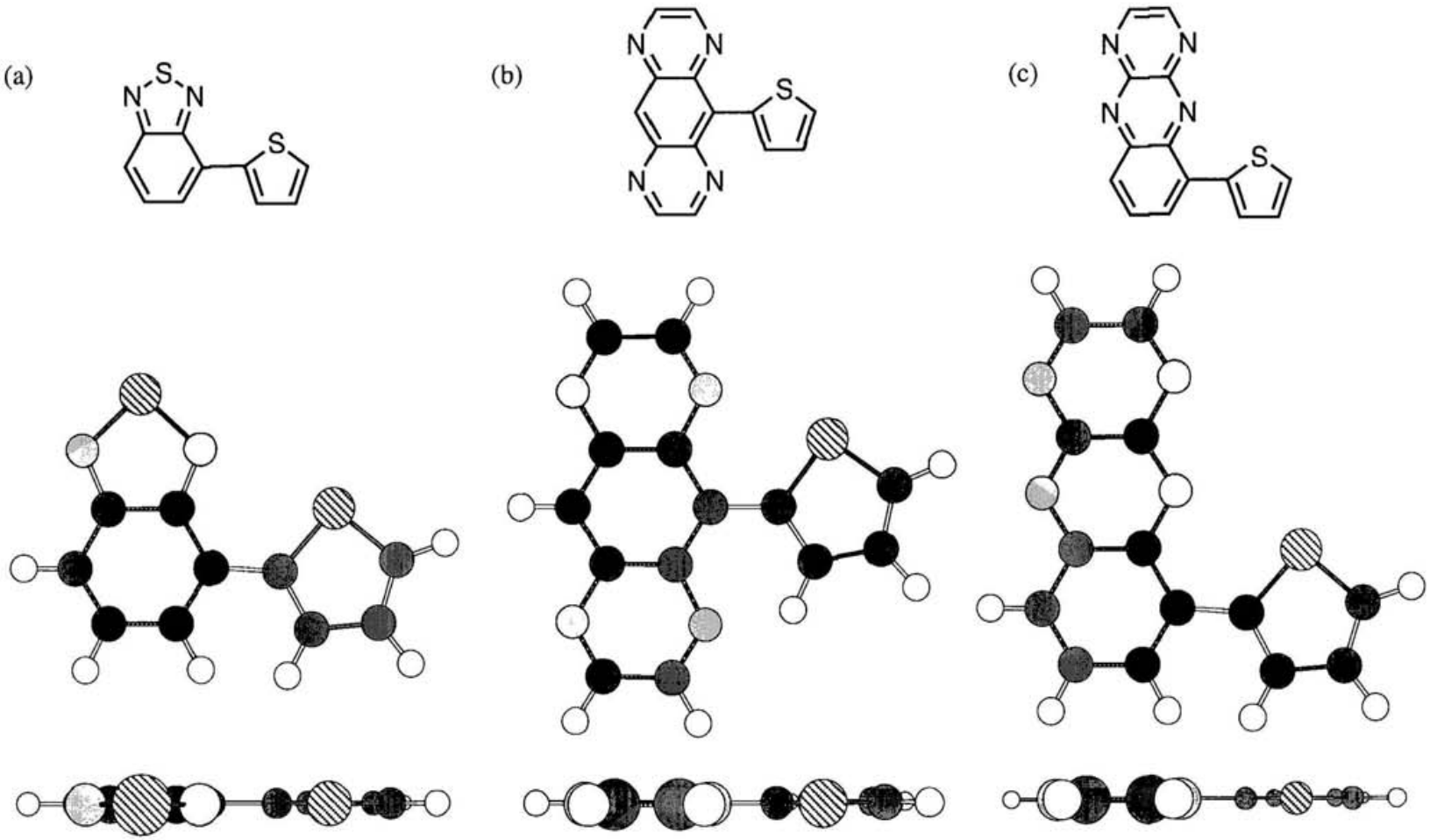


**Figure 5.** PM3-optimized structures composed of o-quinoid-acceptor heterocycles [(a) BT, (b) GPQ and (c) BPQ] and thiophene, showing top (middle) and side (lower) views.

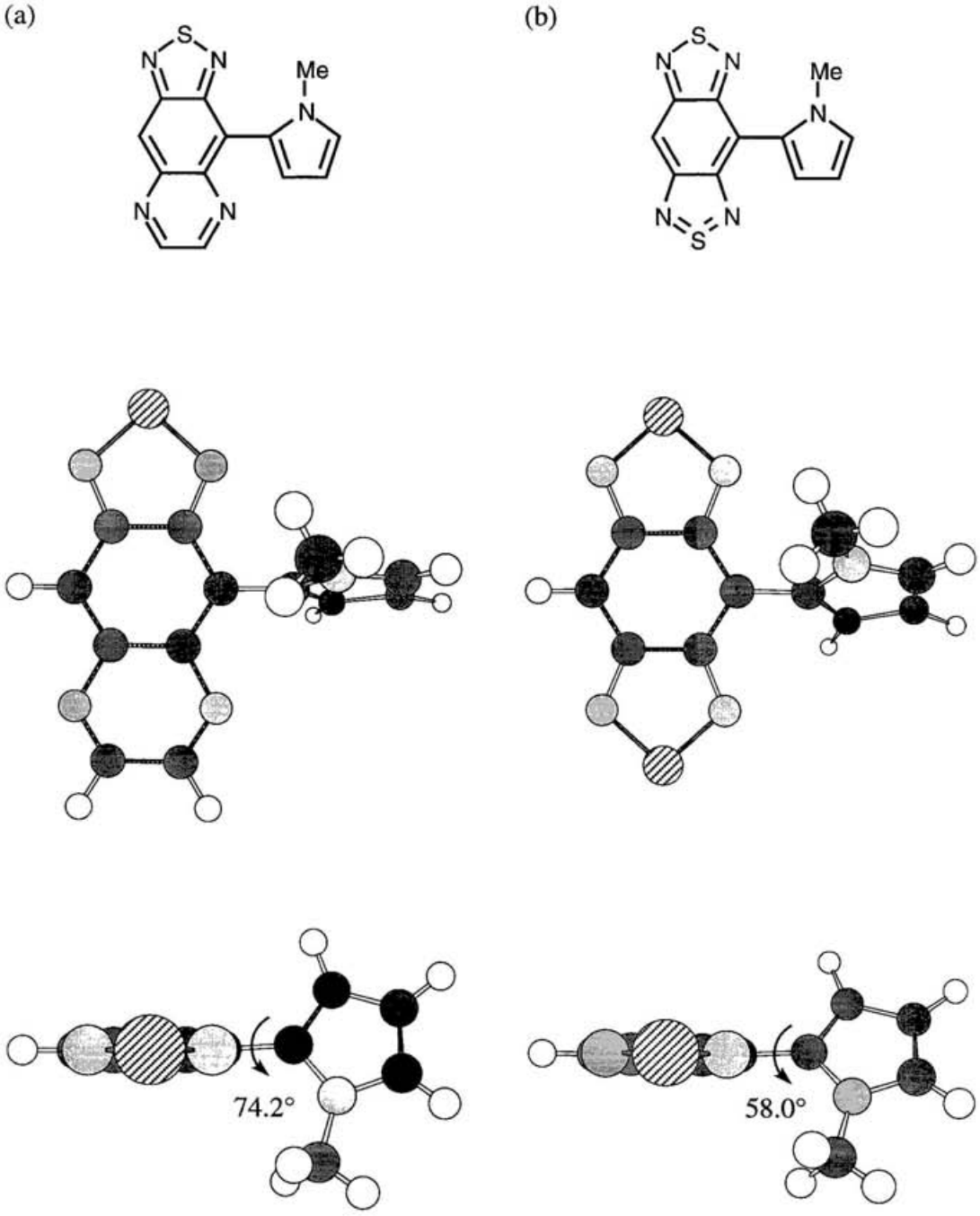


**Figure 6.** PM3-optimized structures composed of *o*-quinoid-acceptor heterocycles [(a) **TQ** and (c) **BBT**] and *N*-methylpyrrole, showing top (middle) and side (lower) views.

and the *o*-quinoid-acceptor units. These conformations would result in the reduction of π-conjugation. Consequently, the absorptions of **8** and **9** are expected to be blue-shifted to those of **4** and **5**. To avoid such nonplanar conformations and manifest the inherent property of pyrrole, the substitution of free pyrrole for *N*-methylpyrrole (**23** and **24**) is required, although the synthesis of free pyrrole derivatives is difficult.

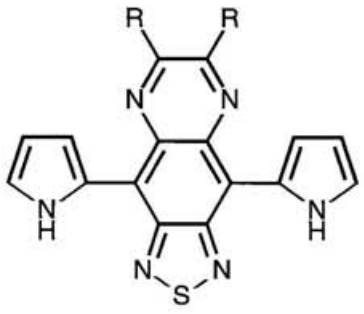

**23**

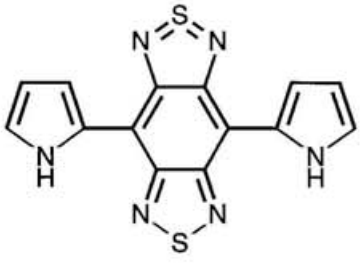

**24**

Cyclic voltammetry measurements on the monomers **1-9** were performed using a Pt disk as a working electrode in PhCN with 0.1 mol $dm^{-3}$ $Bu_4NClO_4$ as a supporting electrolyte. The cyclic voltammograms of the monomers showed both an irreversible oxidation wave and a reversible or quasi-reversible reduction wave (in the case of **7**, an irreversible wave was observed), demonstrating their amphoteric redox property and extended π-system. Their redox peak potentials are summarized in Table 2. The oxidation peak potentials ($E_{pa}$) of the series of monomers vary from 0.78 to 1.23 V *vs* SCE, whereas the reduction peak potentials ($E_{pc}$) are in the range of –0.53 to –1.51 V. This large potential width of the latter indicates that the cathodic peak potentials reflect the wide range of LUMO levels of the *o*-quinoid-acceptor heterocycles. Among the monomers **1-7**, the **BBT** derivative **5** exhibits the highest electron-accepting ability, while the **QU** derivatives **2a,b** show the lowest one. The relative ease of reduction is in the following order: **5 > 4 > 7 > 6 > 3 > 1 > 2**. This order also corresponds approximately to the order of increasing LUMO levels of *o*-quinoid-acceptor heterocycles as shown in Figure 7. As regards *N*-methylpyrrole derivatives **8** and **9**, their anodic peak potentials (0.78-0.86 V) are observed at lower potentials than those of thiophene derivatives **1-7** (0.86-1.23 V), showing that

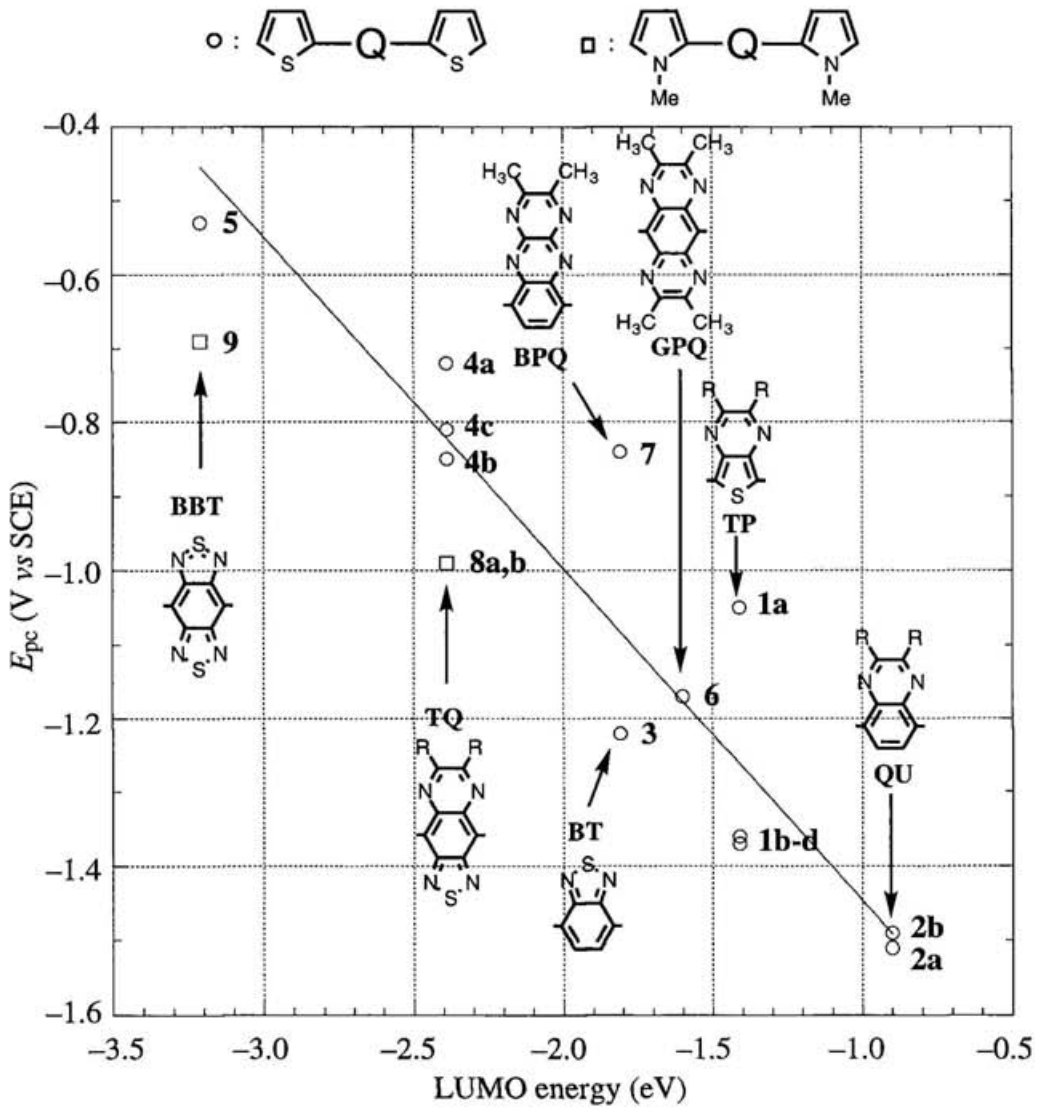


**Figure 7.** Reduction peak potentials of monomers *vs* LUMO energies of *o*-quinoid-acceptor segments. Inserted line: $y = -0.448x + 1.895$, $r = 0.928$.

*N*-methylpyrrole has a slightly higher electron-donating ability than thiophene. This property also explains the fact that the cathodic peak potentials of **8** and **9** are lower than those of **1-7**. The difference between anodic and cathodic potentials ($\Delta E = E_{pa} - E_{pc}$) approximately corresponds to that of HOMO-LUMO separation determined by the absorption maxima as shown in Figure 8. Among the thiophene derivatives **1-7**, **5** has the smallest $\Delta E$ value of 1.48 V and **2** have the largest $\Delta E$ values of 2.66-2.67 V. The order of increasing $\Delta E$ values is **5** < **4** < **7** < **6** < **1** < **3** < **2**. The $\Delta E$ values of the *N*-methylpyrrole derivatives **8** and **9** (1.87-1.89 and 1.47 V, respectively) are comparable to those of the thiophene derivatives **4** and **5** (1.70-1.90 and 1.48 V, respectively), showing that $\Delta E$ is primarily affected by the

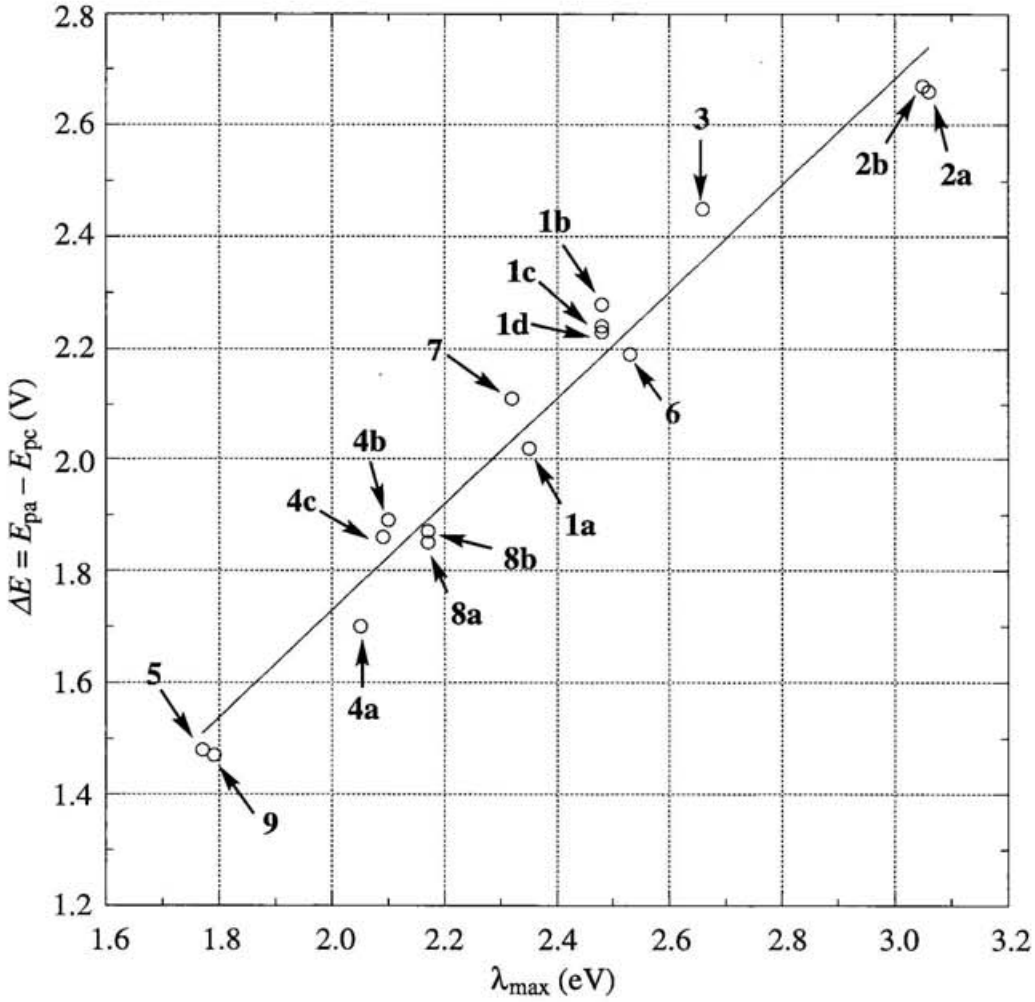


**Figure 8.** The differences between oxidation and reduction peak potentials *vs* absorption maxima in eV. Inserted line: $y = 0.954x - 0.178$, $r = 0.985$.

*o*-quinoid-acceptor moiety. Consequently, these results indicate that the introduction of stronger *o*-quinoid-acceptor heterocycle segment is favorable for reducing HOMO-LUMO separation.

## 2.3 Experimental

**General.** Melting points were measured on a Yanaco MP-500D or a Büchi 535 melting point apparatus and are uncorrected. IR spectra were recorded as KBr pressed pellets on a Perkin-Elmer 1640 FT-IR spectrometer. $^{1}H$ NMR and $^{13}C$ NMR spectra were recorded on a JEOL GX400 FT spectrometer at 400 and 100 MHz, or on a JEOL EX270 FT spectrometer at 270 and 67.8 MHz, respectively. $^{1}H$ chemical shifts ($\delta$) are reported in ppm downfield from tetramethylsilane (TMS), and $^{13}C$ resonances were recorded using the 77.0 ppm $CDCl_3$ resonance of the solvent as an internal reference and are reported in ppm downfield from TMS. UV-vis spectra were recorded on a Shimadzu UV-3101PC spectrometer. Electron impact mass spectra [MS (EI)] were obtained at 70 eV on a Shimadzu QP-1000EX. The *m/z* values listed below are followed by relative intensities given in parentheses. Elemental analyses were carried out on a Yanaco MT-3 CHN corder. High resolution mass determinations (HRMS) were obtained on a Shimadzu Kratos Concept 1s mass spectrometer. Column chromatography was performed on silica gel (Wakogel C-300). All reactions were performed under argon. Tetrahydrofuran (THF) and acetonitrile (MeCN) were distilled under argon from $LiAlH_4$ and $CaH_2$, respectively, prior to use. Pyridine was distilled under argon from NaOH. Benzonitrile (PhCN) was purified under argon by passing through Merck aluminium oxide 90 (neutral, activity I). All other reagents and solvents purchased from Tokyo Kasei, Kanto, Wako, Aldrich, or Merck were used without further purification unless otherwise noted. 2,5-Dibromo-3,4-dinitrothiophene[10] (**10**), 7,8-tetradecanedione,[12] 14,15-octacosanedione,[13] tributyl(thien-2-yl)stannane,[11] tributyl(*N*-methylpyrrol-2-yl)stannane,[20] and dimethyl oxaldiimidate[19] (**19**) were prepared according to literature methods.

**3',4'-Diamino-2,2':5',2''-terthiophene (12).** To a solution of 2,5-dibromo-3,4-dinitrothiophene (**10**) (5.01 g, 15.1 mmol) and tributyl(thien-2-yl)stannane (13.47 g, 36.1 mmol) in THF (100 mL), $PdCl_2(PPh_3)_2$ (108 mg, 1 mol%) was added. The mixture was refluxed for 16 h. After cooling, the reaction mixture was concentrated under reduced

pressure. To the residue hexane was added and then the resulting yellow precipitate was filtered off, washed with hexane and collected. Recrystallization from methanol-toluene gave a dinitro compound (**11**) (2.88 g, 60%), mp 149-151 °C; IR (KBr) 3076, 1541, 1418, 1387, 1305, 706 $cm^{-1}$; $^1H$ NMR (270 MHz, $CDCl_3$) δ 7.17 (dd, *J* = 3.6, 5.3 Hz, 2H), 7.54 (dd, *J* = 1.0, 3.6 Hz, 2H), 7.61 (dd, *J* = 1.0, 5.3 Hz, 2H); UV-vis ($CHCl_3$) $\lambda_{max}$ 379 (sh) nm (log ε 3.90), 310 (4.08), 268 (4.14); MS (EI) *m/z* (relative intensity) 338 ($M^+$, 100), 246 (33), 202 (48). Anal. Calcd for $C_{12}H_6N_2S_3O_4$: C, 42.60; H, 1.79; N, 8.28. Found: C, 42.49; H, 2.04; N, 8.15. The dinitro compound **11** (2.88 g, 9.05 mmol) was suspended in ethanol (30 mL) and concentrated HCl (60 mL). To the mixture a solution of anhydrous $SnCl_2$ (51.19 g, 270 mmol) in EtOH (60 mL) was added. The mixture was stirred at 30 °C for 18 h and poured into a cold 25% NaOH (200 mL). Toluene (100 mL) was added to the above mixture, and then the reaction mixture was shaken vigorously and filtered through Celite. The phases were separated and the aqueous layer was extracted with toluene. The combined organic layer was washed with brine and dried over $Na_2SO_4$. After removal of the solvent under reduced pressure, recrystallization from ethanol afforded the title compound **12** (1.56 g, 62%) as yellowish brown needles, mp 96-96.5 °C; IR (KBr) 3219 (N–H), 3096, 1633, 1531, 1444, 691 $cm^{-1}$; $^1H$ NMR (400 MHz, $CDCl_3$) δ 3.72 (brs, 4H, $NH_2$), 7.05-7.09 (m, 4H), 7.25 (dd, *J* = 1.5, 4.9 Hz, 2H); $^{13}C$ NMR (100 MHz, $CDCl_3$) δ 110.0, 123.9, 124.0, 127.7, 133.6, 135.9; UV-vis ($CHCl_3$) $\lambda_{max}$ 358 nm (log ε 4.25); MS (EI) *m/z* (relative intensity) 278 ($M^+$, 100), 127 (21). Anal. Calcd for $C_{12}H_{10}N_2S_3$: C, 51.77; H, 3.62; N, 10.06. Found: C, 51.69; H, 3.71; N, 9.93.

**General Procedure for the Preparation of 2,3-Dialkyl-5,7-dithien-2-ylthieno[3,4-*b*]pyrazines (1).** A mixture of 0.1-0.2 mmol of diamine **12** and 1.4 equiv of 2,3-dihydroxy-1,4-dioxane (for compound **1a**) or 1.2-2 equiv of 1,2-diketones (diacetyl, 7,8-tetradecanedione, and 14,15-octacosanedione for compounds **1b-d**, respectively) was stirred at 60 °C in MeOH (5-10 mL) for 1 h. After removal of the solvent under reduced pressure, the crude product was purified by column chromatography and recrystallization.

**1a**: yield 52%; reddish purple needles; mp 179-179.5 °C (from hexane); IR (KBr)

3098, 1490, 1354, 1016, 844, 694 $cm^{-1}$; $^1H$ NMR (400 MHz, $CDCl_3$) δ 7.12 (dd, *J* = 3.7, 5.2 Hz, 2H), 7.40 (dd, *J* = 0.9, 5.2 Hz, 2H), 7.63 (dd, *J* = 0.9, 3.7 Hz, 2H), 8.50 (s, 2H); $^{13}C$ NMR (100 MHz, $CDCl_3$) δ 118.1, 118.7, 119.8, 120.4, 127.0, 132.1, 137.3; UV-vis ($CHCl_3$) $\lambda_{max}$ 532 nm (log ε 3.93), 346 (4.25), 300 (4.31); MS (EI) *m/z* (relative intensity) 300 ($M^+$, 100). Anal. Calcd for $C_{14}H_8N_2S_3$: C, 55.97; H, 2.68; N, 9.32. Found: C, 55.75; H, 2.98; N, 9.16.

**1b**: yield 82%; red needles; mp 210-211 °C (from ethanol-toluene); IR (KBr) 3064, 2360, 1495, 1378, 1260, 1228, 694 $cm^{-1}$; $^1H$ NMR (400 MHz, $CDCl_3$) δ 2.67 (s, 6H, $CH_3$), 7.11 (dd, *J* = 3.7, 5.2 Hz, 2H), 7.36 (dd, *J* = 1.2, 5.2 Hz, 2H), 7.63 (dd, *J* = 1.2, 3.7 Hz, 2H); $^{13}C$ NMR (100 MHz, $CDCl_3$) δ 23.7, 123.7, 124.4, 126.0, 127.2, 134.7, 138.0, 153.4; UV-vis ($CHCl_3$) $\lambda_{max}$ 500 nm (log ε 3.99), 343 (4.25), 303 (4.37); MS (EI) *m/z* (relative intensity) 328 ($M^+$, 100), 202 (18), 101 (21). Anal. Calcd for $C_{16}H_{12}N_2S_3$: C, 58.50; H, 3.68; N, 8.53. Found: C, 58.42; H, 3.78; N, 8.61.

**1c**: yield 85%; red fibers; mp 116-116.5 °C (from ethanol); IR (KBr) 2920, 2850, 2362, 1470, 688 $cm^{-1}$; $^1H$ NMR (400 MHz, $CDCl_3$) δ 0.89 (t, *J* = 7.0 Hz, 6H, $CH_2CH_2[CH_2]_3CH_3$), 1.21-1.41 (m, 12H, $CH_2CH_2[CH_2]_3CH_3$), 1.47 (dd, *J* = 6.7, 7.0 Hz, 4H, $CH_2CH_2[CH_2]_3CH_3$), 2.14 (t, *J* = 7.0 Hz, 4H, $CH_2CH_2[CH_2]_3CH_3$), 7.10 (dd, *J* = 3.7, 5.2 Hz, 2H), 7.36 (dd, *J* = 1.2, 5.2 Hz, 2H), 7.61 (dd, *J* = 1.2, 3.7 Hz, 2H); $^{13}C$ NMR(100 MHz, $CDCl_3$) δ 14.2, 22.7, 26.7, 29.1, 31.9, 35.0, 123.5, 123.8, 126.0, 127.0, 135.0, 137.6, 156.2; UV-vis ($CHCl_3$) $\lambda_{max}$ 502 nm (log ε 4.01), 340 (4.24), 305 (4.39); MS (EI) *m/z* (relative intensity) 468 ($M^+$, 100), 398 (34), 355 (28), 328 (29). Anal. Calcd for $C_{26}H_{32}N_2S_3$: C, 66.62; H, 6.88; N, 5.98. Found: C, 66.67; H, 6.87; N, 6.14.

**1d**: yield 75%; red solid; mp 65-67 °C (from ethanol-toluene); IR (KBr) 3067, 2924, 2846, 1470, 1228, 810, 689 $cm^{-1}$; $^1H$ NMR (400 MHz, $CDCl_3$) δ 0.88 (t, *J* = 6.7 Hz, 6H, $CH_2CH_2[CH_2]_{10}CH_3$), 1.20-1.53 (m, 40H, $CH_2CH_2[CH_2]_{10}CH_3$), 1.93 (quintet, *J* = 7.3 Hz, 4H, $CH_2CH_2[CH_2]_{10}CH_3$), 2.85 (t, *J* = 7.3 Hz, 4H, $CH_2CH_2[CH_2]_{10}CH_3$), 7.06 (dd, *J* = 3.7, 5.2 Hz, 2H), 7.32 (dd, *J* = 0.9, 5.2 Hz, 2H), 7.56 (dd, *J* = 0.9, 3.7 Hz, 2H); $^{13}C$ NMR (100 MHz, $CDCl_3$) δ 14.1 ($[CH_2]_{12}CH_3$), 22.7 ($[CH_2]_{11}CH_2CH_3$), 26.7 ($[CH_2]_{10}CH_2C_2H_5$), 29.4 ($[CH_2]_9CH_2C_3H_7$), 29.6

([$CH_2$]$_8$$CH_2C_4H_9$), 29.7 ([$CH_2$]$_2$[$CH_2$]$_6C_5H_{11}$), 31.9 ($CH_2CH_2C_{11}H_{23}$), 35.0 ($CH_2C_{12}H_{25}$), 123.5, 123.8, 126.0, 127.0, 135.0, 137.6, 156.2; UV-vis ($CHCl_3$) $\lambda_{max}$ 500 nm (log ε 4.01), 342 (4.21), 307 (4.36); MS (EI) *m/z* (relative intensity) 664 ($M^+$, 100), 496 (22), 329 (23). Anal. Calcd for $C_{40}H_{60}N_2S_3$: C, 72.23; H, 9.09; N, 4.21. Found: C, 72.30; H, 8.89; N, 4.07.

**4,7-Dithien-2-yl-2,1,3-benzothiadiazole (3).** To a solution of 4,7-dibromo-2,1,3-benzothiadiazole (**13**) (4.05 g, 15.0 mmol) and tributyl(thien-2-yl)stannane (13.47 g, 36.1 mmol) in THF (100 mL), $PdCl_2(PPh_3)_2$ (213 mg, 2 mol%) was added. The mixture was refluxed for 3 h. After removal of the solvent under reduced pressure, the residue was purified by column chromatography on silica gel (eluent: $CH_2Cl_2$/hexane, 1:1). Recrystallization from ethanol-toluene gave the title compound **2** (3.70 g, 82%) as red needles, mp 121-123 °C: IR (KBr) 3096, 1540, 1483, 1423, 1216, 826, 701 $cm^{-1}$; $^1H$ NMR (400 MHz, $CDCl_3$) δ 7.21 (dd, *J* = 3.7, 4.9 Hz, 2H), 7.45 (dd, *J* = 0.9, 4.9 Hz, 2H), 7.86 (s, 2H), 8.11 (dd, *J* = 0.9, 3.7 Hz, 2H); $^{13}C$ NMR (100 MHz, $CDCl_3$) δ 125.8, 126.0, 126.8, 127.5, 128.0, 139.3, 152.6; UV-vis ($CHCl_3$) λmax 446 nm (log ε 4.11), 307 (4.35), 256 (4.12); MS (EI) *m/z* (relative intensity) 300 ($M^+$, 100); Anal. Calcd for $C_{14}H_8N_2S_3$: C, 55.97; H, 2.68; N, 9.32. Found: C, 56.10; H, 2.87; N, 9.31.

**1,2-Diamino-3,6-dithien-2-ylbenzene (14).** A mixture of **3** (300 mg, 1.00 mmol) and zinc dust (1.33 g, 20.3 mmol) in acetic acid (15 mL) was refluxed for 15 min. The reaction mixture was filtered and the residue was washed with $Et_2O$. $Et_2O$ (100 mL) was added to the filtrate and the solution was washed with 5% NaOH and brine. The organic layer was dried over $MgSO_4$. After removal of the solvent under reduced pressure, purification by column chromatography on silica gel (eluent: $CH_2Cl_2$) afforded the title compound **10** (257 mg, 94%) as a pink solid, mp 109-109.5 °C (from ethanol); IR (KBr) 3388 (N–H), 3097, 1630, 1444, 1213, 844, 803, 754, 705 $cm^{-1}$; $^1H$ NMR (400 MHz, $CDCl_3$) δ 3.86 (brs, 4H, $NH_2$), 6.87 (s, 2H), 7.13 (dd, *J* = 3.7, 5.2 Hz, 2H), 7.18 (dd, *J* = 0.9, 3.7 Hz, 2H), 7.36 (dd, *J* = 0.9, 5.2 Hz, 2H); $^{13}C$ NMR (100 MHz, $CDCl_3$) δ

114.0, 114.4, 118.5, 119.0, 120.5, 126.0, 134.0; UV-vis ($CHCl_3$) $\lambda_{max}$ 297 nm (log ε 4.19); MS (EI) *m/z* (relative intensity) 272 ($M^+$, 100), 227 (33). Anal. Calcd for $C_{14}H_{12}N_2S_2$: C, 61.73; H, 4.44; N, 10.28. Found: C, 61.59; H, 4.46; N, 10.22.

**General Procedure for the Preparation of 2,3-Dialkyl-5,8-dithien-2-ylquinoxalines (2).** A mixture of diamine **14** (100 mg, 0.37 mmol) and 1.0-1.5 equiv. of 1,2-diketones (diacetyl and 7,8-tetradecanedione for compounds **2a** and **2b**, respectively) in acetic acid (5 mL) was stirred at room temperature for 10 min. After removal of the solvent under reduced pressure, the residue was purified by column chromatography and recrystallization.

**2a**: yield 89%; yellow needles; mp 237-238 °C (from ethanol); IR (KBr) 3067, 2915, 1474, 1399, 1368, 1226, 832, 696 $cm^{-1}$; $^1H$ NMR (400 MHz, $CDCl_3$) δ 2.81 (s, 6H, $CH_3$), 7.17 (dd, *J* = 3.7, 5.7 Hz, 2H), 7.48 (dd, *J* = 0.6, 5.2 Hz, 2H), 7.85 (dd, *J* = 0.6, 3.7 Hz, 2H), 8.03 (s, 2H); $^{13}C$ NMR (100 MHz, $CDCl_3$) δ 15.7, 119.2, 119.4, 119.6, 121.3, 123.9, 130.5, 132.1, 145.3; UV-vis ($CHCl_3$) $\lambda_{max}$ 405 nm (log ε 4.12), 302 (4.30), 275 (4.45); MS (EI) *m/z* (relative intensity) 322 ($M^+$, 100), 307 (36). Anal. Calcd for $C_{18}H_{14}N_2S_2$: C, 67.05; H, 4.38; N, 8.69. Found: C, 66.09; H, 4.59; N, 8.62.

**2b**: yield 90%; yellow fibers; mp 125-126 °C (from ethanol); IR (KBr) 2924, 2852, 2361, 1468, 1293, 1166, 850, 696 $cm^{-1}$; $^1H$ NMR (400 MHz, $CDCl_3$) δ 0.91 (t, *J* = 7.5 Hz, 6H, $CH_2CH_2[CH_2]_3CH_3$), 1.31-1.46 (m, 12H, $CH_2CH_2[CH_2]_3CH_3$), 2.03 (quintet, *J* = 7.6 Hz, 4H, $CH_2CH_2[CH_2]_3CH_3$), 3.09 (t, *J* = 7.6 Hz, 4H, $CH_2CH_2[CH_2]_3CH_3$), 7.17 (dd, *J* = 3.6, 4.9 Hz, 2H), 7.49 (d, *J* = 4.9 Hz, 2H), 7.84 (d, *J* = 3.6 Hz, 2H), 8.05 (s, 2H); $^{13}C$ NMR (100 MHz, $CDCl_3$) δ 7.1, 15.6, 20.9, 22.3, 24.8, 28.0, 119.0, 119.1, 119.4, 121.3, 123.9, 130.3, 132.1, 148.4; UV-vis ($CHCl_3$) $\lambda_{max}$ 407 nm (log ε 4.10), 277 (4.45); MS (EI) *m/z* (relative intensity) 462 ($M^+$, 59), 392 (100), 322 (64). Anal. Calcd for $C_{28}H_{34}N_2S_2$: C, 72.68; H, 7.41; N, 6.05. Found: C, 72.46; H, 7.33; N, 6.06.

**4,7-Dibromo-5,6-dinitro-2,1,3-benzothiadiazole**[16] **(15).** The compound

was prepared according to the procedure of improved nitration of Coon.[26] To 99% trifluoromethanesulfonic acid (25 g), 94% fuming nitric acid (2.1 mL) was added dropwise. After stirring for 5 min with a powerful stirrer, 4,7-dibromo-2,1,3-benzothiadiazole (**13**) (3.24 g, 12.0 mmol) was added in one portion. The mixture was stirred at 60 °C for 9 h and poured into ice. The resulting yellow solid was extracted with dichloromethane. The extract was washed thoroughly with 20% $Na_2CO_3$ and water, and dried over $MgSO_4$. After removal of the solvent under reduced pressure, recrystallization of the residue from methanol gave the title compound **15** (2.94 g, 64%) as yellow plates, mp 189.5-190.5 °C (lit.[16] mp 202-203.5 °C).

**5,6-Dinitro-4,7-dithien-2-yl-2,1,3-benzothiadiazole (16).** To a solution of 4,7-dibromo-5,6-dinitro-2,1,3-benzothiadiazole (**15**) (3.80 g, 9.9 mmol) and tributyl(thien-2-yl)stannane (8.51 g, 22.8 mmol) in THF (30 mL), $PdCl_2(PPh_3)_2$ (143 mg, 2 mol%) was added. The mixture was refluxed for 3 h. After this was cooled to room temperature, an orange solid appeared. The solid was filtered off, washed with MeCN, and collected. Recrystallization from THF gave the title compound **16** (1.82 g, 47%) as an orange solid, mp 259-260 °C: IR (KBr) 3076, 1541, 1418, 1387, 1305, 706 $cm^{-1}$; $^1H$ NMR (270 MHz, $CDCl_3$) $\delta$ 7.23 (dd, $J$ = 3.6, 5.3 Hz, 2H), 7.52 (dd, $J$ = 1.2, 3.6 Hz, 2H), 7.74 (dd, $J$ = 1.2, 5.3 Hz, 2H); UV-vis ($CHCl_3$) $\lambda_{max}$ 428 nm (log $\varepsilon$ 4.02), 290 (4.23); MS (EI) *m/z* (relative intensity) 390 ($M^+$, 100), 285 (56), 221 (50), 133 (63), 127 (52). Anal. Calcd for $C_{14}H_6N_4O_4S_3$: C, 43.07; H, 1.55; N, 14.35. Found: C, 43.06; H, 1.84; N, 14.05.

**5,6-Diamino-4,7-dithien-2-yl-2,1,3-benzothiadiazole (17).** A mixture of dinitro compound **16** (780 mg, 2.0 mmol) and iron dust (1.33 g, 24.0 mmol) in acetic acid (40 mL) was stirred at 30 °C for 4 h. The reaction mixture was poured into cold 5% NaOH (50 mL) and then a yellow solid appeared. The solution was extracted with $Et_2O$. The organic layer was washed with brine and dried over $Na_2SO_4$. After removal of the solvent under reduced pressure, the residue was purified by column chromatography on silica gel

(eluent: $CH_2Cl_2$). Recrystallization from $CHCl_3$ gave the title compound **17** (383 mg, 58%) as yellow plates, mp 240-242 °C: IR (KBr) 3298 (N–H), 2360, 1622, 1436, 1361, 692 $cm^{-1}$; $^1H$ NMR (400 MHz, $CDCl_3$) δ 4.39 (brs, 4H, $NH_2$), 7.25 (dd, $J$ = 3.7, 5.2 Hz, 2H), 7.36 (dd, $J$ = 1.2, 3.7 Hz, 2H), 7.55 (dd, $J$ = 1.2, 5.2 Hz, 2H); $^{13}C$ NMR (100 MHz, $CDCl_3$) δ 100.1, 120.2, 120.4, 121.5, 128.2, 132.3, 143.9; UV-vis ($CHCl_3$) $\lambda_{max}$ 362 nm (log ε 4.20), 297 (3.98); MS (EI) *m/z* (relative intensity) 330 ($M^+$, 100), 285 (21), 264 (16). Anal. Calcd for $C_{14}H_{10}N_4S_3$: C, 50.89; H, 3.05; N, 16.96. Found: C, 50.79; H, 3.11; N, 16.90.

**General Procedure for the Preparation of 6,7-Dialkyl-4,9-dithien-2-yl[1,2,5]thiadiazolo[3,4-*g*]quinoxalines (4).** A mixture of 0.1-0.2 mmol of diamine **17** and 1.4 equiv of 2,3-dihydroxy-1,4-dioxane (for compound **4a**) or 1.6-2.0 equiv of 1,2-diketones (diacetyl and 7,8-tetradecanedione for compound **4b** and **4c**, respectively) in acetic acid was stirred at 60 °C for 10 min. After removal of the solvent under reduced pressure, the residue was purified by column chromatography and recrystallization.

**4a**: yield 50%; blue solid; mp 253-255 °C (from ethanol-toluene); IR (KBr) 2362, 1440, 1228, 908, 706 $cm^{-1}$; $^1H$ NMR (270 MHz, $CDCl_3$) δ 7.32 (dd, $J$ = 4.0, 5.0 Hz, 2H), 7.70 (dd, $J$ = 1.0, 5.0 Hz, 2H), 8.87 (dd, $J$ = 1.0, 4.0 Hz, 2H), 8.98 (s, 2H); UV-vis ($CHCl_3$) $\lambda_{max}$ 606 nm (log ε 4.01), 322 (4.38); MS (EI) *m/z* (relative intensity) 352 ($M^+$, 100), 307 (23). Anal. Calcd for $C_{16}H_8N_4S_3$: C, 54.53; H, 2.29; N, 15.90. Found: C, 54.79; H, 2.58; N, 15.79.

**4b**: yield 82%; blue needles; mp 257-259 °C (from ethanol-toluene); IR (KBr) 1447, 1427, 1364, 1230, 829, 702 $cm^{-1}$; $^1H$ NMR (400 MHz, $CDCl_3$) δ 2.83 (s, 6H, $CH_3$), 7.30 (dd, $J$ = 4.0, 5.0 Hz, 2H), 7.64 (dd $J$ = 0.6, 5.2 Hz, 2H), 8.98 (dd, $J$ = 0.6, 4.0 Hz, 2H); UV-vis ($CHCl_3$) $\lambda_{max}$ 591 nm (log ε 4.06), 320 (4.08), 285 (4.19); MS (EI) *m/z* (relative intensity) 380 ($M^+$, 100), 365 (40), 347 (34). Anal. Calcd for $C_{28}H_{32}N_4S_3$: C, 64.15; H, 4.85; N, 22.44. Found: C, 64.19; H, 5.10; N, 22.43.

**4c**: yield 75%; blue needles; mp 114-115 °C (from ethanol); IR (KBr) 2948, 1442,

1421, 1230, 833, 707 $cm^{-1}$; $^1H$ NMR (400 MHz, $CDCl_3$) δ 0.92 (t, $J$ = 7.3 Hz, 6H, $CH_2CH_2[CH_2]_3CH_3$), 1.35-1.58 (m, 12H, $CH_2CH_2[CH_2]_3CH_3$), 2.07 (quintet, $J$ = 7.6 Hz, 4H, $CH_2CH_2[CH_2]_3CH_3$), 3.14 (t, $J$ = 7.6 Hz, 4H, $CH_2CH_2[CH_2]_3CH_3$), 7.31 (dd, $J$ = 4.0, 5.2 Hz, 2H), 7.65 (dd $J$ = 0.6, 5.2 Hz, 2H), 8.98 (dd, $J$ = 0.6, 4.0 Hz, 2H); $^{13}C$ NMR (100 MHz, $CDCl_3$) δ 14.1, 22.6, 27.9, 29.3, 31.8, 35.4, 126.5, 130.6, 132.6, 135.1, 135.8, 151.4, 152.8, 157.3; UV-vis ($CHCl_3$) $\lambda_{max}$ 593 nm (log ε 4.07), 319 (4.46), 282 (4.55); MS (EI) *m/z* (relative intensity) 520 ($M^+$, 100), 450 (51), 435 (26), 381 (44). Anal. Calcd for $C_{28}H_{32}N_4S_3$: C, 64.58; H, 6.19; N, 10.76. Found: C, 64.52; H, 6.08; N, 10.60.

**4,8-Dithien-2-yl-2λ$^4$δ$^2$-benzo[1,2-*c*;4,5-*c*']bis[1,2,5]thiadiazole (5).** A mixture of diamine **17** (996 mg, 3.0 mmol), *N*-sulfinylaniline (848 mg, 6.0 mmol), and chlorotrimethylsilane (592 mg, 5.4 mmol) in pyridine (15 mL) was stirred at 80 °C for 24 h. To the reaction solution tetrachloromethane (50 mL) was added, and the resulting solid was filtered off and collected. The solid was sublimed at 300 °C/0.05 Torr to give blue crystals of **5** (880 mg, 82%), mp 334-336 °C: IR (KBr) 1445, 1422, 1174, 849, 689 $cm^{-1}$; UV-vis ($CHCl_3$) $\lambda_{max}$ 706 nm (log ε 4.07), 336 (4.53); MS (EI) *m/z* (relative intensity) 358 ($M^+$, 100), 147 (16). Anal. Calcd for $C_{14}H_6N_4S_4$: C, 46.92; H, 1.69; N, 15.65. Found: C, 47.18; H, 1.99; N, 15.73.

**2,3,7,8-Tetramethyl-5,10-dithien-2-ylpyrazino[2,3-*g*]quinoxaline (6).** A mixture of dinitrobenzothiadiazole **16** (197 mg, 0.51 mmol) and zinc dust (693 mg, 10.6 mmol) in acetic acid (5 mL) was stirred at 60 °C for 1 h until the reaction mixture turned white. After cooling to rt, diacetyl (0.35 g, 4.1 mmol) was added to the solution and the mixture was stirred for 1 h. After removal of the solvent under reduced pressure, the residue was purified by column chromatography on silica gel (eluent: $CH_2Cl_2$). Recrystallization from THF gave the title compound **6** (108 mg, 53%) as an orange-red solid, mp 175-176 °C (decomp.); IR (KBr) 3064, 1602, 1410, 1361, 1316, 1190, 827, 695 $cm^{-1}$; $^1H$ NMR (270 MHz, $CDCl_3$) δ 5.23 (s, 12H, $CH_3$), 7.29 (dd, $J$ = 4.0, 5.3 Hz, 2H), 7.65 (dd, $J$ = 1.0,

5.3 Hz, 2H), 8.38 (dd, $J$ = 1.0, 4.0 Hz, 2H); UV-vis ($CHCl_3$) $\lambda_{max}$ 491 nm (log ε 3.96), 385 (3.85), 294 (4.72); MS (EI) *m/z* (relative intensity) 402 ($M^+$, 100), 387 (38), 369 (33). Anal. Calcd for $C_{22}H_{18}N_4S_2$: C, 65.65; H, 4.51; N, 13.92. Found; C, 65.71; H, 4.57; N 13.82.

**2,3-Diamino-5,8-dithien-2-ylquinoxaline (20).** A mixture of dimethyl oxaldiimidate (**19**) (228 mg, 2.0 mmol) and diamine **14** in methanol (5.0 mL) was stirred at 50 °C. After 10 min, acetic acid (0.5 mL) was added to the solution and the mixture was stirred for 1 h additionally. After removal of the solvent under reduced pressure, the residue was purified twice by column chromatography on silica gel (eluent: toluene/ethyl acetate, 2:1 and $CH_2Cl_2$). Recrystallization from toluene afforded the title compound **20** (187 mg, 58%) as yellow needles, mp 243 °C (decomp.); IR (KBr) 3305 (N–H), 1643, 1487, 1312, 851, 811, 696 $cm^{-1}$; $^1H$ NMR (270 MHz, $CDCl_3$) δ 4.72 (brs, 4H, N$H_2$), 7.14 (dd, $J$ = 3.6, 5.3 Hz, 2H), 7.41 (dd, $J$ = 0.7, 5.3 Hz, 2H), 7.73 (dd, $J$ = 0.7, 3.6 Hz, 2H); UV-vis ($CHCl_3$) $\lambda_{max}$ 369 nm (log ε 4.32), 286 (4.38); MS (EI) *m/z* (relative intensity) 324 ($M^+$, 100), 291 (10). Anal. Calcd for $C_{16}H_{12}N_4S_2$: C, 59.24; H, 3.73; N, 17.27. Found C, 59.39; H, 3.85; N, 17.23.

**2,3-Dimethyl-6,9-dithien-2-ylpyrazino[2,3-*b*]quinoxaline (7).** A mixture of diamine **20** (65 mg, 0.20 mmol) and diacetyl (34 mg, 0.40 mmol) in acetic acid (3 mL) was stirred at room temperature for 10 min. After removal of the solvent under reduced pressure, recrystallization from THF gave the title compound **7** (64 mg, 86%) as a red solid, mp 280 °C (decomp.); IR (KBr) 3057, 1474, 1421, 1391, 1254, 733 $cm^{-1}$; $^1H$ NMR (270 MHz, $CDCl_3$) δ 2.97 (s, 6H, C$H_3$), 7.21-7.23 (m, 2H), 7.55 (dd, $J$ = 1.0, 5.3 Hz, 2H), 8.02 (dd, $J$ = 1.0, 3.6 Hz, 2H), 8.28 (s, 2H); UV-vis ($CHCl_3$) $\lambda_{max}$ 533 nm (log ε 3.64), 384 (4.13), 308 (4.56); MS (EI) *m/z* (relative intensity) 374 ($M^+$, 100), 329 (23), 291 (19). Anal. Calcd for $C_{20}H_{14}N_4S_2$: C, 64.15; H, 3.77; N, 14.96. Found; C, 63.90; H, 3.99; N, 14.82.

**5,6-Diamino-4,7-bis(*N*-methylpyrrol-2-yl)-2,1,3-benzothiadiazole (22).** According to the same procedures for the preparation of **16** and **17**, the reaction with 4,7-dibromo-5,6-dinitro-2,1,3-benzothiadiazole (**15**) (2.69 g, 7.0 mmol), tributyl(*N*-methylpyrrol-2-yl)stannane (5.75 g, 15.5 mmol), $PdCl_2(PPh_3)_2$ (98 mg, 2 mol%), and THF (20 mL), followed by reduction with iron dust (4.66 g, 81.8 mmol) in acetic acid (100 mL) afforded the title compound **22** (1.66 g, 73%) as a yellow solid, mp 186 °C (decomp.); IR (KBr) 3322 (N–H), 2940, 1623, 1475, 1444, 1303, 735 $cm^{-1}$; $^1H$ NMR (400 MHz, $CDCl_3$) δ 3.46 (s, 4H, $CH_2H$), 3.47 (s, 2H, $CH_2H$), 4.29 (brs, 4H, $NH_2$), 6.33–6.36 (m, 4H), 6.88 (dd, $J$ = 1.8, 2.1 Hz, 2H); $^{13}C$ NMR (100 MHz, $CDCl_3$) δ 34.9, 105.6, 108.3, 110.0, 123.8, 125.5, 140.7, 151.3; UV-vis ($CHCl_3$) $\lambda_{max}$ 364 nm (log ε 4.14); MS (EI) *m/z* (relative intensity) 324 ($M^+$, 100), 282 (21); HRMS (EI) Calcd for $C_{16}H_{16}N_6S$ 324.1157, Found 324.1159.

**General Procedure for the Preparation of 6,7-Dialkyl-4,9-bis(*N*-methylpyrrol-2-yl)[1,2,5]thiadiazolo[3,4-*g*]quinoxalines (8).** According to the same procedure for the preparation of **4**, the title compounds **8** were synthesized from 0.1-0.2 mmol of diamine **22** and 1.5-2.0 equiv of 1,2-diketones (diacetyl and 7,8-tetradecanedione for compound **8a** and **8b**, respectively).

**8a**: yield 62%; bluish violet solid; mp 211-213 °C (decomp.) (from ethanol); IR (KBr) 3099, 2942, 1546, 1480, 1390, 1279, 850, 711 $cm^{-1}$; $^1H$ NMR (400 MHz, $CDCl_3$) δ 2.72 (s, 6H, $CH_3$), 3.57 (s, 6H, $NCH_3$), 6.47 (dd, $J$ = 2.1, 3.7 Hz, 2H), 6.66 (dd, $J$ = 1.8, 3.7 Hz, 2H), 6.98 (dd, $J$ = 1.8, 2.1 Hz, 2H); $^{13}C$ NMR (100 MHz, $CDCl_3$) δ 23.8 ($CH_3$), 36.1 ($NCH_3$), 108.5, 114.2, 121.6, 124.9, 127.5, 137.2, 153.5, 154.9; UV-vis ($CHCl_3$) $\lambda_{max}$ 572 nm (log ε 3.90), 369 (4.02), 356 (4.02); MS (EI) *m/z* (relative intensity) 374 ($M^+$, 100), 332 (28). Anal. Calcd for $C_{20}H_{18}N_6S$: C, 64.15; H, 4.85; N, 22.44. Found: C, 64.19; H, 5.10; N, 22.43.

**8b**: yield 59%; bluish violet solid; mp 109-110 °C (from ethanol); IR (KBr) 3097, 2923, 2855, 1546, 1487, 1460, 1279, 712 $cm^{-1}$; $^1H$ NMR (400 MHz, $CDCl_3$) δ 0.90 (t, $J$ = 7.0 Hz, 6H, $CH_2CH_2[CH_2]_3CH_3$), 1.27-1.49 (m, 12H, $CH_2CH_2[CH_2]_3CH_3$), 1.82

(quintet, $J$ = 7.6 Hz, 4H, $CH_2CH_2[CH_2]_3CH_3$), 2.97 (t, $J$ = 7.6 Hz, 4H, $CH_2CH_2[CH_2]_3CH_3$), 3.56 (s, 6H, $NCH_3$), 6.45 (dd, $J$ = 2.1, 3.6 Hz, 2H), 6.63 (dd, $J$ = 1.5, 3.6 Hz, 2H), 6.97 (dd, $J$ = 1.8, 2.1 Hz, 2H); $^{13}C$ NMR (100 MHz, $CDCl_3$) δ 14.1, 22.6, 27.4, 29.3, 31.7, 35.5, 36.0 ($NCH_3$), 108.4, 114.0, 121.6, 124.5, 127.5, 137.6, 153.5, 157.9; UV-vis ($CHCl_3$) $\lambda_{max}$ 571 nm (log ε 3.90), 371 (4.09), 357 (4.07); MS (EI) *m/z* (relative intensity) 514 ($M^+$, 88), 444 (21), 280 (30), 107 (100). Anal. Calcd for $C_{28}H_{32}N_4S_3$: C, 70.00; H, 7.44; N, 16.33. Found: C, 70.28; H, 7.37; N, 16.19.

**4,8-Bis(*N*-methylpyrrol-2-yl)-2λ$^4$δ$^2$-benzo[1,2-*c*;4,5-*c*']bis[1,2,5]-thiadiazole (9).** According to the same procedure for the preparation of **5**, the title compound **9** was synthesized from diamine **22** (246 mg, 0.76 mmol), *N*-sulfinylaniline (457 mg, 3.3 mmol), chlorotrimethylsilane (163 mg, 1.5 mmol), and pyridine (2 mL) as a blue solid: yield 28%; mp 279-280 °C (from toluene-$CH_2Cl_2$); IR (KBr) 3096, 2945, 1539, 1464, 1058, 838, 725, 604 $cm^{-1}$; $^1H$ NMR (400 MHz, $CDCl_3$) δ 3.72 (s, 6H, $CH_3$), 6.47 (dd, $J$ = 2.7, 4.0 Hz, 2H), 6.83 (dd, $J$ = 1.8, 4.0 Hz, 2H), 7.02 (dd, $J$ = 1.8, 2.7 Hz, 2H); $^{13}C$ NMR (100 MHz, $CDCl_3$) δ 36.5, 109.5, 113.2, 115.5, 126.5, 126.6, 127.9, 153.0; UV-vis ($CHCl_3$) $\lambda_{max}$ 694 nm (log ε 4.06), 353 (4.44), 300 (4.33), 261 (4.24); MS (EI) *m/z* (relative intensity) 352 ($M^+$, 100). Anal. Calcd for $C_{16}H_{12}N_6S_2$: C, 54.53; H, 3.43; N, 23.85. Found; C, 54.42; H, 3.64; 23.64.

**Computational Method.** The energy level of each heterocyclic segment and the geometries of monomers were calculated by using the MNDO-PM3 method in the MOPAC 6.1 program.[21] These calculations were performed with the Sony-Tektronix CAChe system.

**X-ray Structure Analyses.** The crystals for the data collections were prepared by slow evaporation of the solvents used for recrystallization (chloroform for **1b**, hexane for **2a**, ethanol/hexane for **4c**, and tetrachloromethane for **5**). An Enraf-Nonius CAD4 diffractometer (40 kV, 32 mA) was used with graphite-monochromated Cu *K*α radiation (λ

= 1.5418 Å), $\theta/2\theta$ scan technique. The atomic parameters and bond lengths and angles are presented at the end of this chapter. A compilation of the crystal data and experimental details are given in Table 3. Cell parameters were determined from least-squares procedures on 25 reflections ($44° < 2\theta < 50°$). No significant variation was observed in intensities of

**Table 3.** Crystal Data for Compounds **1b**, **2a**, **4c**, and **5**.

| compd | **1b** | **2a** | **4c** | **5** |
|---|---|---|---|---|
| formula | $C_{16}H_{12}N_2S_3$ | $C_{18}H_{14}N_2S_2$ | $C_{28}H_{32}N_4S_3$ | $C_{14}H_6N_4S_4$ |
| formula wt | 328.46 | 322.45 | 520.77 | 358.47 |
| cryst syst | orthorhombic | monoclinic | triclinic | monoclinic |
| space group | $P2_12_12_1$ | $P2_1/a$ | $P\bar{1}$ | $P2_1/n$ |
| $a$, Å | 5.689(1) | 6.337(3) | 11.717(4) | 17.393(8) |
| $b$, Å | 8.084(1) | 20.570(3) | 16.005(4) | 4.818(2) |
| $c$, Å | 32.842(2) | 12.007(4) | 7.552(3) | 8.345(4) |
| $\alpha$, deg | 90.0 | 90.0 | 92.04(2) | 90.0 |
| $\beta$, deg | 90.0 | 99.69(2) | 104.46(2) | 99.17(2) |
| $\gamma$, deg | 90.0 | 90.0 | 97.63(2) | 90.0 |
| $V$, Å$^3$ | 1510.4(2) | 1542.9(10) | 1342.2(8) | 690.3(6) |
| $Z$ | 4 | 4 | 2 | 2 |
| cryst size, mm | 0.35 × 0.04 × 0.03 | 0.45 × 0.10 × 0.05 | 0.45 × 0.15 × 0.10 | 0.25 × 0.10 × 0.05 |
| $d_{calcd}$, g cm$^{-3}$ | 1.45 | 1.39 | 1.29 | 1.72 |
| radiation | Cu $K\alpha$ | Cu $K\alpha$ | Cu $K\alpha$ | Cu $K\alpha$ |
| $2\theta_{max}$, deg | 1, 70 | 1, 70 | 1, 70 | 1, 70 |
| obsd unique data | 1477 ($3\sigma$) | 1454 ($3\sigma$) | 3557 ($3\sigma$) | 1052 ($3\sigma$) |
| $R$ | 0.053 | 0.092 | 0.073 | 0.063 |
| $R_w$ | 0.060 | 0.084 | 0.076 | 0.067 |
| largest peak, e/Å$^3$ | 0.72 | 0.39 | 0.72 | 0.80 |

three standards monitored every 7200 s. The structures were solved by the direct method using the MULTAN78[27] or SHELXS86[28] program and refined by the block-diagonal least-squares analysis based on *F* values using UNICS III program package.[29] Thiophene rings were statistically disordered by the 180° rotation in the crystal. New ideal atoms of X [S $\alpha$% and C (100–$\alpha$)%] and Y [S (100–$\alpha$)% and C $\alpha$%] were prepared from mixed atom scattering factors taken from the International Tables[30] and applied at the disorder-positions. All the non-hydrogen atoms of the molecule were refined with anisotropic temperatures factors. At the final stage, hydrogen atoms were included in the refinement with isotropic temperature factors. These calculations were carried out in the Computer Center of Institute for Molecular Science.

**Electrochemistry.** Cyclic voltammetry of monomers was carried out with a Toho Technical Research Polarization Unit PS-07 potentiostat/galvanostat in a three-compartment cell in PhCN or MeCN containing 0.1 mol $dm^{-3}$ $Bu_4NClO_4$ at a scan rate of 100 mV $s^{-1}$. Solutions were degassed by argon bubbling before use, and an argon stream was maintained over the solutions during measurements. Pt disk (2.0 $mm^{-2}$), Pt wire, and SCE were used as the working, counter, and reference electrodes, respectively.

## 2.4 References and Notes


(1) (a) Patil, A. O.; Heeger, A. J.; Wudl, F. *Chem. Rev.* **1988**, *88*, 183. (b) Gorman, C. B.; Grubbs, R. H. In *Conjugated Polymers*; Brédas, J.-L., Silbey, R., Eds.; Kluwer Academic Publishers: Dordrecht, 1991; p 31. (c) Roncali, J. *Chem. Rev.* **1992**, *92*, 711. (d) Scherf. U; Müllen, K. *Synthesis* **1992**, 23.

(2) Musmanni, S.; Ferraris, J. P. *J. Chem. Soc., Chem. Commun.* **1993**, 172.

(3) Nayak, K.; Marynick, D. S. *Macromolecules* **1990**, *23*, 2237.

(4) Gronowitz, S.; Peters, D. *Heterocycles* **1990**, *30*, 645.

(5) Tamao, K.; Kodama, S.; Nakajima, I.; Kumada, M. *Tetrahedron* **1982**, *38*, 3347.

(6) Hoshino, Y.; Miyaura, N.; Suzuki, A. *Bull. Chem. Soc. Jpn.* **1988**, *61*, 3008.

(7) Stille, J. K. *Angew. Chem., Int. Ed. Engl.* **1986**, *25*, 508.

(8) Baily, T. R. *Tetrahedron Lett.* **1986**, *27*, 4407.

(9) Benincori, T.; Brenna, E.; Sannicolo, F.; Trimarco, L.; Moro, G.; Pitea, D.; Pilati, T.; Zerbi, G.; Zotti, G. *J. Chem. Soc., Chem. Commun.* **1995**, 881.

(10) Mozingo, R.; Harris, S. A.; Wolf, D. E.; Hoffhine, C. E., Jr.; Eaton, N. R.; Folkers, K. *J. Am. Chem. Soc.* **1945**, *67*, 2092.

(11) Pinhey, J. T.; Roche, E. G. *J. Chem. Soc., Perkin Trans. 1* **1988**, 2415.

(12) Srinivasan, N. S.; Lee, D. G. *J. Org. Chem.* **1979**, *44*, 1574.

(13) Khalique, A. *Sci. Res.* **1967**, *4*.129.

(14) Venuti, M. C. *Synthesis* **1982**, 61.

(15) Pilgram, K.; Zupan, M.; Skiles, R. *J. Heterocycl. Chem.* **1970**, *7*, 629.

(16) Uno, T.; Takagi, K.; Tomoeda, M. *Chem. Pharm. Bull.* **1980**, *28*, 1909.

(17) Cava, M. P.; Lakshmikantham, M. V. *Acc. Chem. Res.* **1975**, *8*, 139.

(18) Ono, K.; Tanaka, S.; Yamashita, Y. *Angew. Chem., Int. Ed. Engl.* **1994**, *33*, 1977.

(19) Weidinger, H.; Kranz, J. *Chem. Ber.* **1964**, *97*, 1599.

(20) Yamamoto, M.; Izuoka, H.; Saiki, M.; Yamada, K. *J. Chem. Soc., Chem. Commun.* **1988**, 560.

(21) Steward, J. J. P. *J. Comput. Chem.* **1989**, *10*, 209, 221.

(22) Müllen, K.; Baumgarten, M.; Tyutyulkov, N.; Karabunarliev, S. *Synth. Met.* **1991**, *40*, 127.

(23) The resonace integrals between adjacent p-orbitals are expressed by $\beta = \beta_0 \cos \theta$ where $\beta_0$ is the standard resonance integral and $\theta$ is the torsional angle.

(24) Hiber, G.; Hanack, M.; Wurst, K.; Strähle, J. *Chem. Ber.* **1991**, *124*, 1597.

(25) The Chemical Society of Japan, Ed. In *Kagaku Binran Kisohen*, 4th ed.; Maruzen: Tokyo, 1993, Vol 2, p725.

(26) Coon, C. L.; Blucher, W. G.; Hill, M. E. *J. Org. Chem.* **1973**, *38*, 4243.

(27) Main, P.; Hull, S. E.; Lessinger, L.; Germain, G.; Declercq, J.-P.; Woolfson, M. M. MULTAN78, A System of Computer Programs for the Automatic Solution of Crystal Structures from X-ray Diffraction Data, Universities of York, England and Louvain, Belgium, 1978.

(28) Sheldrick, G. M. SHELXS86, Program for Crystal Structure Determination, University of Goettingen, Germany, 1986.

(29) Sakurai, T.; Kobayashi, K. *Rikagaku Kenkyusho Hokoku* **1979**, *55*, 69.

(30) *International Tables for X-ray Crystallography*, Vol 4, Kynoch Press; Birmingham, 1974.

## 2.5 Supplementary Materials

2,3-Dimethyl-5,7-dithien-2-ylthieno[3,4-*b*]pyrazine (**1b**)

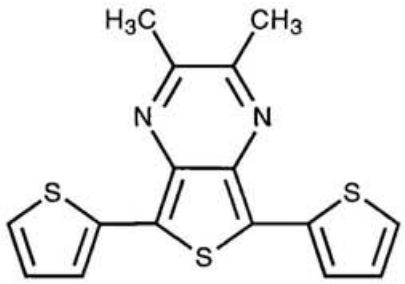


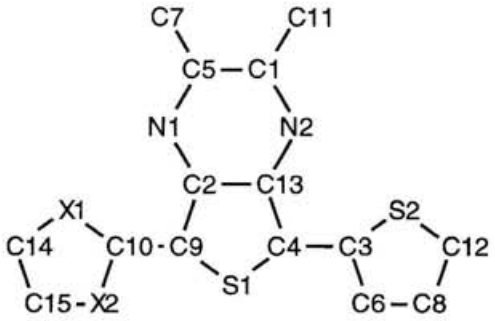


X = 50% S + 50% C

**Table 4.** Positional parameters of non-H atoms with estimated deviations in parentheses.

| atom | X | Y | Z | *Beq* / Å$^2$ |
|---|---|---|---|---|
| S1 | 0.7120 (3) | 0.2115 (2) | 0.3757 (0) | 3.5 |
| S2 | 0.8622 (3) | 0.5693 (2) | 0.4717 (1) | 5.1 |
| N1 | 0.2088 (8) | 0.5066 (6) | 0.3423 (1) | 3.3 |
| N2 | 0.4763 (8) | 0.6437 (5) | 0.4081 (1) | 3.3 |
| C1 | 0.2975 (11) | 0.7193 (7) | 0.3922 (2) | 3.4 |
| C2 | 0.3966 (10) | 0.4237 (6) | 0.3587 (1) | 3.0 |
| C3 | 0.8854 (10) | 0.4115 (6) | 0.4363 (1) | 3.1 |
| C4 | 0.7134 (11) | 0.3891 (6) | 0.4045 (1) | 3.3 |
| C5 | 0.1593 (10) | 0.6492 (6) | 0.3585 (2) | 3.3 |
| C6 | 1.0907 (9) | 0.3144 (6) | 0.4431 (1) | 2.8 |
| C7 | –0.0485 (11) | 0.7436 (7) | 0.3422 (2) | 4.3 |
| C8 | 1.2126 (12) | 0.3765 (8) | 0.4775 (2) | 4.7 |
| C9 | 0.4751 (10) | 0.2698 (6) | 0.3459 (1) | 3.1 |
| C10 | 0.3911 (11) | 0.1650 (6) | 0.3131 (2) | 3.3 |
| C11 | 0.2305 (13) | 0.8842 (7) | 0.4091 (2) | 4.8 |
| C12 | 1.1132 (13) | 0.5087 (9) | 0.4951 (2) | 5.1 |
| C13 | 0.5291 (9) | 0.4917 (6) | 0.3912 (1) | 2.9 |
| C14 | 0.1591 (13) | 0.0425 (9) | 0.2592 (2) | 5.4 |
| C15 | 0.3443 (15) | –0.0515 (9) | 0.2649 (2) | 6.8 |
| X1 | 0.1452 (4) | 0.2011 (3) | 0.2887 (1) | 3.4 |
| X2 | 0.5227 (6) | 0.0072 (4) | 0.2957 (1) | 6.8 |

**Table 5.** Bond lengths with estimated deviations in parentheses.

| atom1 | atom2 | distance / Å | atom1 | atom2 | distance / Å |
|---|---|---|---|---|---|
| S1 | C4 | 1.719 (5) | S1 | C9 | 1.731 (5) |
| S2 | C3 | 1.730 (5) | S2 | C12 | 1.695 (7) |
| N1 | C2 | 1.372 (7) | N1 | C5 | 1.301 (7) |
| N2 | C1 | 1.297 (7) | N2 | C13 | 1.380 (7) |
| C1 | C5 | 1.470 (7) | C1 | C11 | 1.494 (8) |
| C2 | C9 | 1.387 (7) | C2 | C13 | 1.418 (7) |
| C3 | C4 | 1.442 (7) | C3 | C6 | 1.425 (8) |
| C4 | C13 | 1.406 (8) | C5 | C7 | 1.502 (8) |
| C6 | C8 | 1.417 (8) | C8 | C12 | 1.341 (9) |
| C9 | C10 | 1.454 (7) | C10 | X1 | 1.638 (6) |
| C10 | X2 | 1.586 (6) | C14 | C15 | 1.313 (11) |
| C14 | X1 | 1.608 (7) | C15 | X2 | 1.509 (8) |

**Table 6.** Bond angles with estimated deviations in parentheses.

| atom1 | atom2 | atom3 | angle / degree | atom1 | atom2 | atom3 | angle / degree |
|---|---|---|---|---|---|---|---|
| C4 | S1 | C9 | 95.0 (3) | C3 | S2 | C12 | 91.6 (3) |
| C2 | N1 | C5 | 116.1 (4) | C1 | N2 | C13 | 115.4 (4) |
| N2 | C1 | C5 | 122.8 (5) | N2 | C1 | C11 | 118.1 (5) |
| C5 | C1 | C11 | 119.1 (5) | N1 | C2 | C9 | 124.7 (5) |
| N1 | C2 | C13 | 121.4 (4) | C9 | C2 | C13 | 113.9 (5) |
| S2 | C3 | C4 | 121.8 (4) | S2 | C3 | C6 | 111.3 (4) |
| C4 | C3 | C6 | 126.9 (4) | S1 | C4 | C3 | 120.4 (4) |
| S1 | C4 | C13 | 108.6 (4) | C3 | C4 | C13 | 131.1 (5) |
| N1 | C5 | C1 | 122.3 (5) | N1 | C5 | C7 | 118.5 (5) |
| C1 | C5 | C7 | 119.3 (5) | C3 | C6 | C8 | 109.3 (5) |
| C6 | C8 | C12 | 114.8 (6) | S1 | C9 | C2 | 108.9 (4) |
| S1 | C9 | C10 | 121.1 (4) | C2 | C9 | C10 | 130.0 (5) |
| C9 | C10 | X1 | 122.7 (4) | C9 | C10 | X2 | 125.6 (5) |
| X1 | C10 | X2 | 111.8 (8) | S2 | C12 | C8 | 112.9 (5) |
| N2 | C13 | C2 | 122.1 (5) | N2 | C13 | C4 | 124.3 (4) |
| C2 | C13 | C4 | 113.7 (4) | C15 | C14 | X1 | 114.5 (5) |
| C14 | C15 | X2 | 117.0 (6) | C10 | X1 | C14 | 96.3 (3) |
| C10 | X2 | C15 | 100.2 (4) | | | | |

2,3-Dimethyl-5,8-dithien-2-ylquinoxaline (**2a**)

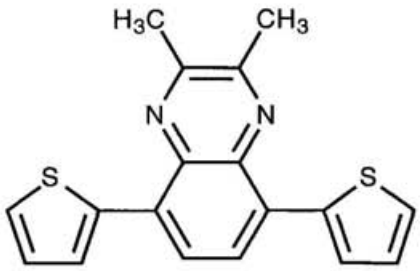


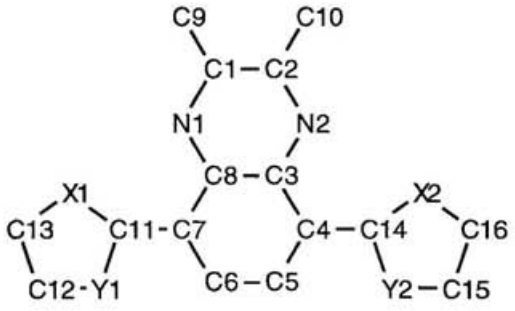


X = 80% S + 20% C, Y = 20% S + 80% C

**Table 7.** Positional parameters of non-H atoms with estimated deviations in parentheses.

| atom | X | Y | Z | *B*eq / Å$^2$ |
|---|---|---|---|---|
| N1 | 0.4474 (10) | 0.4221 (3) | 0.2744 (5) | 4.7 |
| N2 | 0.6254 (11) | 0.4262 (3) | 0.0772 (6) | 4.8 |
| C1 | 0.6170 (13) | 0.4577 (4) | 0.2672 (7) | 4.7 |
| C2 | 0.7081 (13) | 0.4596 (4) | 0.1677 (7) | 4.6 |
| C3 | 0.4473 (13) | 0.3888 (4) | 0.0823 (7) | 4.5 |
| C4 | 0.3603 (13) | 0.3518 (4) | –0.0156 (7) | 4.7 |
| C5 | 0.1758 (14) | 0.3155 (5) | –0.0081 (7) | 5.5 |
| C6 | 0.0865 (14) | 0.3137 (4) | 0.0910 (7) | 5.5 |
| C7 | 0.1746 (13) | 0.3480 (4) | 0.1877 (7) | 4.6 |
| C8 | 0.3563 (12) | 0.5015 (4) | 0.1604 (8) | 4.1 |
| C9 | 0.7093 (15) | 0.4950 (5) | 0.3730 (8) | 6.3 |
| C10 | 0.9035 (15) | 0.5015 (5) | 0.1604 (8) | 6.0 |
| C11 | 0.0791 (13) | 0.3421 (4) | 0.2894 (7) | 4.6 |
| C12 | –0.1612 (16) | 0.3100 (5) | 0.4129 (9) | 6.7 |
| C13 | –0.0021 (18) | 0.3387 (5) | 0.4865 (9) | 7.3 |
| C14 | 0.4502 (15) | 0.3512 (5) | –0.1194 (8) | 6.0 |
| C15 | 0.5013 (20) | 0.3235 (6) | –0.3058 (9) | 8.7 |
| C16 | 0.6548 (20) | 0.3674 (7) | –0.2758 (9) | 9.1 |
| X1 | 0.1970 (4) | 0.3690 (1) | 0.4208 (2) | 5.1 |
| X2 | 0.6620 (5) | 0.3966 (2) | –0.1427 (3) | 6.7 |
| Y1 | –0.1258 (12) | 0.3087 (4) | 0.2952 (7) | 8.6 |
| Y2 | 0.3670 (13) | 0.3115 (4) | –0.2229 (6) | 8.1 |

**Table 8.** Bond lengths with estimated deviations in parentheses.

| atom1 | atom2 | distance / Å | atom1 | atom2 | distance / Å |
|---|---|---|---|---|---|
| N1 | C1 | 1.315 (11) | N1 | C8 | 1.372 (10) |
| N2 | C2 | 1.318 (10) | N2 | C3 | 1.375 (11) |
| C1 | C2 | 1.413 (13) | C1 | C9 | 1.515 (12) |
| C2 | C10 | 1.523 (13) | C3 | C4 | 1.432 (11) |
| C3 | C8 | 1.416 (12) | C4 | C5 | 1.404 (12) |
| C4 | C14 | 1.454 (13) | C5 | C6 | 1.417 (13) |
| C6 | C7 | 1.393 (12) | C7 | C8 | 1.408 (11) |
| C7 | C11 | 1.457 (13) | C11 | X1 | 1.719 (9) |
| C11 | Y1 | 1.480 (12) | C12 | C13 | 1.360 (14) |
| C12 | Y1 | 1.468 (13) | C13 | X1 | 1.714 (12) |
| C14 | X2 | 1.697 (11) | C14 | Y2 | 1.505 (13) |
| C15 | C16 | 1.332 (18) | C15 | Y2 | 1.436 (15) |
| C16 | X2 | 1.702 (14) | | | |

**Table 9.** Bond angles with estimated deviations in parentheses.

| atom1 | atom2 | atom3 | angle / degree | atom1 | atom2 | atom3 | angle / degree |
|---|---|---|---|---|---|---|---|
| C1 | N1 | C8 | 118.8 (7) | C2 | N2 | C3 | 118.1 (7) |
| N1 | C1 | C9 | 121.7 (7) | N1 | C1 | C9 | 115.6 (8) |
| C2 | C1 | C9 | 122.7 (8) | N2 | C2 | C1 | 121.4 (8) |
| N2 | C2 | C10 | 117.6 (8) | N2 | C3 | C4 | 117.8 (8) |
| N2 | C3 | C8 | 120.7 (7) | C4 | C3 | C8 | 121.5 (7) |
| C3 | C4 | C5 | 116.0 (8) | C3 | C4 | C14 | 123.8 (8) |
| C5 | C4 | C14 | 120.1 (7) | C4 | C5 | C6 | 122.0 (8) |
| C5 | C6 | C7 | 122.1 (8) | C6 | C7 | C8 | 117.5 (8) |
| C6 | C7 | C11 | 119.5 (8) | C8 | C7 | C11 | 123.0 (7) |
| N1 | C8 | C3 | 119.3 (7) | N1 | C8 | C7 | 120.8 (7) |
| C3 | C8 | C7 | 120.8 (7) | C7 | C11 | X1 | 124.4 (6) |
| C7 | C11 | Y1 | 124.7 (7) | X1 | C11 | Y1 | 110.8 (6) |
| C13 | C12 | Y1 | 114.6 (10) | C12 | C13 | X1 | 112.4 (9) |
| C4 | C14 | X2 | 124.8 (7) | C4 | C14 | Y2 | 125.3 (8) |
| X2 | C14 | Y2 | 109.9 (7) | C16 | C15 | Y2 | 114.8 (10) |
| C15 | C16 | X2 | 113.4 (10) | C11 | X1 | C13 | 93.8 (5) |
| C14 | X2 | C16 | 93.6 (6) | C11 | Y1 | C12 | 108.3 (7) |
| C14 | Y2 | C15 | 108.3 (8) | | | | |

6,7-Dihexyl-4,9-dithien-2-yl[1,2,5]thiadiazolo[3,4-*g*]quinoxaline (**4c**)

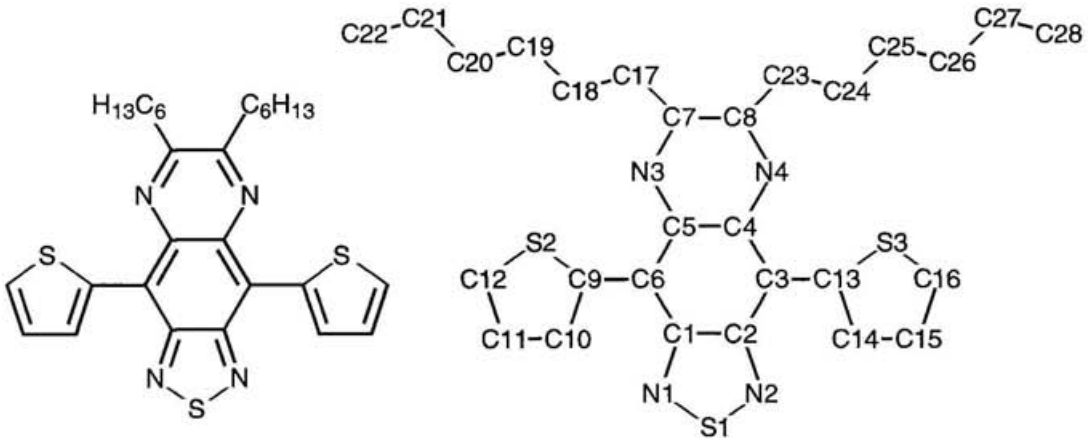


**Table 10.** Positional parameters of non-H atoms with estimated deviations in parentheses.

| atom | X | Y | Z | *B*eq / Å$^2$ |
|---|---|---|---|---|
| S1 | 0.5471 (1) | 0.5911 (1) | 0.2582 (2) | 5.8 |
| S2 | 0.0714 (1) | 0.3505 (1) | 0.2095 (2) | 5.2 |
| S3 | 0.1999 (1) | 0.8489 (1) | 0.3120 (2) | 6.5 |
| N1 | 0.4423 (3) | 0.5141 (2) | 0.2479 (5) | 5.1 |
| N2 | 0.4816 (3) | 0.6705 (2) | 0.2758 (5) | 5.1 |
| N3 | 0.0314 (3) | 0.5125 (2) | 0.2562 (4) | 3.3 |
| N4 | 0.0751 (3) | 0.6893 (2) | 0.2851 (4) | 3.7 |
| C1 | 0.3451 (3) | 0.5497 (2) | 0.2591 (5) | 3.9 |
| C2 | 0.3669 (3) | 0.6410 (2) | 0.2739 (5) | 3.9 |
| C3 | 0.2778 (3) | 0.6917 (2) | 0.2841 (4) | 3.6 |
| C4 | 0.1658 (3) | 0.6450 (2) | 0.2768 (4) | 3.3 |
| C5 | 0.1438 (3) | 0.5544 (2) | 0.2623 (4) | 3.3 |
| C6 | 0.2311 (3) | 0.5030 (2) | 0.2549 (5) | 3.6 |
| C7 | –0.0525 (3) | 0.5569 (2) | 0.2629 (4) | 3.3 |
| C8 | –0.0313 (3) | 0.6482 (2) | 0.2765 (4) | 3.4 |
| C9 | 0.2118 (3) | 0.4106 (2) | 0.2438 (5) | 4.1 |
| C10 | 0.3055 (4) | 0.3562 (2) | 0.2596 (5) | 4.7 |
| C11 | 0.2490 (5) | 0.2694 (3) | 0.2426 (7) | 6.1 |
| C12 | 0.1282 (5) | 0.2574 (3) | 0.2127 (6) | 5.8 |
| C13 | 0.3033 (4) | 0.7835 (2) | 0.2959 (5) | 4.1 |
| C14 | 0.4149 (4) | 0.8335 (3) | 0.2988 (6) | 5.2 |
| C15 | 0.4063 (5) | 0.9207 (3) | 0.3078 (6) | 6.1 |
| C16 | 0.2985 (5) | 0.9378 (3) | 0.3198 (7) | 6.6 |

| atom | X | Y | Z | $B_{eq}$ / Å$^2$ |
|---|---|---|---|---|
| C17 | –0.1752 (3) | 0.5114 (2) | 0.2554 (5) | 3.7 |
| C18 | –0.1895 (3) | 0.4162 (2) | 0.2361 (5) | 3.7 |
| C19 | –0.3165 (3) | 0.3743 (2) | 0.2297 (5) | 3.9 |
| C20 | –0.3307 (3) | 0.2782 (2) | 0.2076 (5) | 4.2 |
| C21 | –0.4579 (4) | 0.2369 (3) | 0.1974 (6) | 5.3 |
| C22 | –0.4743 (5) | 0.1399 (3) | 0.1777 (7) | 6.5 |
| C23 | –0.1338 (3) | 0.6958 (3) | 0.2772 (5) | 4.5 |
| C24 | –0.1039 (4) | 0.7914 (3) | 0.2948 (6) | 5.1 |
| C25 | –0.2184 (5) | 0.8328 (3) | 0.2771 (7) | 6.6 |
| C26 | –0.1957 (7) | 0.9281 (4) | 0.3082 (9) | 9.3 |
| C27 | –0.1480 (8) | 0.9712 (4) | 0.1614 (11) | 11.4 |
| C28 | –0.1301 (9) | 1.0666 (5) | 0.1937 (11) | 12.8 |

**Table 11.** Bond lengths with estimated deviations in parentheses.

| atom1 | atom2 | distance / Å | atom1 | atom2 | distance / Å |
|---|---|---|---|---|---|
| S1 | N1 | 1.604 (4) | S1 | N2 | 1.589 (4) |
| S2 | C9 | 1.738 (4) | S2 | C12 | 1.709 (5) |
| S3 | C13 | 1.728 (5) | S3 | C16 | 1.698 (5) |
| N1 | C1 | 1.361 (6) | N2 | C2 | 1.360 (5) |
| N3 | C5 | 1.385 (4) | N3 | C7 | 1.298 (5) |
| N4 | C4 | 1.369 (5) | N4 | C8 | 1.313 (5) |
| C1 | C2 | 1.444 (5) | C1 | C6 | 1.433 (5) |
| C2 | C3 | 1.423 (6) | C3 | C4 | 1.407 (5) |
| C3 | C13 | 1.454 (5) | C4 | C5 | 1.433 (5) |
| C5 | C6 | 1.407 (5) | C6 | C9 | 1.460 (5) |
| C7 | C8 | 1.444 (5) | C7 | C17 | 1.508 (5) |
| C9 | C10 | 1.472 (6) | C10 | C11 | 1.441 (6) |
| C11 | C12 | 1.354 (7) | C13 | C14 | 1.433 (6) |
| C14 | C15 | 1.414 (6) | C15 | C16 | 1.355 (8) |
| C17 | C18 | 1.507 (5) | C18 | C19 | 1.536 (5) |
| C19 | C20 | 1.523 (5) | C20 | C21 | 1.527 (6) |
| C21 | C22 | 1.534 (6) | C23 | C24 | 1.516 (6) |
| C24 | C25 | 1.548 (7) | C25 | C26 | 1.512 (8) |
| C26 | C27 | 1.523 (12) | C27 | C28 | 1.515 (10) |

**Table 12.** Bond angles with estimated deviations in parentheses.

| atom1 | atom2 | atom3 | angle / degree | atom1 | atom2 | atom3 | angle / degree |
|---|---|---|---|---|---|---|---|
| N1 | S1 | N2 | 101.7 (2) | C9 | S2 | C12 | 92.7 (3) |
| C13 | S3 | C16 | 92.7 (2) | S1 | N1 | C1 | 106.1 (3) |
| S1 | N2 | C2 | 107.7 (3) | C5 | N3 | C7 | 118.7 (3) |
| C4 | N4 | C8 | 119.5 (3) | N1 | C1 | C2 | 113.3 (3) |
| N1 | C1 | C6 | 124.5 (4) | C2 | C1 | C6 | 122.2 (4) |
| N2 | C2 | C1 | 111.3 (4) | N2 | C2 | C3 | 125.5 (3) |
| C1 | C2 | C3 | 123.2 (3) | C2 | C3 | C4 | 113.9 (3) |
| C2 | C3 | C13 | 121.3 (3) | C4 | C3 | C13 | 124.8 (4) |
| N4 | C4 | C3 | 117.5 (3) | N4 | C4 | C5 | 119.5 (3) |
| C3 | C4 | C5 | 123.1 (3) | N3 | C5 | C4 | 120.0 (3) |
| N3 | C5 | C6 | 116.1 (3) | C4 | C5 | C6 | 124.0 (3) |
| C1 | C6 | C5 | 113.6 (3) | C1 | C6 | C9 | 121.3 (4) |
| C5 | C6 | C9 | 125.1 (3) | N3 | C7 | C8 | 121.8 (3) |
| N3 | C7 | C17 | 118.7 (3) | C8 | C7 | C17 | 119.6 (3) |
| N4 | C8 | C7 | 120.7 (3) | N4 | C8 | C23 | 120.3 (3) |
| C7 | C8 | C23 | 119.0 (3) | S2 | C9 | C6 | 123.3 (3) |
| S2 | C9 | C10 | 110.9 (3) | C6 | C9 | C10 | 125.8 (3) |
| C9 | C10 | C11 | 108.1 (4) | C10 | C11 | C12 | 115.8 (5) |
| S2 | C12 | C11 | 112.4 (3) | S3 | C13 | C3 | 123.6 (3) |
| S3 | C13 | C14 | 109.8 (3) | C3 | C13 | C14 | 126.6 (4) |
| C13 | C14 | C15 | 111.0 (4) | C14 | C15 | C16 | 113.9 (4) |
| S3 | C16 | C15 | 112.5 (4) | C7 | C17 | C18 | 115.7 (3) |
| C17 | C18 | C19 | 112.8 (3) | C18 | C19 | C20 | 112.4 (3) |
| C19 | C20 | C21 | 112.2 (4) | C20 | C21 | C22 | 113.3 (4) |
| C8 | C23 | C24 | 115.8 (3) | C23 | C24 | C25 | 110.8 (4) |
| C24 | C25 | C26 | 114.5 (4) | C25 | C26 | C27 | 113.1 (6) |
| C26 | C27 | C28 | 111.6 (7) | | | | |

4,8-Dithien-2-yl-2λ$^4$δ$^2$-benzo[1,2-*c*;4,5-*c*']bis[1,2,5]thiadiazole (**5**)

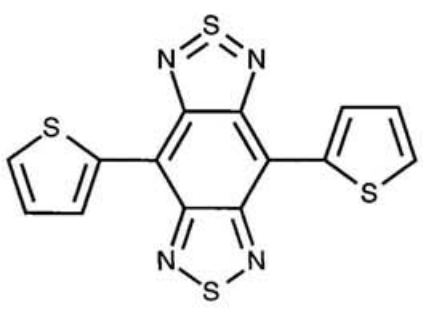


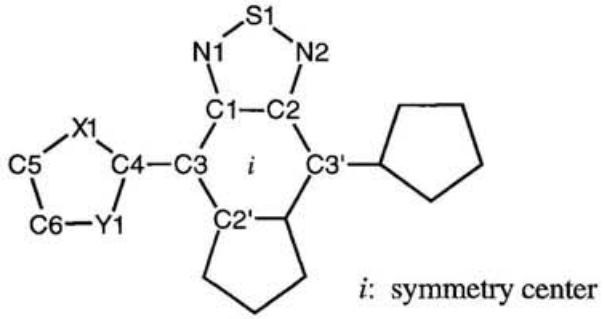


*i*: symmetry center

X = 75% S + 25% C, Y = 25% S + 75% C

**Table 13.** Positional parameters of non-H atoms with estimated deviations in parentheses.

| atom | X | Y | Z | *B*eq / Å$^2$ |
|---|---|---|---|---|
| S1 | 0.0914 (1) | 0.0608 (3) | 0.3945 (1) | 4.6 |
| N1 | 0.1121 (2) | –0.1367 (9) | 0.2549 (4) | 3.6 |
| N2 | 0.0169 (2) | 0.2224 (9) | 0.3037 (5) | 3.9 |
| C1 | 0.0592 (2) | –0.0853 (9) | 0.1212 (5) | 2.7 |
| C2 | 0.0029 (2) | 0.1276 (9) | 0.1498 (5) | 2.8 |
| C3 | 0.0580 (2) | –0.2169 (9) | –0.0294 (5) | 2.6 |
| C4 | 0.1147 (2) | –0.4297 (9) | –0.0587 (5) | 2.8 |
| C5 | 0.2259 (2) | –0.7590 (10) | –0.0312 (6) | 3.7 |
| C6 | 0.1835 (3) | –0.7697 (10) | –0.1841 (6) | 3.9 |
| X1 | 0.1902 (1) | –0.5302 (3) | 0.0919 (2) | 3.7 |
| Y1 | 0.1141 (2) | –0.5716 (7) | –0.2324 (5) | 5.0 |

**Table 14.** Bond lengths with estimated deviations in parentheses.

| atom1 | atom2 | distance / Å | atom1 | atom2 | distance / Å |
|---|---|---|---|---|---|
| S1 | N1 | 1.589 (4) | S1 | N2 | 1.596 (4) |
| N1 | C1 | 1.352 (5) | N2 | C2 | 1.348 (5) |
| C1 | C2 | 1.464 (6) | C1 | C3 | 1.405 (6) |
| C3 | C4 | 1.405 (5) | C4 | X1 | 1.736 (4) |
| C4 | Y1 | 1.736 (4) | C5 | X1 | 1.665 (5) |
| C5 | C6 | 1.348 (6) | C6 | Y1 | 1.541 (6) |

**Table 15.** Bond angles with estimated deviations in parentheses.

| atom1 | atom2 | atom3 | angle / degree | atom1 | atom2 | atom3 | angle / degree |
|---|---|---|---|---|---|---|---|
| N1 | S1 | N2 | 101.9 (2) | S1 | N1 | C1 | 107.0 (3) |
| S1 | N2 | C2 | 107.3 (3) | N1 | C1 | C2 | 112.3 (4) |
| N1 | C1 | C3 | 112.3 (4) | C2 | C1 | C3 | 123.2 (3) |
| N2 | C2 | C1 | 111.6 (3) | N2 | C2 | C3' | 125.4 (4) |
| C1 | C2 | C3' | 123.0 (4) | C1 | C3 | C2' | 113.8 (4) |
| C1 | C3 | C4 | 123.3 (3) | C2' | C3 | C4 | 122.9 (4) |
| C3 | C4 | X1 | 121.6 (3) | C3 | C4 | Y1 | 122.7 (3) |
| X1 | C4 | Y1 | 115.6 (3) | C6 | C5 | X1 | 116.1 (4) |
| C5 | C6 | Y1 | 118.7 (4) | C4 | X1 | C5 | 91.7 (2) |
| C4 | Y1 | C6 | 97.8 (3) | | | | |

# Chapter 3 Syntheses and Properties of Polymers Composed of Aromatic-Donor and *o*-Quinoid-Acceptor Segments.

Abstract: Electrochemical polymerization of a series of triheterocyclic monomers composed of aromatic-donor and *o*-quinoid-acceptor segments on Pt and ITO electrodes by repetitive potential sweeps was attempted. All the cyclic voltammograms showed the outlooks indicating the growth of polymers deposited on an electrode. Only one polymer containing pyrazino[2,3-*b*]quinoxaline as *o*-quinoid acceptor unit displayed the deformation of the cyclic voltammogram over a period of polymerization. The resulting polymers were relatively stable under ordinary conditions but insoluble in all the organic solvents even when longer alkyl chains were introduced. Cyclic voltammograms of the polymers on a Pt disk electrode were measured under certain strict conditions. Most of the polymers containing thiophene units showed both p- and n-doping processes. The p-doping wave was broad and irreversible, while the n-doping wave was sharp and quasi-reversible in the case of the polymers having no alkyl substituents. On the other hand, the polymers with *N*-methylpyrrole units hardly showed n-doping. Some polymers exhibited characteristic waves probably due to the charge trapping. From the onset potentials between p- and n-doping, electrochemical bandgaps were estimated. Electronic spectra of the polymers on an ITO-coated glass electrode were measured. From the onset of the absorbance, optical bandgaps were determined. As oxidized electrochemically, many polymers displayed electrochromic phenomena. The bandgaps were a range of 0.5 to 1.8 eV. The value of 0.5 eV is one of the narrowest bandgap reported so far.

## 3.1 Introduction

Since the discovery of the first narrow-bandgap polymer, poly(benzo[c]thiophene) (**1**),[1] the search for polymers possessing narrow bandgaps is a current topic because such polymers are expected to be promising candidates for intrinsic organic conductors and nonlinear optical devices.[2,3] To develop new series of narrow-bandgap polymers, the author has designed the alternating copolymer composed of aromatic-donor and *o*-quinoid-acceptor segments, and a variety of monomers was synthesized. In Chapter 2, properties of monomers (**2-10**) were surveyed and their features were demonstrated in conjunction with *o*-quinoid-acceptor units. In this chapter, the attempt to polymerize the monomers by electrochemical oxidative polymerization is stated. Properties of the polymers are discussed

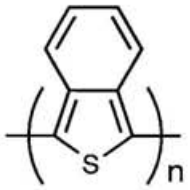

**1**

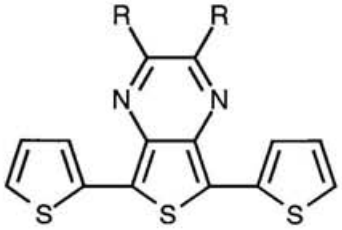

**2**

**a** : R = H
**b** : R = $CH_3$
**c** : R = $C_6H_{13}$
**d** : R = $C_{13}H_{27}$

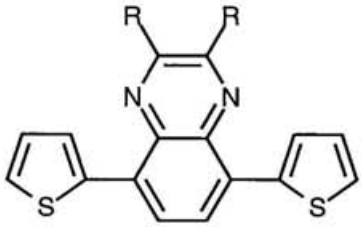

**3**

**a** : R = $CH_3$
**b** : R = $C_6H_{13}$

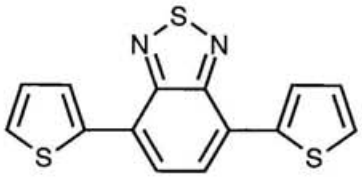

**4**

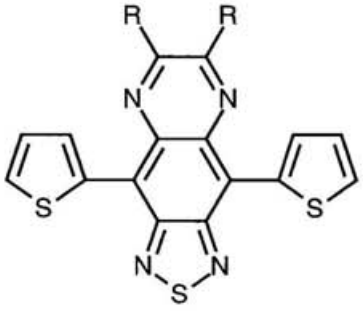

**5**

**a** : R = H
**b** : R = $CH_3$
**c** : R = $C_6H_{13}$

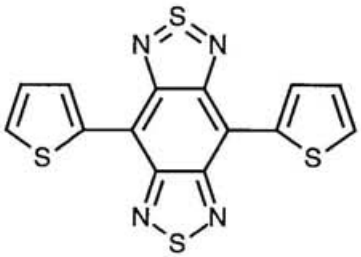

**6**

using cyclic voltammetry and electronic spectra. The correlation between structures and properties of the polymers are examined.

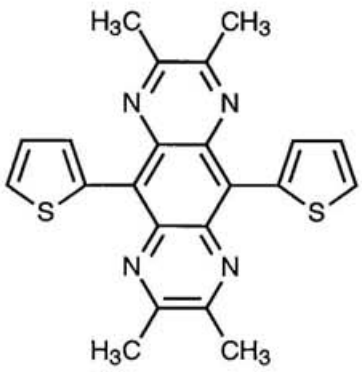

**7**

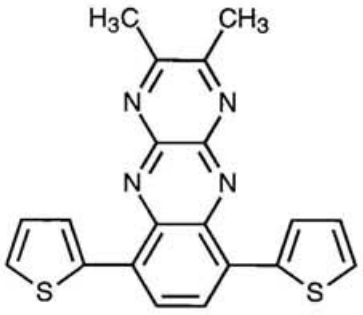

**8**

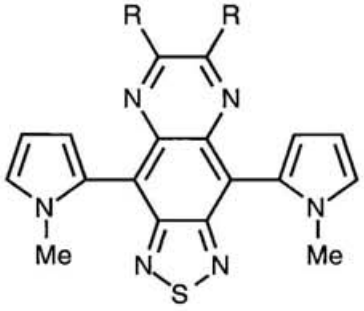

**a** : R = $CH_3$
**b** : R = $C_6H_{13}$

**9**

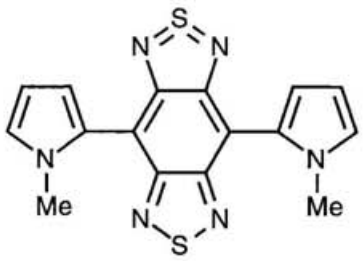

**10**

## 3.2 Results and Discussion

### 3.2.1 Electrochemical Polymerization

Polymerization was attempted by repetitive potential-sweep anodic oxidation onto Pt disk and indium tin oxide (ITO) coated glass electrodes in PhCN containing 0.1 mol $dm^{-3}$ Bu4NClO4 (for **6**, Bu4NBF4) at a scan rate of 100 mV $s^{-1}$. The concentration of monomers ranged from $10^{-4}$ to $2 \times 10^{-3}$ mol $dm^{-3}$. For **2a,b**, **3a**, **4**, and **9a,b**, MeCN was also used. The optimized experimental conditions are summarized in Table 1. The polymerization smoothly occurred except for **6** and **7** whose polymerization needed a prolonged time (3-4 h) due to low efficiency. The initial modes of growth of polymers by

**Table 1.** Experimental conditions[a] of electropolymerization.

| monomer | Pt disk electrode | | ITO electrode | |
|---|---|---|---|---|
| | scan range[b] | solvent | scan range[b] | solvent |
| **2a** | –0.3 ~ +0.9 | MeCN | –0.3 ~ +0.9 | MeCN |
| **2b** | –0.4 ~ +1.1 | PhCN | –0.3 ~ +0.85 | MeCN |
| **2c** | –0.3 ~ +1.2 | PhCN | –0.3 ~ +1.0 | PhCN |
| **2d** | –0.3 ~ +1.2 | PhCN | –0.3 ~ +1.05 | PhCN |
| **3a** | 0 ~ +1.15 | MeCN | 0 ~ +1.05 | MeCN |
| **3b** | –0.3 ~ +1.2 | PhCN | –0.2 ~ +1.2 | PhCN |
| **4** | 0 ~ +1.15 | MeCN | 0 ~ +1.15 | MeCN |
| **5a** | –0.1 ~ +1.1 | PhCN | –0.1 ~ +1.1 | PhCN |
| **5b** | –0.1 ~ +1.1 | PhCN | –0.1 ~ +1.1 | PhCN |
| **5c** | –0.1 ~ +1.2 | PhCN | –0.1 ~ +1.2 | PhCN |
| **6** | 0 ~ +1.125 | PhCN | 0 ~ +1.125 | PhCN |
| **7** | –0.1 ~ +1.0 | PhCN | 0 ~ +1.1 | PhCN |
| **8** | 0 ~ +1.25 | PhCN | 0 ~ +1.2 | PhCN |
| **9a** | –0.3 ~ +0.8 | MeCN | –0.3 ~ +0.8 | MeCN |
| **9b** | –0.2 ~ +0.8 | MeCN | –0.1 ~ +0.85 | MeCN |
| **10** | –0.5 ~ +0.9 | PhCN | –0.5 ~ +0.9 | PhCN |

[a] monomer: $10^{-4}$ to $2 \times 10^{-3}$ mol dm$^{-3}$; electrolyte: $Bu_4NClO_4$ (0.1 mol dm$^{-3}$) ($Bu_4NBF_4$ for **6**); scan rate: 100 mV s$^{-1}$. [b] V *vs* SCE.

electropolymerization are shown in Figures 1a-i. In all the Figures, the appearance of new peaks in lower-potential region than the oxidation potentials of monomers and the tendency for peak currents to grow linearly with potential cycling are observed as has been seen in many cases of the electrochemical polymerization. In the case of polymerization of **8**, however, the deformation of waves that both the anodic onset and peak potential shift to higher positive potentials over a period of polymerization is found as shown in Figure 2. This finding may suggest the possibility of degradation of conjugation in the course of polymerization process. All the polymers were obtained as insoluble film-type deposits even when long alkyl chains were introduced as in monomers **2**, **3**, **5**, and **9**. After polymerization, electrochemical reduction of the resulting polymers gave dedoped polymers.

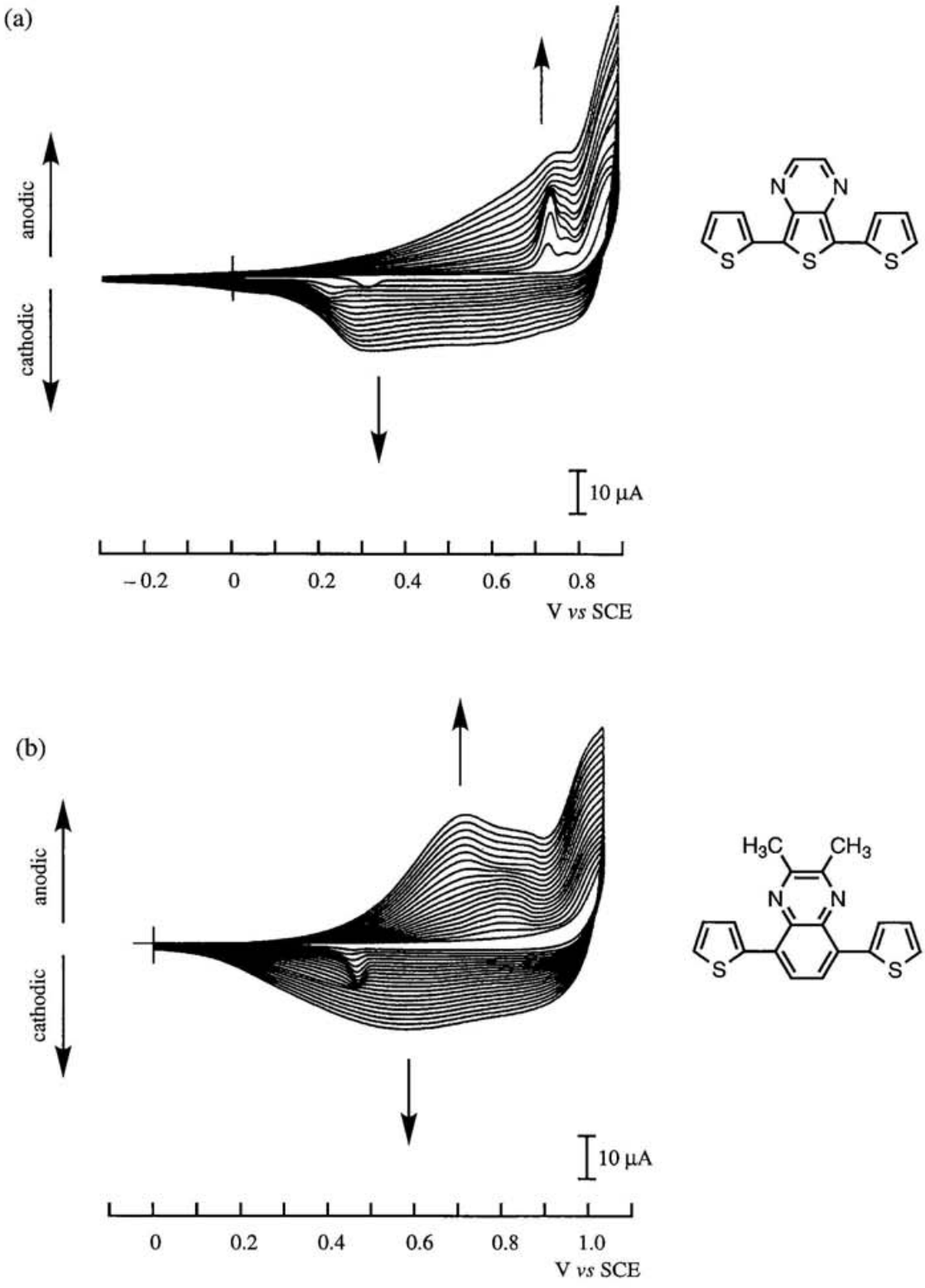


**Figure 1.** Multisweep cyclic voltammetry for the electropolymerization of (a) **2a**, (b) **3a**, (c) **4**, (d) **5a**, (e) **6**, (f) **7**, (g) **8**, (h) **9a**, and (i) **10** on a Pt disk in PhCN (MeCN for **2a**, **3a**, **4**, and **9a**) containing 0.1 mol $dm^{-3}$ $Bu_4NClO_4$ ($Bu_4NBF_4$ for **6**), scan rate 100 mV $s^{-1}$.

(c)

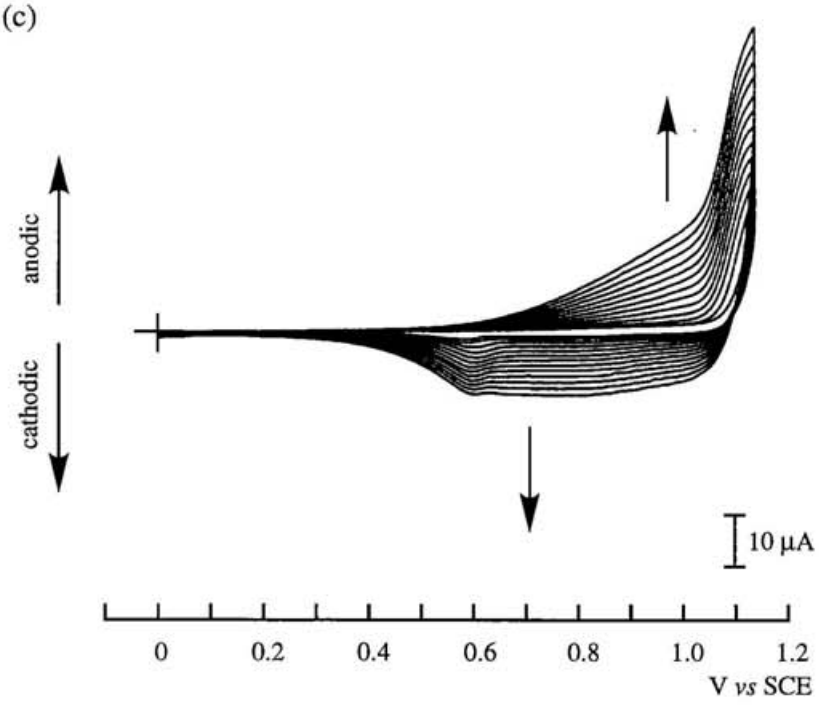
anodic
cathodic
10 μA
0
0.2
0.4
0.6
0.8
1.0
1.2
V *vs* SCE

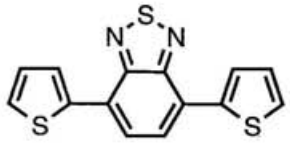
S
N
N
S
S

(d)

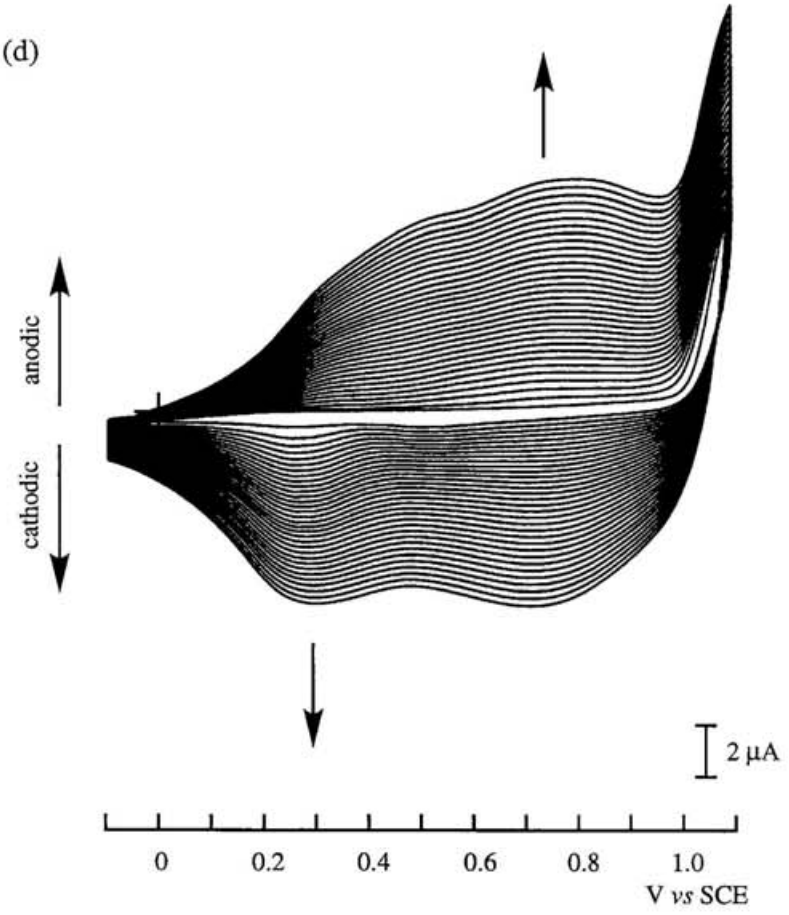
anodic
cathodic
2 μA
0
0.2
0.4
0.6
0.8
1.0
V *vs* SCE

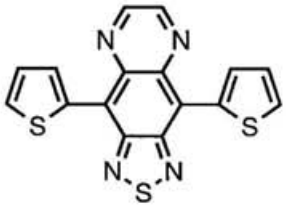
N
N
S
S
N
S
N

(e)

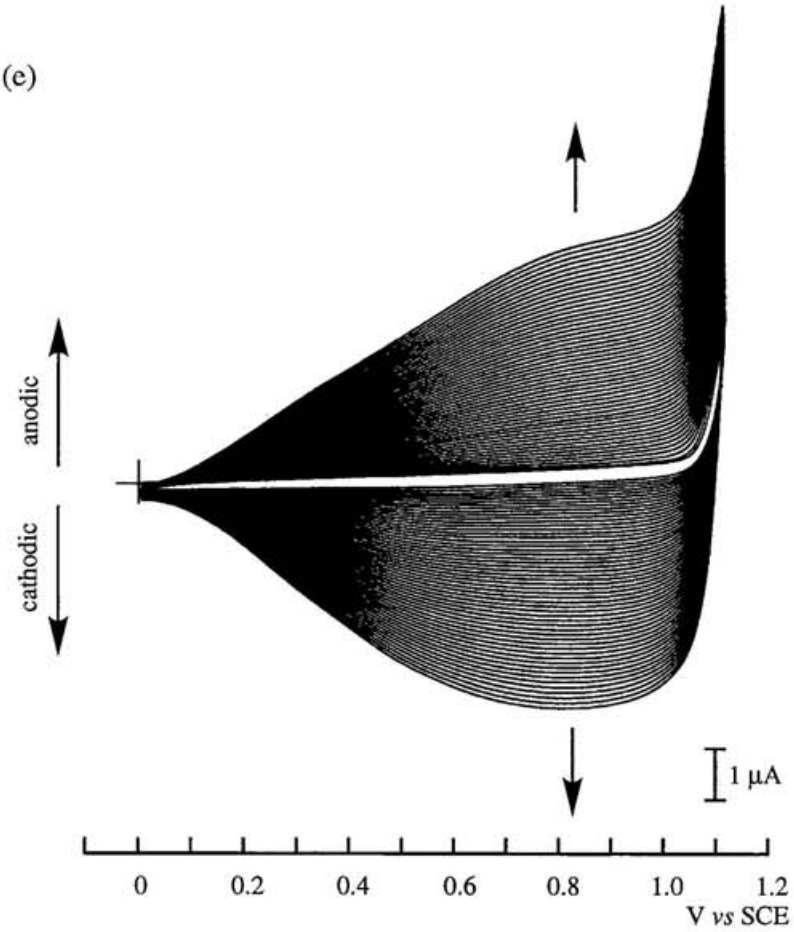
anodic
cathodic
1 μA
0
0.2
0.4
0.6
0.8
1.0
1.2
V vs SCE

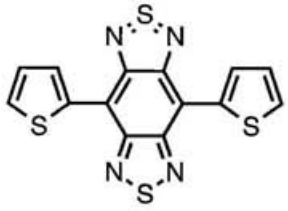
N
S
N
S
S
N
S
N

(f)

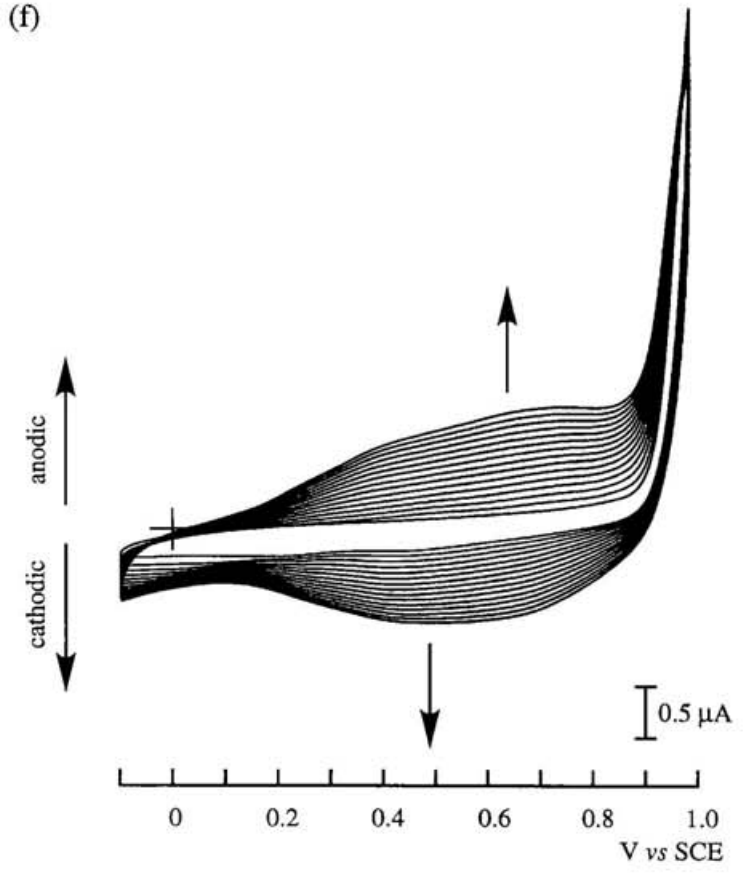
anodic
cathodic
0.5 μA
0
0.2
0.4
0.6
0.8
1.0
V vs SCE

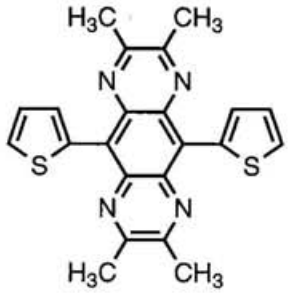
H3C
CH3
N
N
S
S
N
N
H3C
CH3

(g)

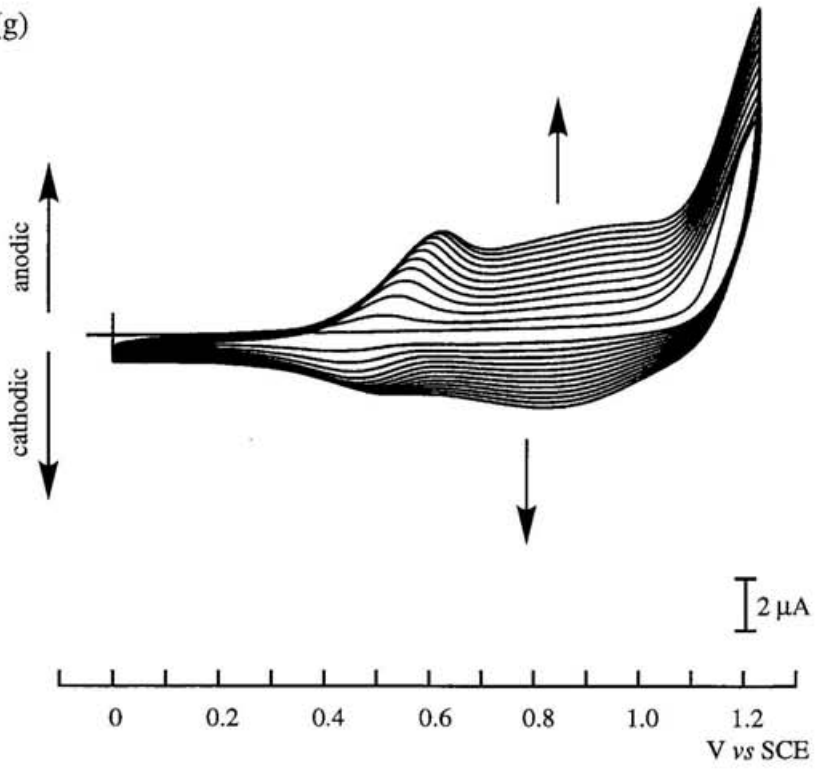
anodic
cathodic
2 μA
0
0.2
0.4
0.6
0.8
1.0
1.2
V *vs* SCE

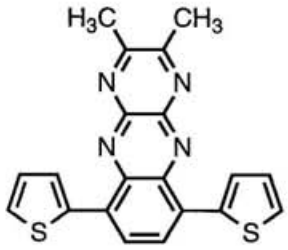
H3C
CH3
N
N
N
N
S
S

(h)

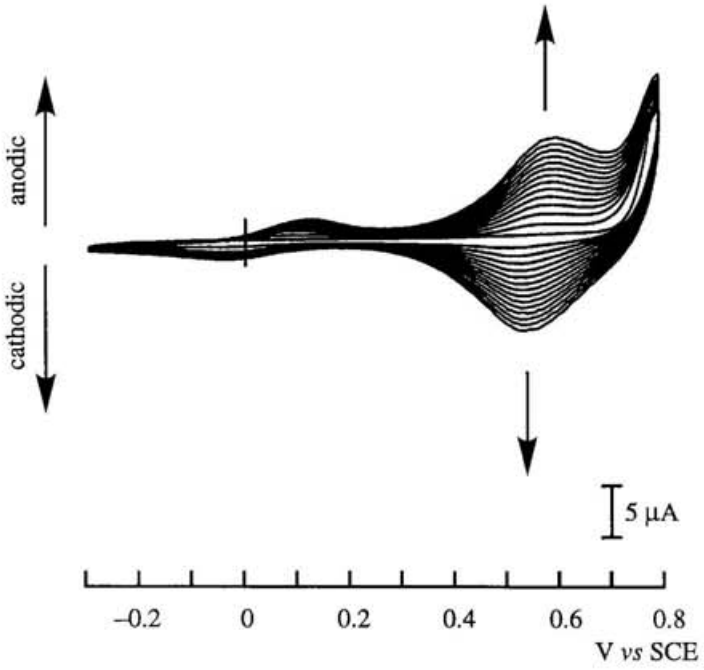
anodic
cathodic
5 μA
–0.2
0
0.2
0.4
0.6
0.8
V *vs* SCE

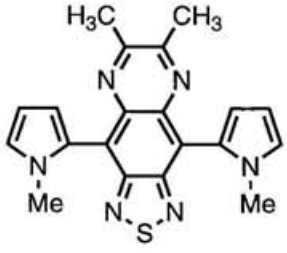
H3C
CH3
N
N
N
Me
N
S
N
N
Me

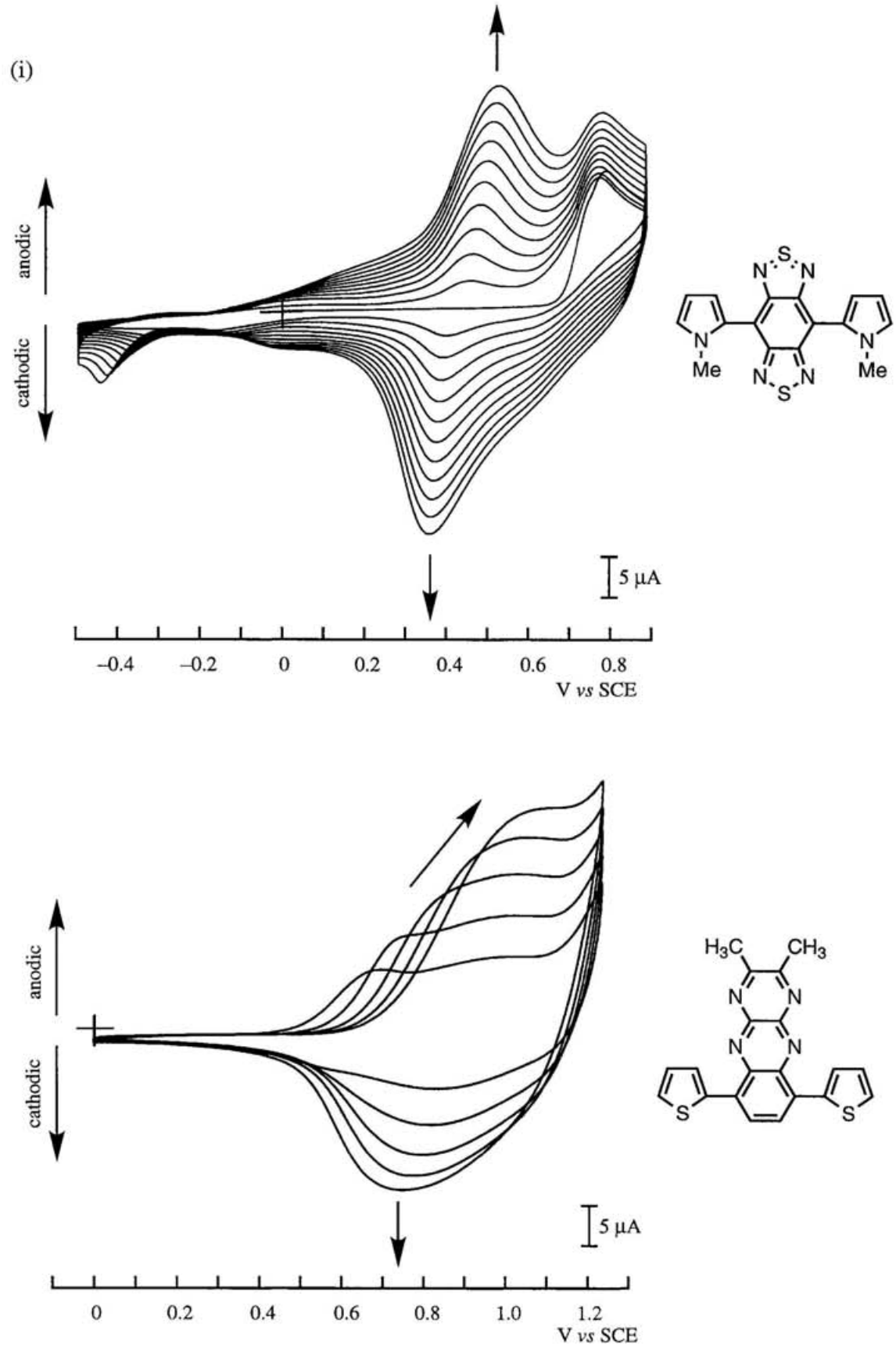


**Figure 2.** Multisweep cyclic voltammetry for the electropolymerization of **8** on a Pt disk in PhCN containing 0.1 mol $dm^{-3}$ $Bu_4NClO_4$, scan rate 100 mV $s^{-1}$. The waves were recorded every 10 minutes.

At that time, the changes of colors were clearly perceived in most of the polymers, indicating the changes of electronic states. In the dedoped state, the colors of the polymers were as follows: dark blue-green for the polymers of **2**, reddish purple for the polymers of **3**, violet for the polymer of **4**, dark green for the polymers of **5**, dark green for the polymer of **6**, dark blue-green for the polymer of **7**, reddish brown for the polymer of **8**, dark blue-violet for the polymers of **9**, and dark yellow-green for the polymer of **10**. All the polymers showed relatively high stability under normal conditions. While the surfaces of most of the polymers were powdery, those of the polymers with longer alkyl chains looked slightly smooth.

### 3.2.2 Electrochemistry and Electronic Spectra of Polymers

To examine the electrochemistry of the resulting polymers, cyclic voltammetry measurements on the polymers on a Pt disk were performed in PhCN with 0.1 mol $dm^{-3}$ $Bu_4NClO_4$ ($Bu_4NBF_4$ for the polymer of **6**) as a supporting electrolyte, at a scan rate of 10 mV $s^{-1}$ to avoid the shifts of peak potentials arising from the IR drop across the films. Cyclic voltammograms of all the polymers are depicted in Figures 3-18. Careful conditions (especially, purification of solvents and oxygen-free atmosphere) were indispensable for gaining reproducible clear cyclic voltammograms. Except for Figure 8, Figures 3a-18a show both p- and n-doping processes, and Figures 3b-18b display p- and n-doping processes separately. Such amphoteric properties are unusual since many polymers such as poly(thiophene) do not show n-doping process due to the instability at negative potentials. The shape of individual p- and n-doping waves in Figures 3a-18a was in almost agreement with that of p- and n-doping waves in Figures 3b-18b, indicating the stability of the doping process. No significant loss of electroactivity was seen after several cycles in every polymer except for the polymer of **3b** (Figure 8) . The characteristics of the resulting polymers are stated as follows.

As represented in Figure 3, almost all the polymers that possess thiophene units

showed redox waves in both p- and n-doping regions, indicating their amphoteric redox property similarly to the corresponding monomers. The p-doping redox wave was broad and irreversible, while the n-doping redox wave was sharp and quasi-reversible similarly to other narrow-bandgap polymers.[4] Within the same polymer backbone containing alkyl substituents, the polymer with shorter alkyl chains exhibited a sharper n-doping wave as seen among Figures 3-6, between Figures 7 and 8, and among Figures 10-12, respectively.

On the other hand, some exceptions were observed in Figures 15-18. The polymers of **8** (Figure 15) and **9a,b** (Figures 16 and 17) hardly exhibited n-doping charge probably due to the slow ion transport rate,[5] and the polymer of **10** (Figure 18) showed the decreasing tendency of n-doping waves with increasing potential sweeps. Although the polymer of **8** has thiophene units, the electrochemical behavior was considerably different from those of other polymers containing thiophene segments. This can be explained by considering that π-conjugation of the polymer was not extended sufficiently. The strange cyclic voltammogram of polymerization in Figure 2 supports this fact. The cyclic voltammograms of the polymers containing *N*-methylpyrrole segments differ from those of the polymers containing thiophene units. This fact may be ascribed to the difference in conformations along the polymer backbone because the monomers **9a,b** and **10** have nonplanar conformations in Chapter 2.

Another unique feature in the shape of doping waves is a prepeak. For example, Figure 3a showed a clear prepeak around 0.1 V *vs* SCE. On the other hand, the prepeak was not observed in Figure 3b that shows p- and n-doping separately. This prepeak would result from the ionic transport processes caused by the charge trapping,[5] which can be monitored by the electrochemical quartz crystal microbarance (EQCM) technique.[6] The other clear prepeaks were found around –1.1 V in Figure 6a, around 0.3 and –1.3 V in Figure 7a, and around 0.2 and –0.8 V in Figure 14a. On the other way, the n-doping processes can be seen in broad regions from 0 to –0.6 V in Figures 10-12 and from 0 to –0.3 V in Figure 13. The strange waves might be ascribed to the above charge trapping or the impurity levels due to structural defects and/or wide distributions of molecular weight. Work is in progress to investigate these phenomena.

It is generally accepted that the difference between p- and n-doping onset potentials can imply an electrochemically estimated bandgap.[7] The p-doping onset potentials of almost all the polymers containing thiophene units are found to start from about 0 V, while the n-doping onset potentials vary from about –0.4 to –1.4 V depending on the *o*-quinoid-acceptor moieties. n-Doping peaks also vary with the structure of *o*-quinoid-acceptor heterocycles. The n-doping cathodic peak potentials, n- and p- doping onset potentials, and electrochemical bandgaps are summarized in Table 2. The determined values of n-doping peak potentials are close to those of reduction peak potentials of the corresponding monomers (Table 2 in Chapter 2), indicating that the structures and properties of the *o*-quinoid-acceptor segments reflect characteristic features of the polymers. The estimated bandgap values (0.5-1.6 eV) suggest that the polymers are narrow bandgap polymers. Particularly, Figure 13 shows that

**Table 2.** Electrochemical properties of all the polymers of **2-10**.

| polymer | $E_{pc}$ / V[a] | $E_{onset}^{n\text{-dope}}$ / V[a] | $E_{onset}^{p\text{-dope}}$ / V[a] | $E_g$[b] / eV |
|---|---|---|---|---|
| poly(**2a**) | –1.33 | –0.9 | 0 | 0.9 |
| poly(**2b**) | –1.42 | –1.2 | 0 | 1.2 |
| poly(**2c**) | –1.40 | –1.2 | 0 | 1.2 |
| poly(**2d**) | –1.38 | –1.2 | 0.2 | 1.4 |
| poly(**3a**) | –1.74 | –1.4 | 0.2 | 1.6 |
| poly(**3b**) | not observed | not observed | not observed | not estimated |
| poly(**4**) | –1.38 | –1.1 | 0 .4 | 1.5 |
| poly(**5a**) | –0.78 | –0.6 | 0 | 0.6 |
| poly(**5b**) | –0.93 | –0.7 | 0.1 | 0.8 |
| poly(**5c**) | –0.92 | –0.7 | 0.1 | 0.8 |
| poly(**6**) | –0.68 | –0.4 | 0.1 | 0.5 |
| poly(**7**) | –1.19 | –0.9 | 0.2 | 1.1 |
| poly(**8**) | not observed | not observed | 0.5 | not estimated |
| poly(**9a**) | not observed | not observed | 0.1 | not estimated |
| poly(**9b**) | not observed | not observed | 0.2 | not estimated |
| poly(**10**) | –0.73 | –0.6 | –0.1 | 0.5 |

[a] 0.1 mol dm$^{-1}$ $Bu_4NClO_4$ [$Bu_4NBF_4$ for poly(**6**)] in PhCN, scan rate 10mV s$^{-1}$, V *vs* SCE. [b] Electrochemical bandgap.

the polymer of **6** has a markedly narrow bandgap. The order of decreasing electrochemical bandgaps corresponds roughly to that of decreasing LUMO energies of *o*-quinoid-acceptor segments in the monomers as shown in Figure 19.

In principle, the bandgap can be determined from electronic spectra using the relation of photon energy (in eV) = 1240 / $\lambda$ (in nm), where $\lambda$ is the onset of absorption.[8] Figures 20-35 show absorption spectra of the polymers of **2-10** as a function of potential at 0.2 V intervals from 0 to 1.0 V.[9]

For the polymer of **2a**, the onset was seen at about 0.6 eV in Figure 20,[10] that is, the bandgap was 0.6 eV. As the polymer was oxidized electrochemically, a new absorption band around 1.1 eV appeared and developed. In proportion to that, an electrochromic phenomenon was observed where the color changed from dark blue-green to transparent blue-black. For the polymer of **2b**, though the onset is seen at about 1.0 eV in Figure 21, the curve from 1 to 1.4 eV seems to be attributed to residual p-doping. Therefore, it is appropriate to regard that the bandgap was about 1.3 eV. For the polymers of **2c,d**, the same tendency was observed in Figures 22 and 23. Both the bandgaps would be 1.3 eV. The polymers of **2b-d** also exhibited the same electrochromic phenomena as the polymer of **2a**. The polymers with alkyl substituents showed large bandgap values. Since the electronic effect of alkyl groups is expected to be small, steric circumstances might be different.

For the polymers of **3a,b** and **4**, the above tendency was observed in Figures 24-26. Their bandgaps were estimated to be 1.7, 1.8 and 1.6 eV, respectively. As the polymers of **3a,b** were oxidized electrochemically, the colors changed from reddish purple to violet. In contrast, as the polymers of **4** were oxidized electrochemically, the color changed from violet to transparent blue-black.

For the polymers of **5a-c**, as shown in Figures 27-29, their bandgaps were estimated to be 0.5, 0.5, and 0.6 eV, respectively. The polymers showed little electrochromic phenomena. Thus, their colors were unchanged from dark green even when oxidized electrochemically. Figures 27-29 exhibit the growth of the absorption in the region ranging from 0.5 to 1.5 eV with electrochemically oxidizing.

For the polymer of **6**, the bandgap was estimated to be 0.5 eV from Figure 30. The

electrochemical behavior of the polymer of **6** resembled those of the polymers of **5**. Thus, as the polymer was oxidized electrochemically, the color changed slightly from dark green to dark somewhat-bluish green, and the absorption intensity increased in the region ranging from 0.5 to 1.0 eV.

For the polymer of **7**, the absorption spectra as shown in Figure 31 displayed the different tendency from Figures stated above. The absorption in the region above 1.8 eV may be mainly based on those of oligomers (dimer or tetramer). The bandgap was estimated to be 0.8 eV from the onset of absorbance. An electrochromic phenomenon was observed that the color changed from dark blue-green to dark brown-green as the polymer of **7** was oxidized electrochemically. Then, the peak around 1.3 eV diminished, and a new peak around 1.0 eV emerged and grew up.

For the polymer of **8**, no clear absorption bands but gentle curves were observed as shown in Figure 32. However, as the polymer was oxidized electrochemically, the color changed from reddish brown to brown, and a new absorption band appeared and developed. Since Figure 32 did not exhibit the absorption peak beyond the monomer **8** (2.32 eV, in Table 2 in Chapter 2), the polymer of **8** would be electroactive deposits without extended $\pi$-conjugation. Therefore, the bandgap was not estimated.

For the polymers of **9a,b**, as shown in Figures 33 and 34, their bandgaps were estimated to be 0.6 and 0.8 eV, respectively. As the polymers were oxidized electrochemically, an absorption peak around 1.1 eV appeared and the absorption developed in all region. However, their colors were unchanged from dark blue-violet similarly to the polymers of **5**. The absorption bands around 1.7 eV may be ascribed to those of oligomers.

For the polymer of **10**, the bandgap was estimated to be 0.6 eV from Figure 35. As the polymer was oxidized electrochemically, all the absorption region increased, and the color changed from dark yellow-green to dark green. The tendency for the change of the absorbance was similar to that for the polymers of **9**.

The bandgaps of the series of the polymers are summarized in Table 3. The bandgap values ranged from 0.5 to 1.8 eV. The bandgap of 0.5 eV is one of the narrowest bandgaps[11,12] among the polymers reported so far. It was observed that the optical

**Table 3.** Optical bandgaps of the polymers of **2-10**.

| polymer | $E_g$ / eV |
|---|---|
| poly(**2a**) | 0.6 |
| poly(**2b**) | 1.3 |
| poly(**2c**) | 1.3 |
| poly(**2d**) | 1.3 |
| poly(**3a**) | 1.7 |
| poly(**3b**) | 1.8 |
| poly(**4**) | 1.6 |
| poly(**5a**) | 0.5 |
| poly(**5b**) | 0.5 |
| poly(**5c**) | 0.6 |
| poly(**6**) | 0.5 |
| poly(**7**) | 0.8 |
| poly(**8**) | not estimated |
| poly(**9a**) | 0.6 |
| poly(**9b**) | 0.8 |
| poly(**10**) | 0.6 |

bandgaps in Tables 3 were in approximate accord with the electrochemical bandgaps in Table 2 as shown in Figure 36. When the values were compared with the polymers containing thiophene segments, the order of increasing bandgaps was poly(**6**) ≤ poly(**5**) < poly(**7**) < poly(**2**) < poly(**4**) < poly(**3**) and was approximately comparable to the order of increasing absorption maxima of the corresponding monomers in eV: **6** < **5** < **8** < **2** < **7** < **4** < **3** (in Table 2 in Chapter 2) as shown in Figure 37. Furthermore, the order of decreasing optical bandgaps corresponded nearly to that of decreasing LUMO energies of *o*-quinoid-acceoptor segments (Figure 38). These results revealed that the molecular design of mixing aromatic-donor and *o*-quinoid-acceptor segments is effective to reduce both HOMO-LUMO gaps and bandgaps. Accordingly, it was elucidated that the introduction of *o*-quinoid-acceptor units with lower LUMO level is powerful strategy. On the other hand, in the case of the polymers

with *N*-methylpyrrole as aromatic-donor segment, regardless of its higher HOMO level, their bandgaps (the polymers of **9** and **10**) were slightly inferior to the polymers with thiophene (the polymers of **5** and **6**) similarly to the comparison of the corresponding monomers. This result would be also ascribed to the difference in conformations between intrachain segments. Conclusively, it was elucidate that the molecular design adopted in this thesis produced new narrow-bandgap systems effectively and that the structural modification tuned the bandgaps subtly.

At the present stage, the *o*-quinoid-acceptor segment has reached to the supreme level. To obtain further-narrower-bandgap polymers in the future, the development of new strong aromatic-donor segments and the various combination of aromatic-donor and *o*-quinoid acceptor segments, for example, $[\text{–A–Q–A–Q–}]_n$ and $[\text{–A–A–Q–Q–A–A–Q–Q–}]_n$ (A: an aromatic-donor unit, Q: an *o*-quinoid-acceptor unit) will be potential. To elucidate the information about the precise structures, characterization of the polymers will be required in more details.

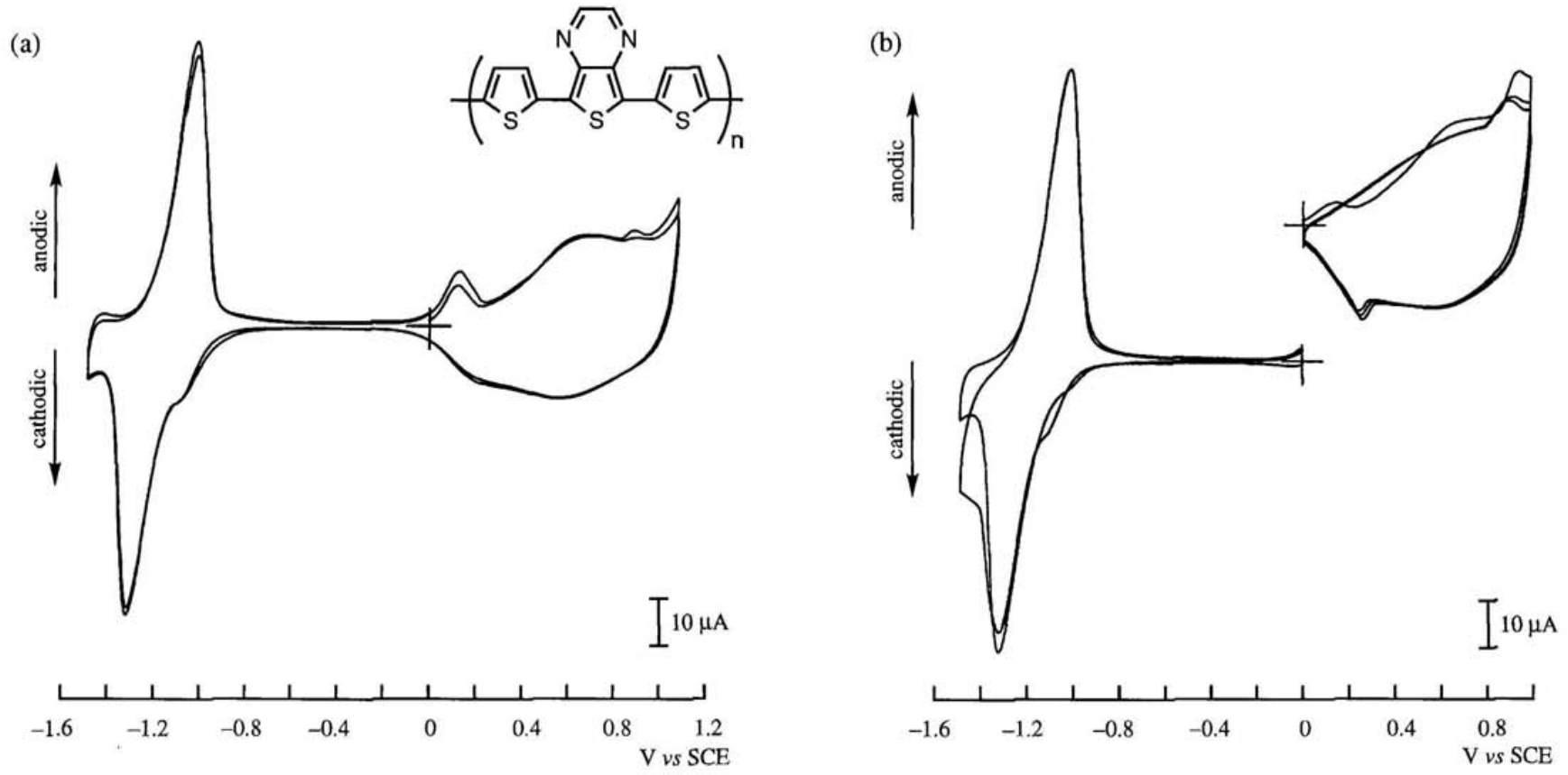


**Figure 3.** Cyclic voltammograms of the polymer of **2a** on a Pt disk in PhCN containing 0.1 mol $dm^{-3}$ $Bu_4NClO_4$, scan rate 10 mV $s^{-1}$, showing (a) both p- and n-doping, and (b) p- and n-doping separately.

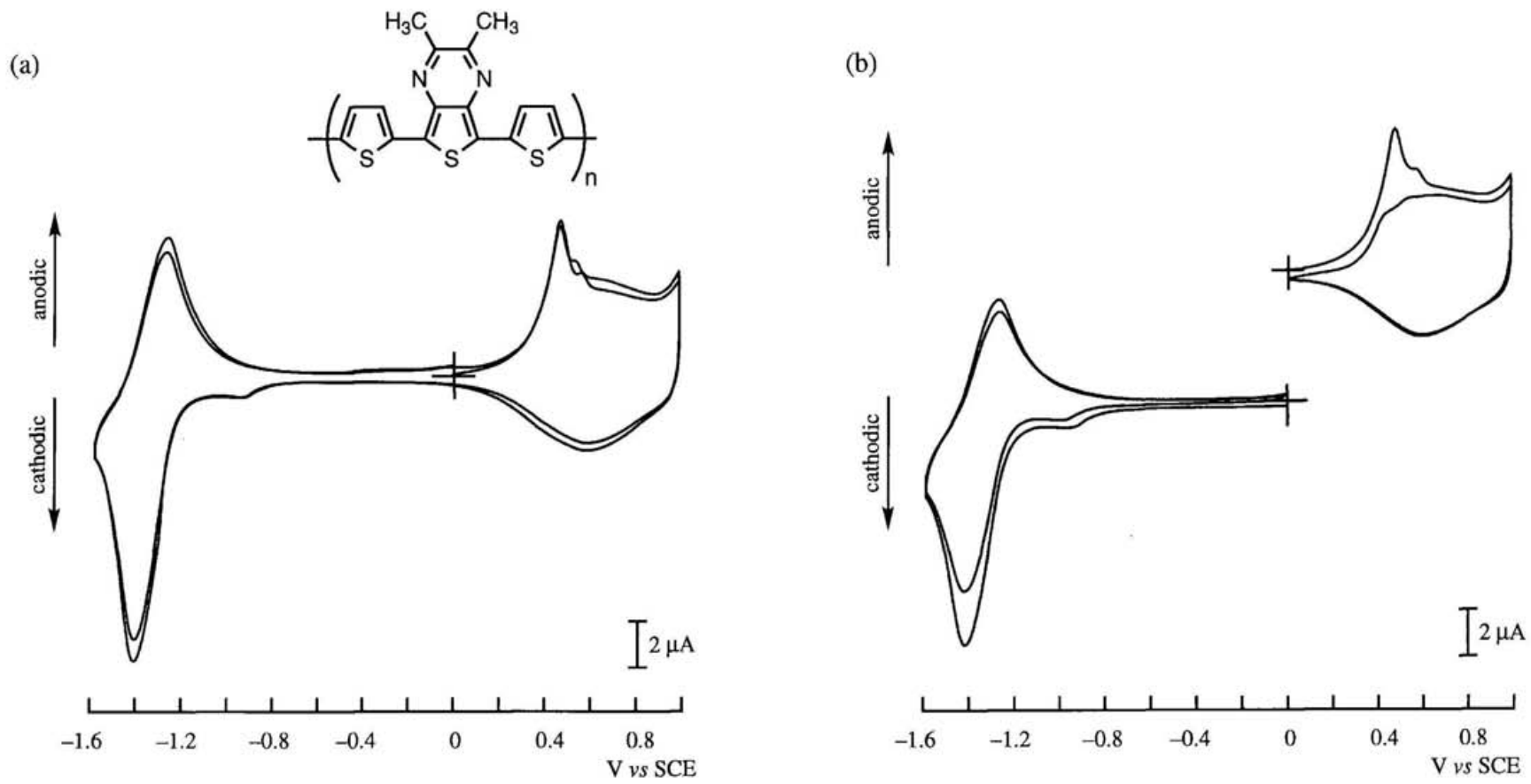


**Figure 4.** Cyclic voltammograms of the polymer of **2b** on a Pt disk in PhCN containing 0.1 mol $dm^{-3}$ $Bu_4NClO_4$, scan rate 10 mV $s^{-1}$, showing (a) both p- and n-doping, and (b) p- and n-doping separately.

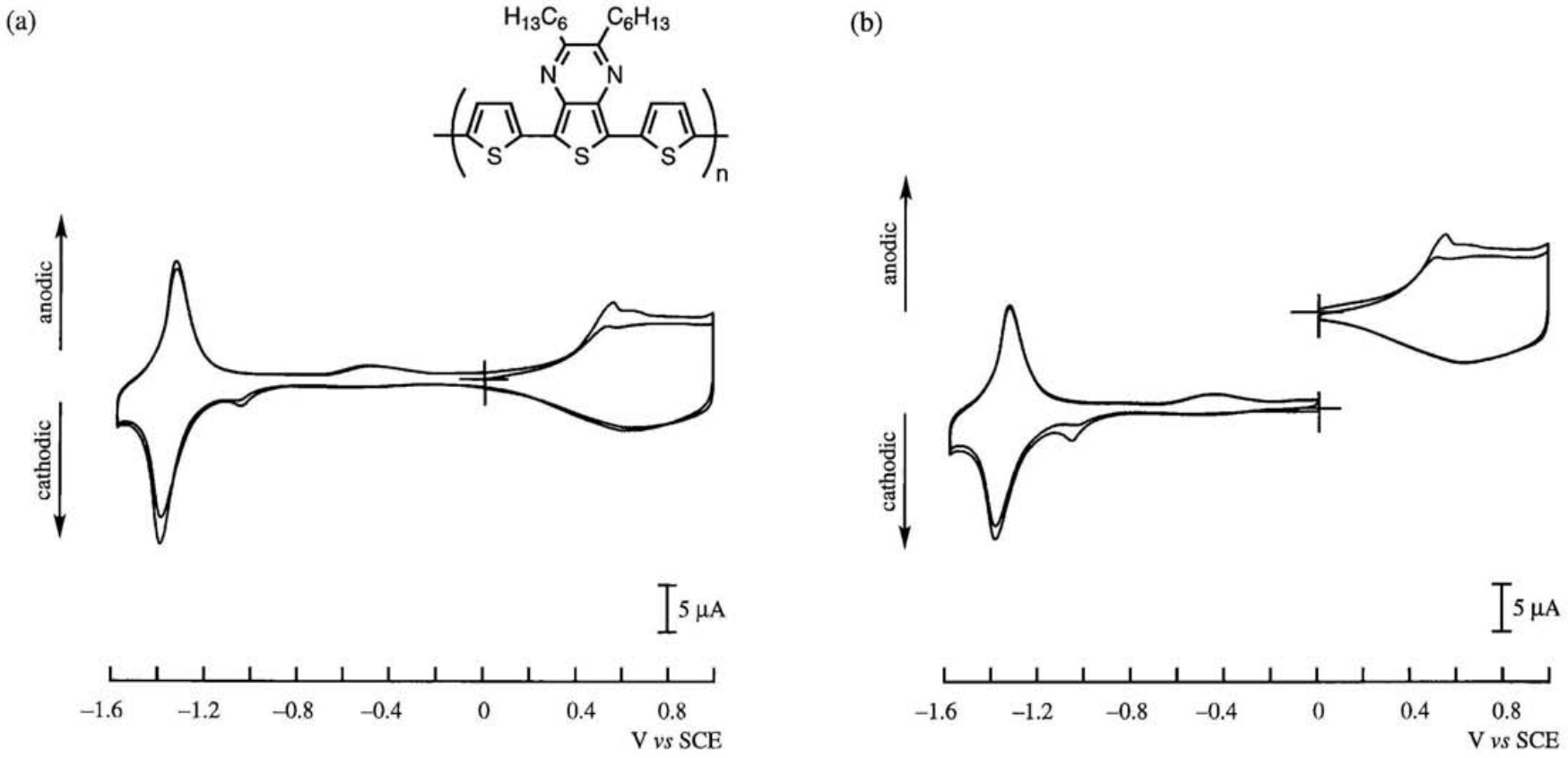


**Figure 5.** Cyclic voltammograms of the polymer of **2c** on a Pt disk in PhCN containing 0.1 mol $dm^{-3}$ $Bu_4NClO_4$, scan rate 10 mV $s^{-1}$, showing (a) both p- and n-doping, and (b) p- and n-doping separately.

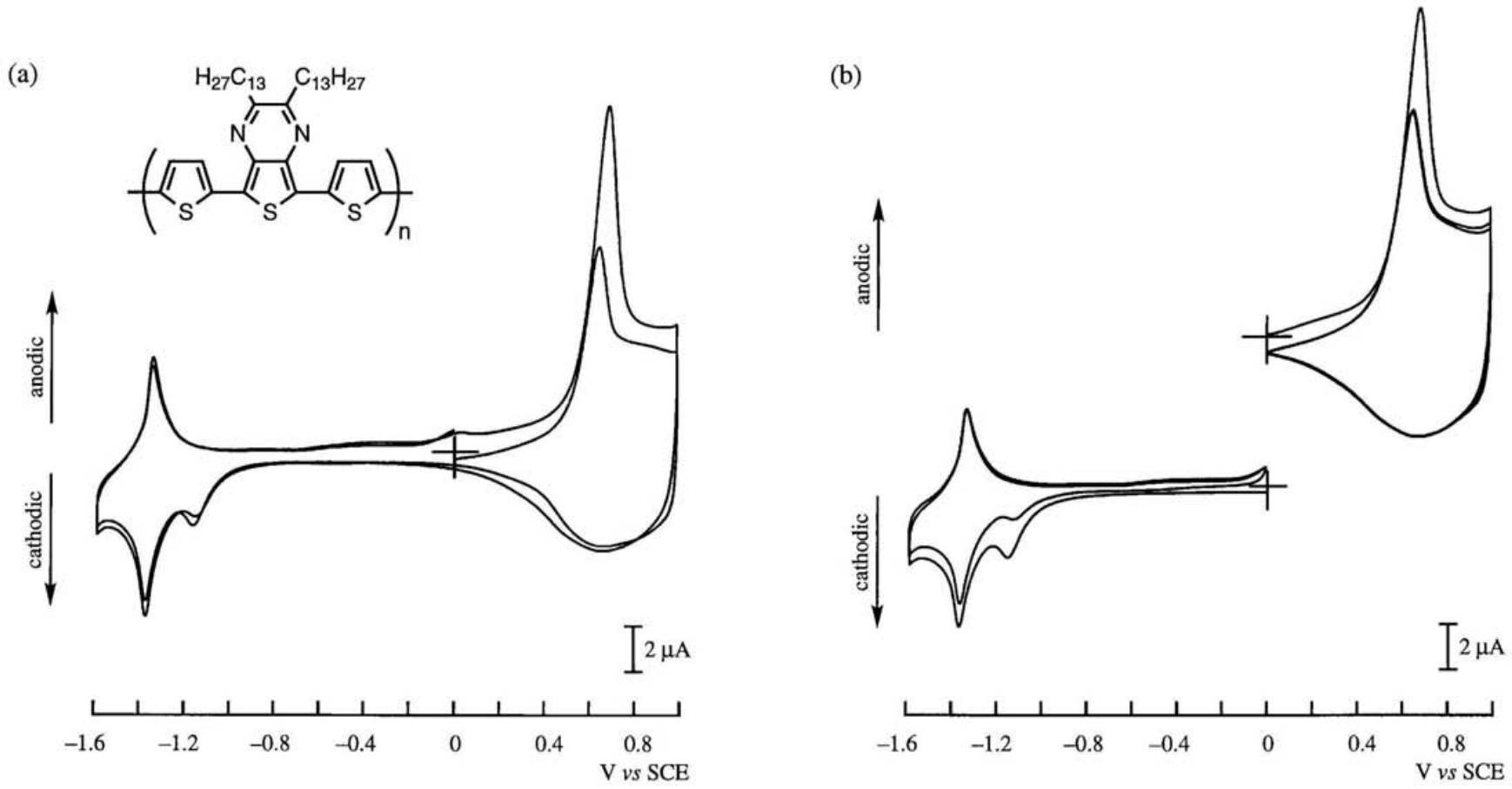


**Figure 6.** Cyclic voltammograms of the polymer of **2d** on a Pt disk in PhCN containing 0.1 mol $dm^{-3}$ $Bu_4NClO_4$, scan rate 10 mV $s^{-1}$, showing (a) both p- and n-doping, and (b) p- and n-doping separately.

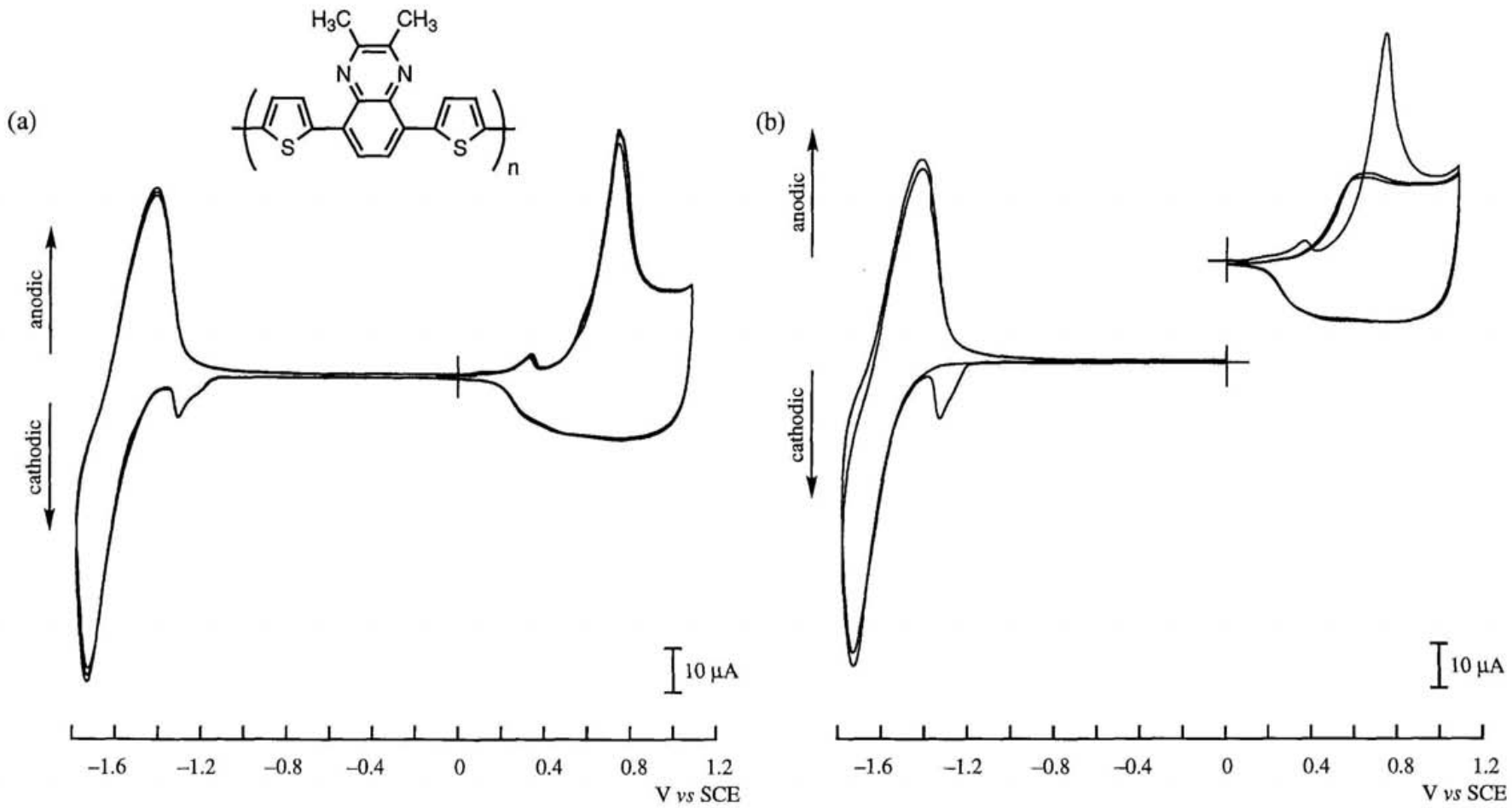


**Figure 7.** Cyclic voltammograms of the polymer of **3a** on a Pt disk in PhCN containing 0.1 mol $dm^{-3}$ $Bu_4NClO_4$, scan rate 10 mV $s^{-1}$, showing (a) both p- and n-doping, and (b) p- and n-doping separately.

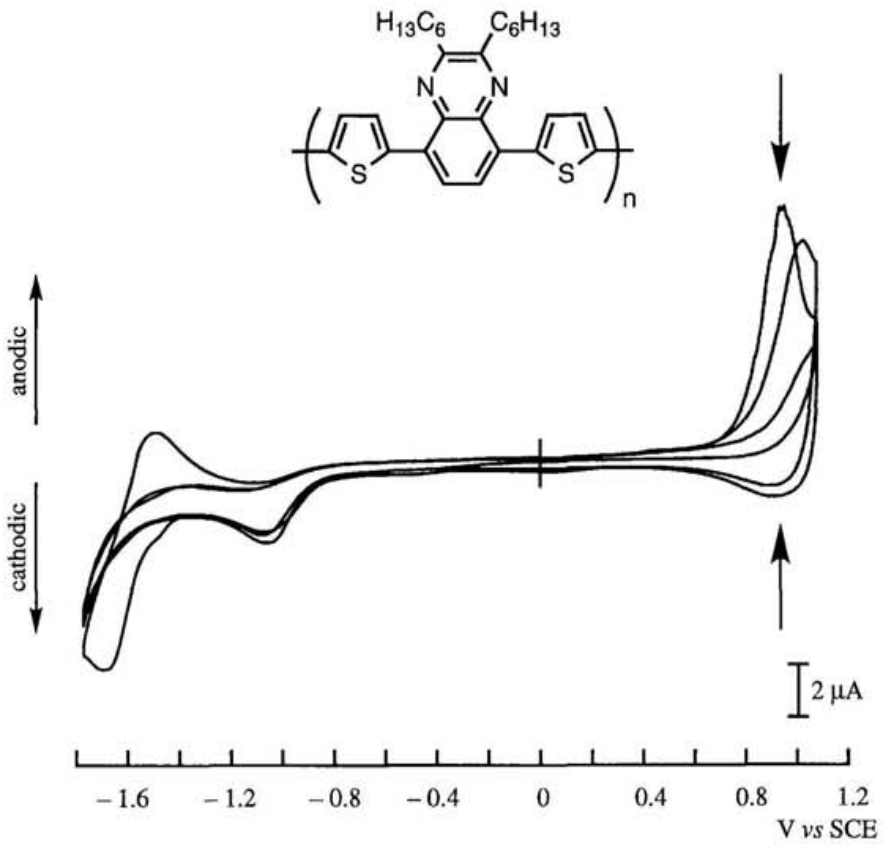


**Figure 8.** Cyclic voltammogram of the polymer of **3b** on a Pt disk in PhCN containing 0.1 mol $dm^{-3}$ $Bu_4NClO_4$, scan rate 10 mV $s^{-1}$, showing both p- and n-doping.

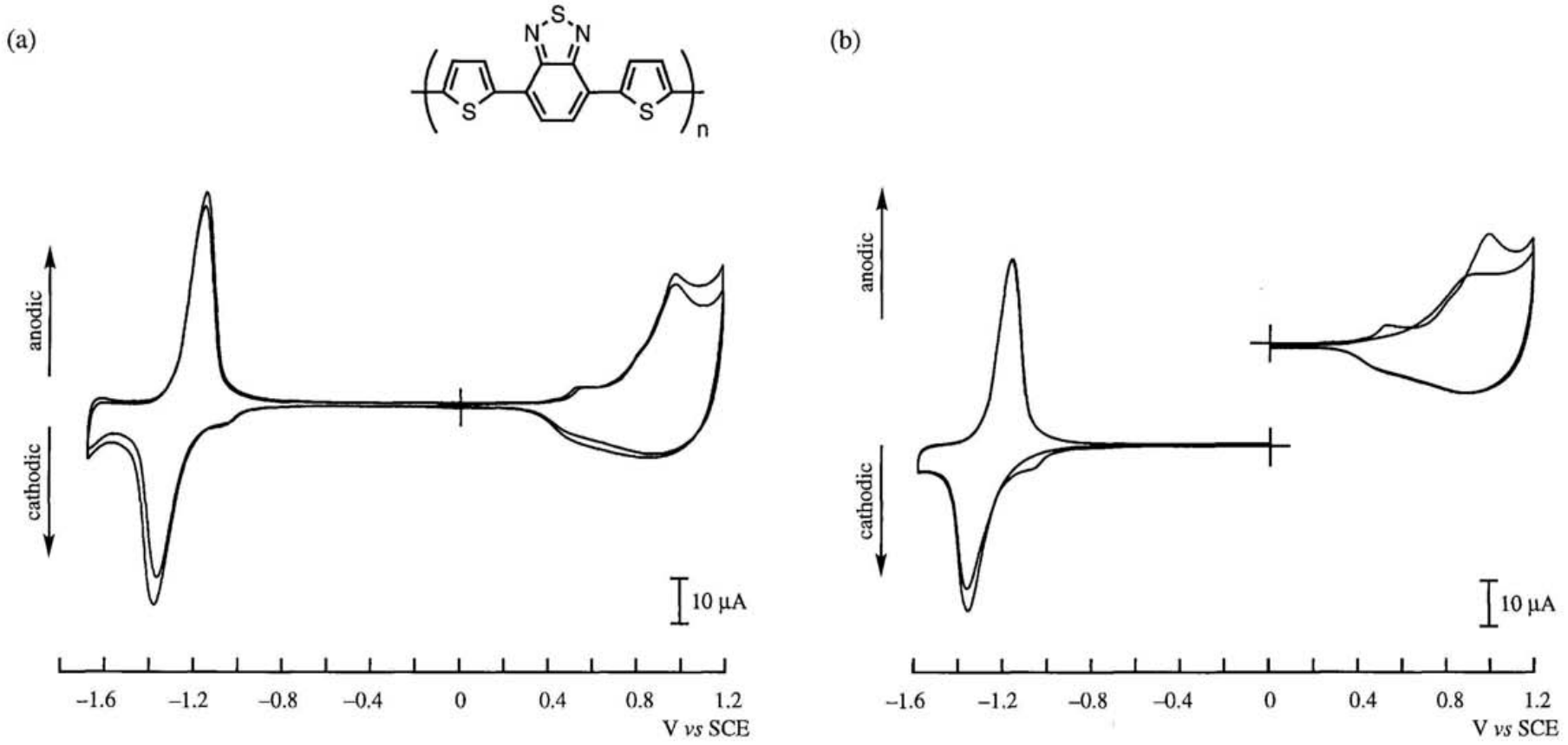


**Figure 9.** Cyclic voltammograms of the polymer of **4** on a Pt disk in PhCN containing 0.1 mol $dm^{-3}$ $Bu_4NClO_4$, scan rate 10 mV $s^{-1}$, showing (a) both p- and n-doping, and (b) p- and n-doping separately.

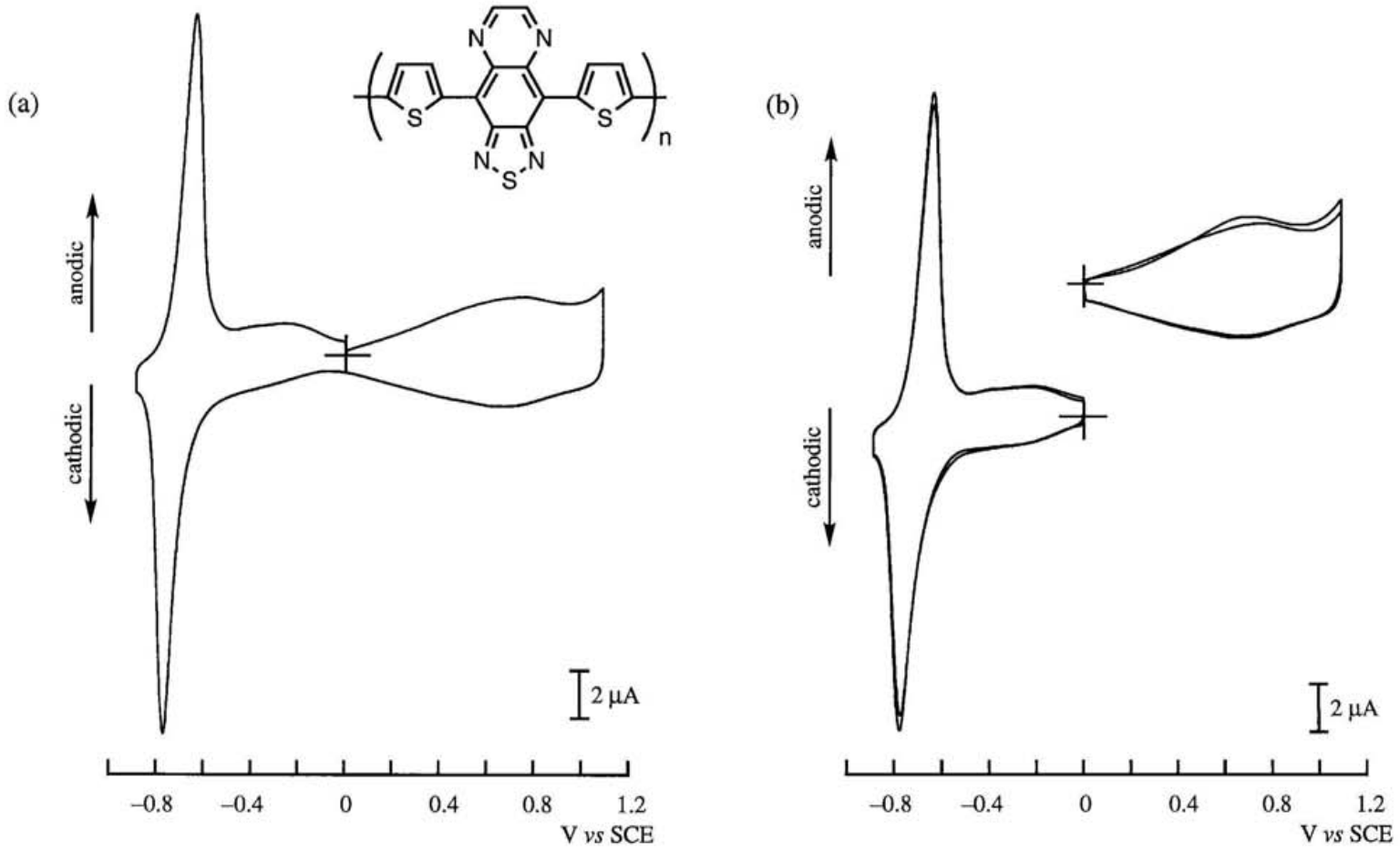


**Figure 10.** Cyclic voltammograms of the polymer of **4a** on a Pt disk in PhCN containing 0.1 mol $dm^{-3}$ $Bu_4NClO_4$, scan rate 10 mV $s^{-1}$, showing (a) both p- and n-doping, and (b) p- and n-doping separately.

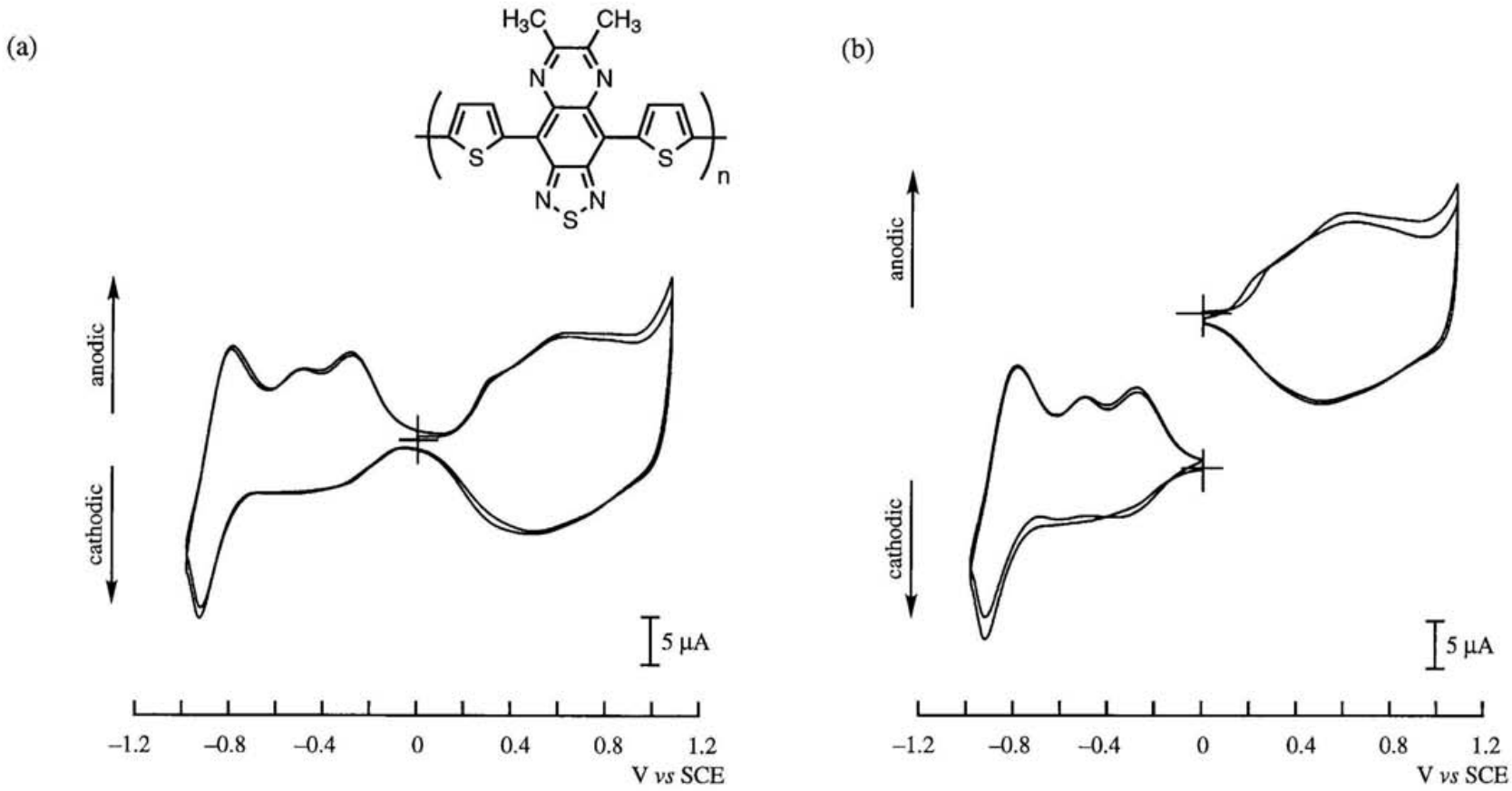


**Figure 11.** Cyclic voltammograms of the polymer of **5b** on a Pt disk in PhCN containing 0.1 mol $dm^{-3}$ $Bu_4NClO_4$, scan rate 10 mV $s^{-1}$, showing (a) both p- and n-doping, and (b) p- and n-doping separately.

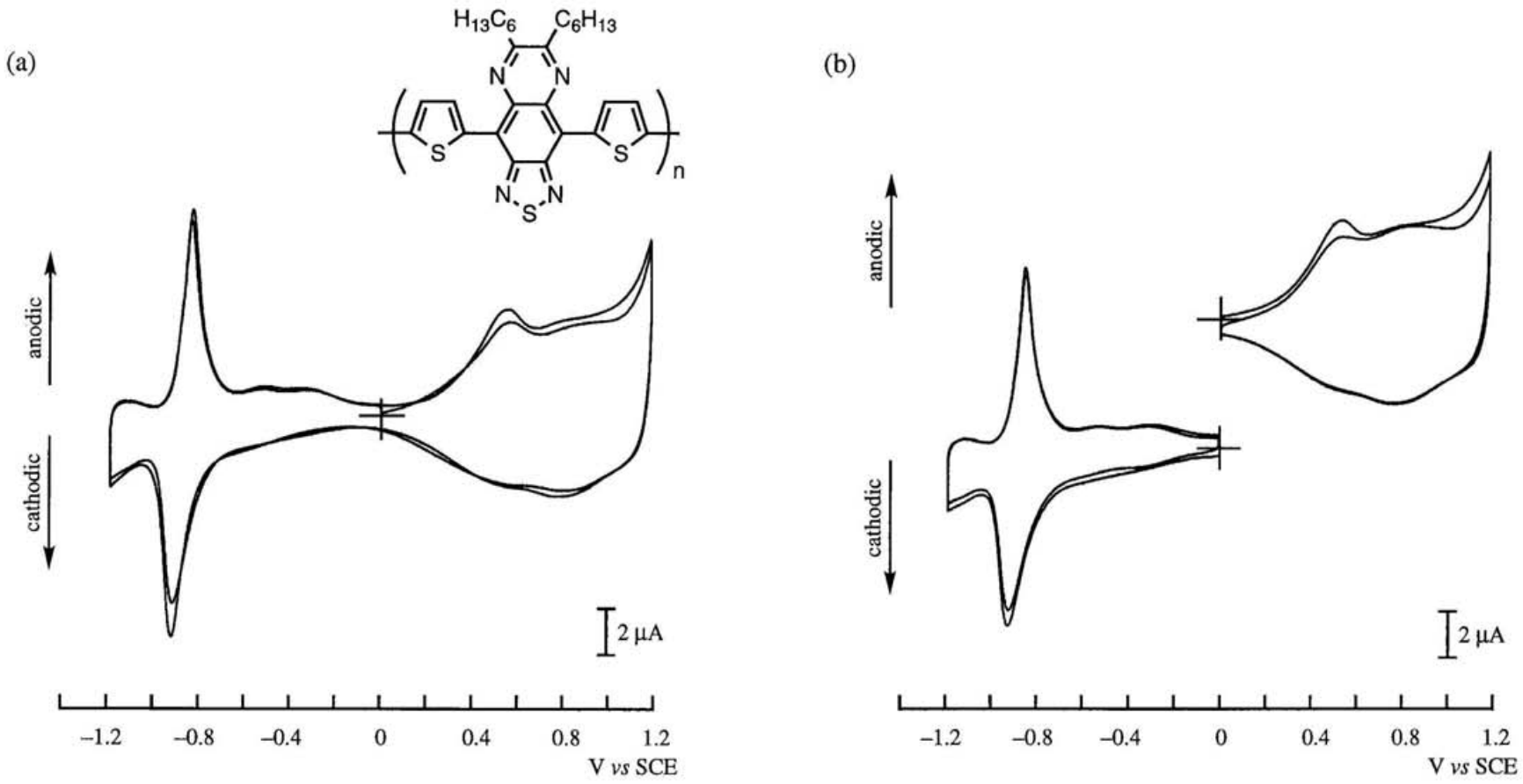


**Figure 12.** Cyclic voltammograms of the polymer of **5c** on a Pt disk in PhCN containing 0.1 mol $dm^{-3}$ $Bu_4NClO_4$, scan rate 10 mV $s^{-1}$, showing (a) both p- and n-doping, and (b) p- and n-doping separately.

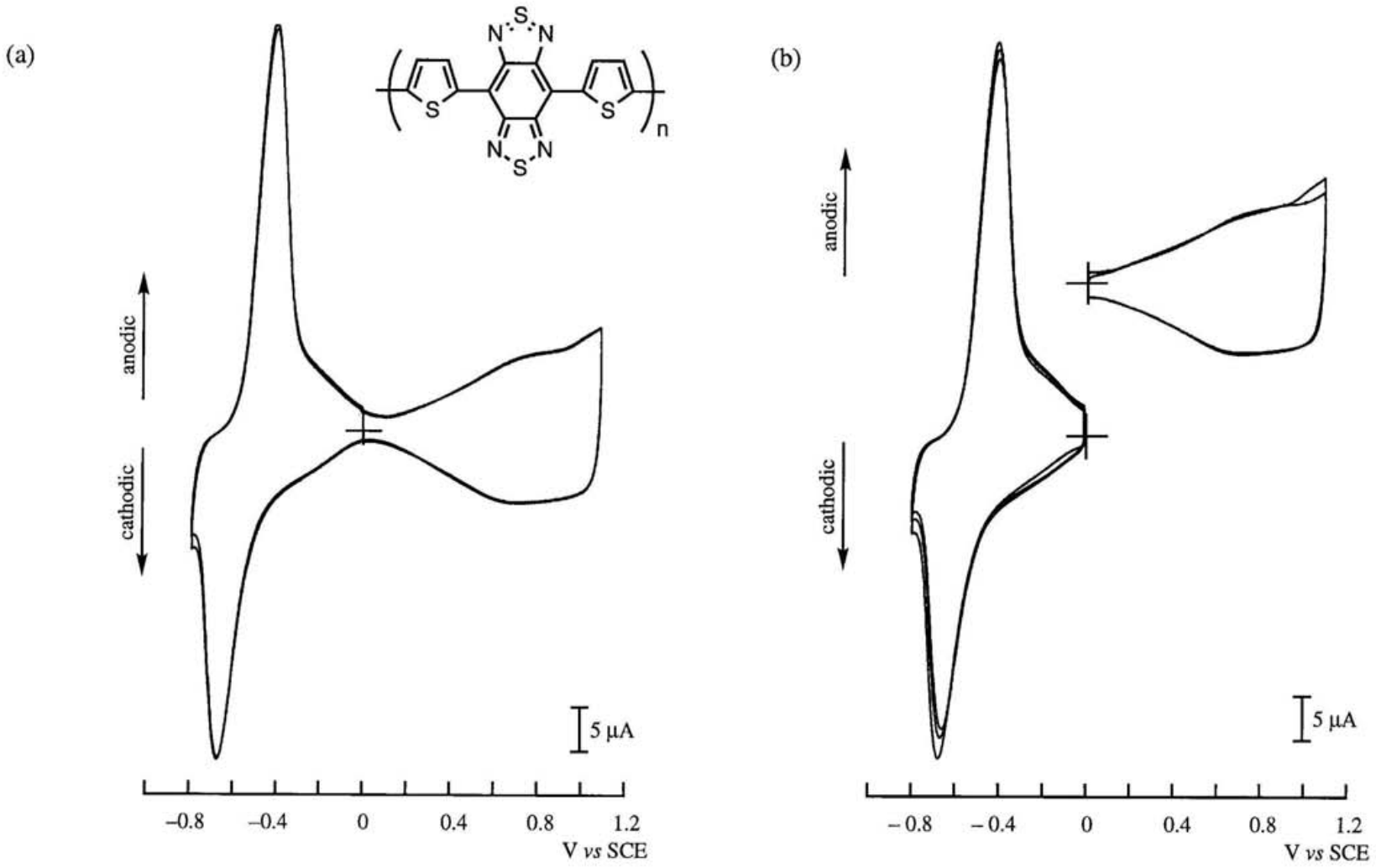


**Figure 13.** Cyclic voltammograms of the polymer of **6** on a Pt disk in PhCN containing 0.1 mol $dm^{-3}$ $Bu_4BF_4$, scan rate 10 mV $s^{-1}$, showing (a) both p- and n-doping, and (b) p- and n-doping separately.

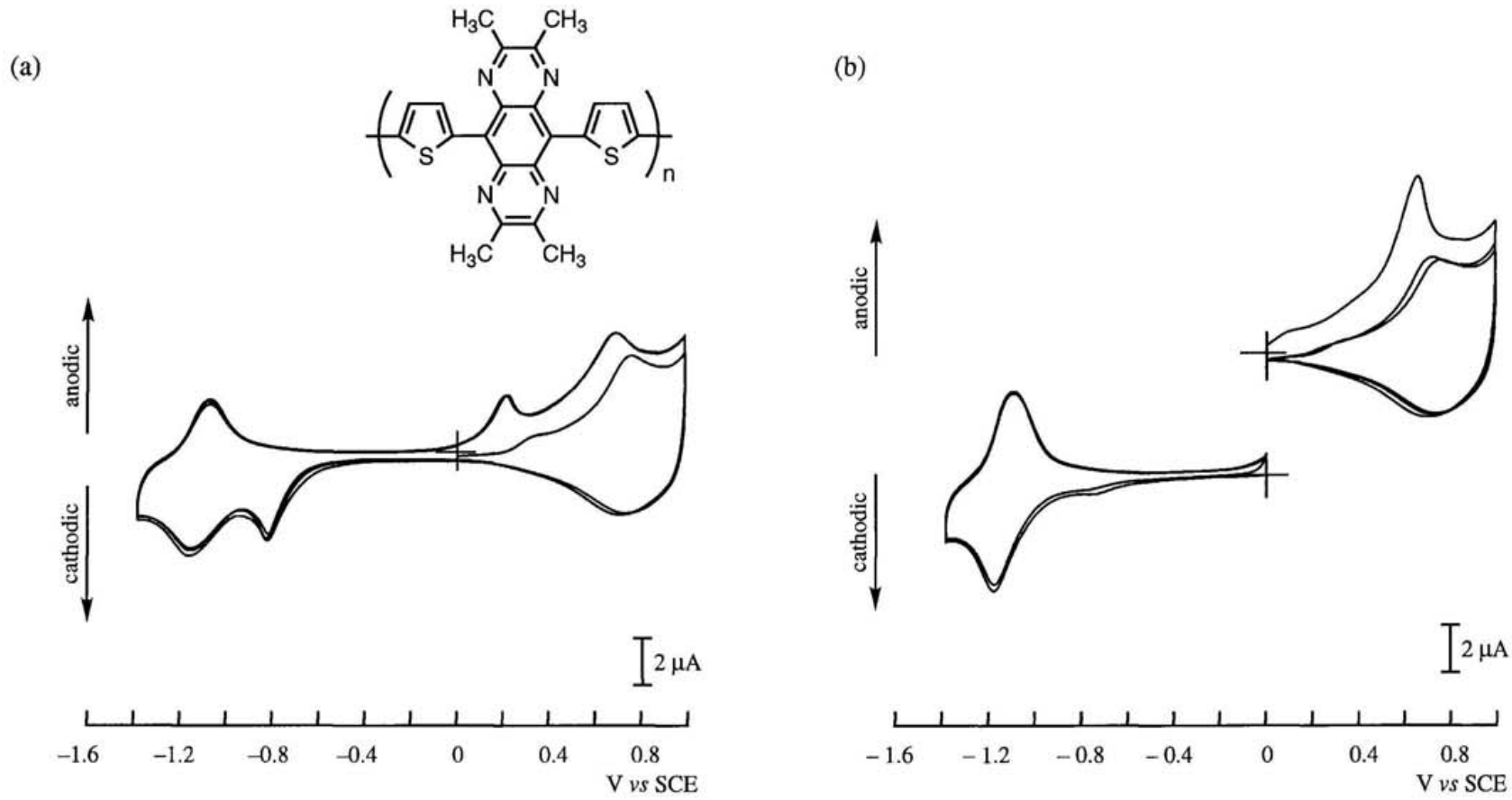


**Figure 14.** Cyclic voltammograms of the polymer of **7** on a Pt disk in PhCN containing 0.1 mol $dm^{-3}$ $Bu_4NClO_4$, scan rate 10 mV $s^{-1}$, showing (a) both p- and n-doping, and (b) p- and n-doping separately.

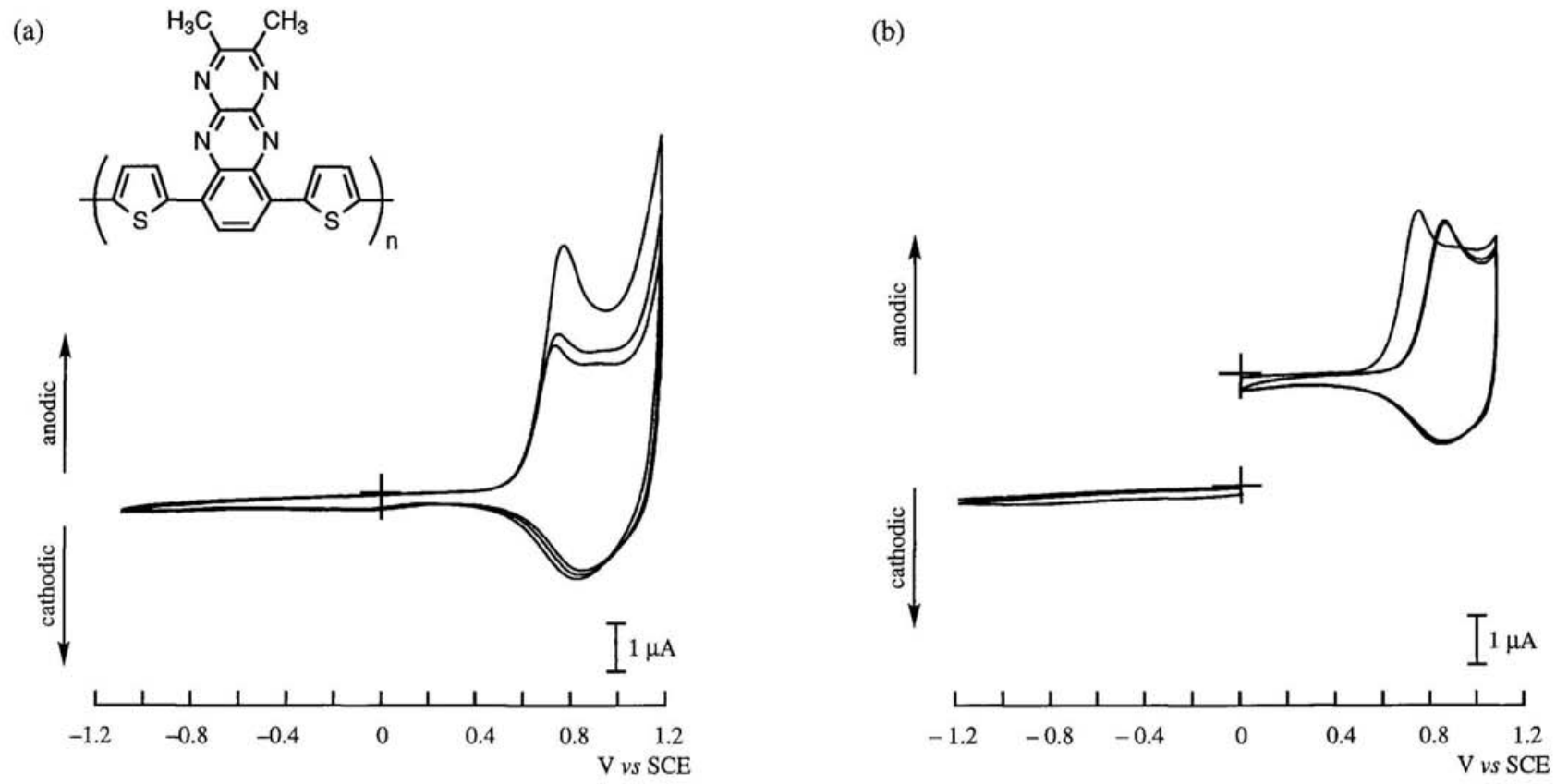


**Figure 15.** Cyclic voltammograms of the polymer of **8** on a Pt disk in PhCN containing 0.1 mol $dm^{-3}$ $Bu_4NClO_4$, scan rate 10 mV $s^{-1}$, showing (a) both p- and n-doping, and (b) p- and n-doping separately.

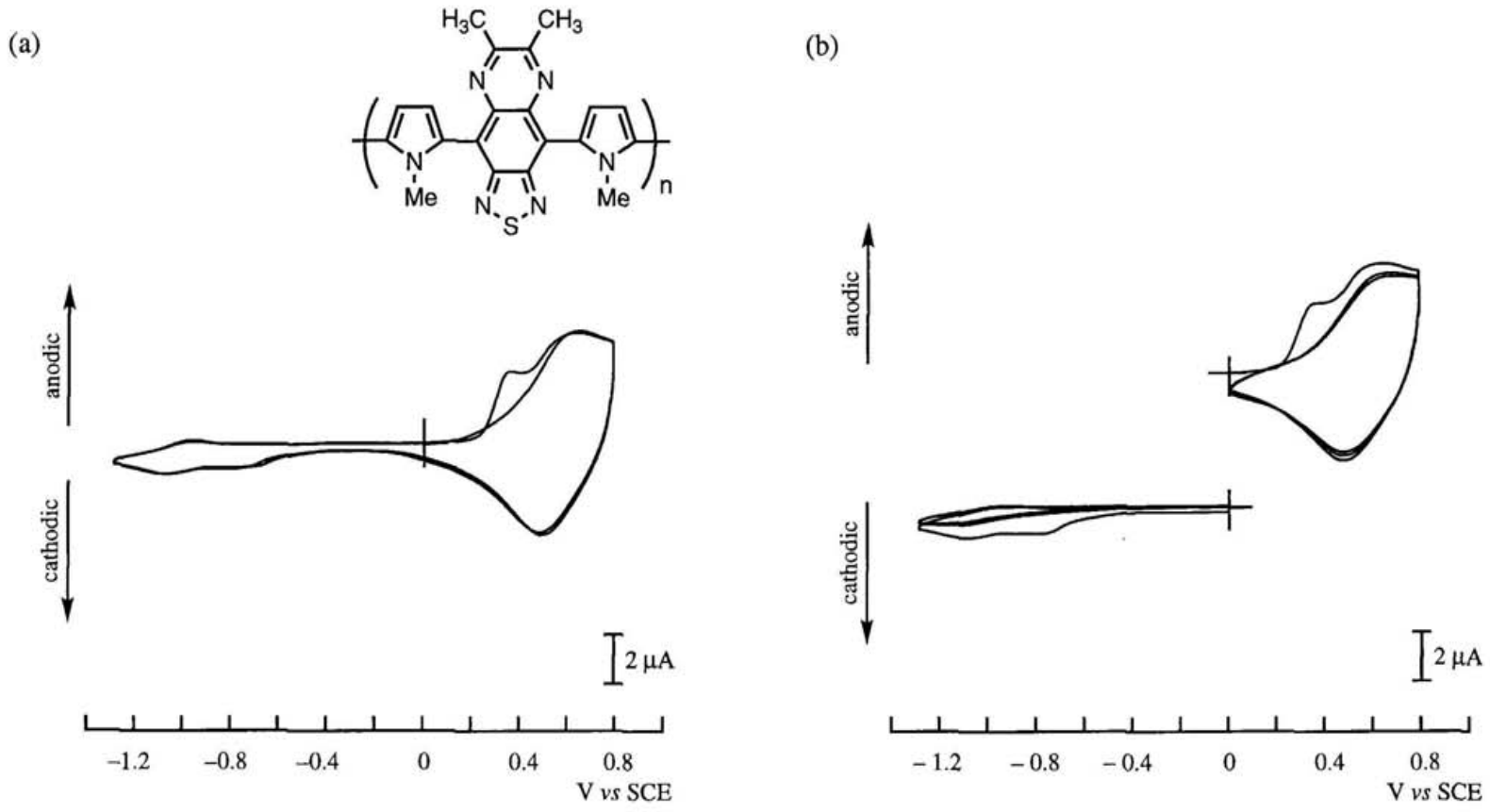


**Figure 16.** Cyclic voltammograms of the polymer of **9a** on a Pt disk in PhCN containing 0.1 mol $dm^{-3}$ $Bu_4NClO_4$, scan rate 10 mV $s^{-1}$, showing (a) both p- and n-doping, and (b) p- and n-doping separately.

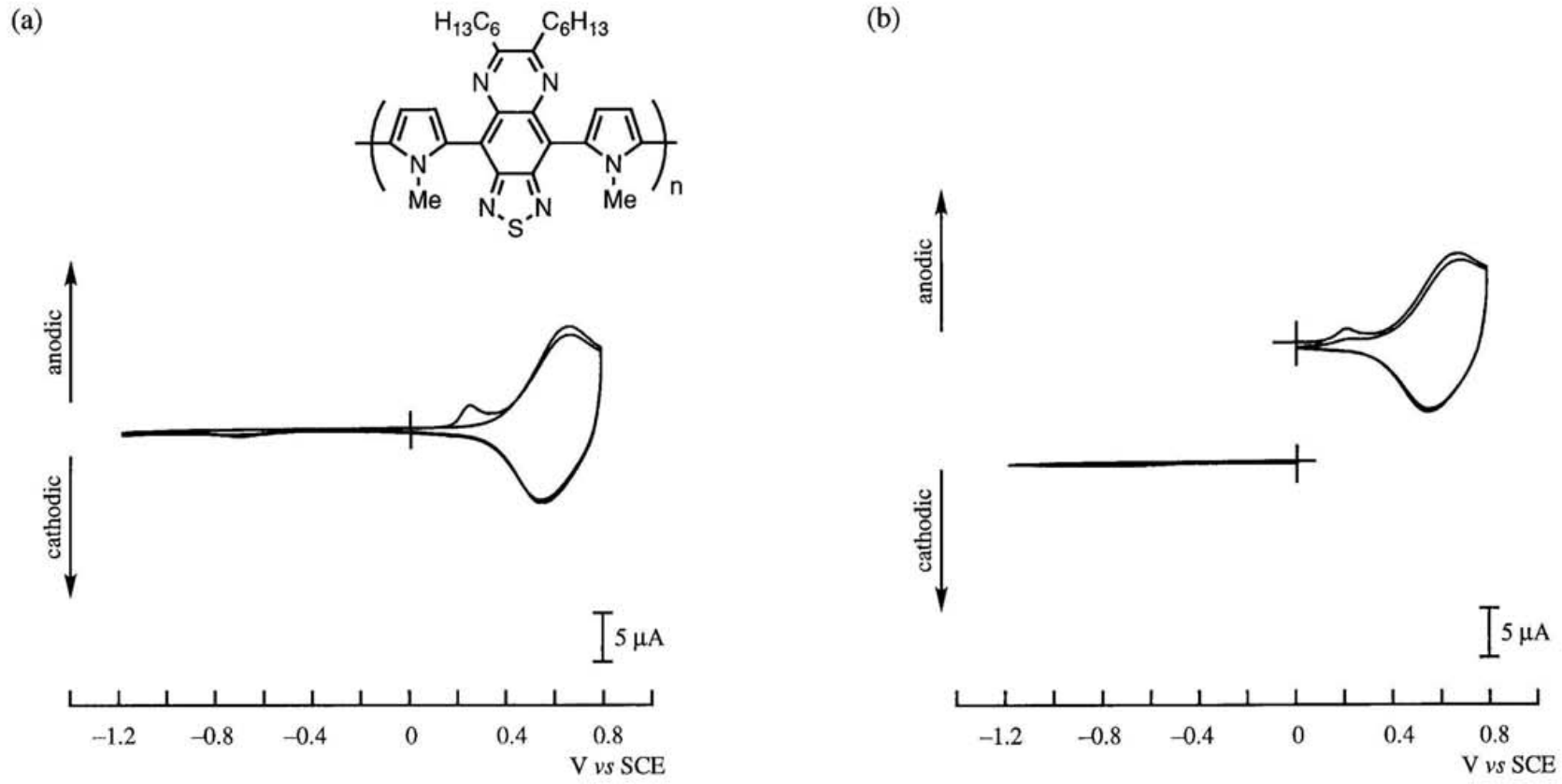


**Figure 17.** Cyclic voltammograms of the polymer of **9b** on a Pt disk in PhCN containing 0.1 mol $dm^{-3}$ $Bu_4NClO_4$, scan rate 10 mV $s^{-1}$, showing (a) both p- and n-doping, and (b) p- and n-doping separately.

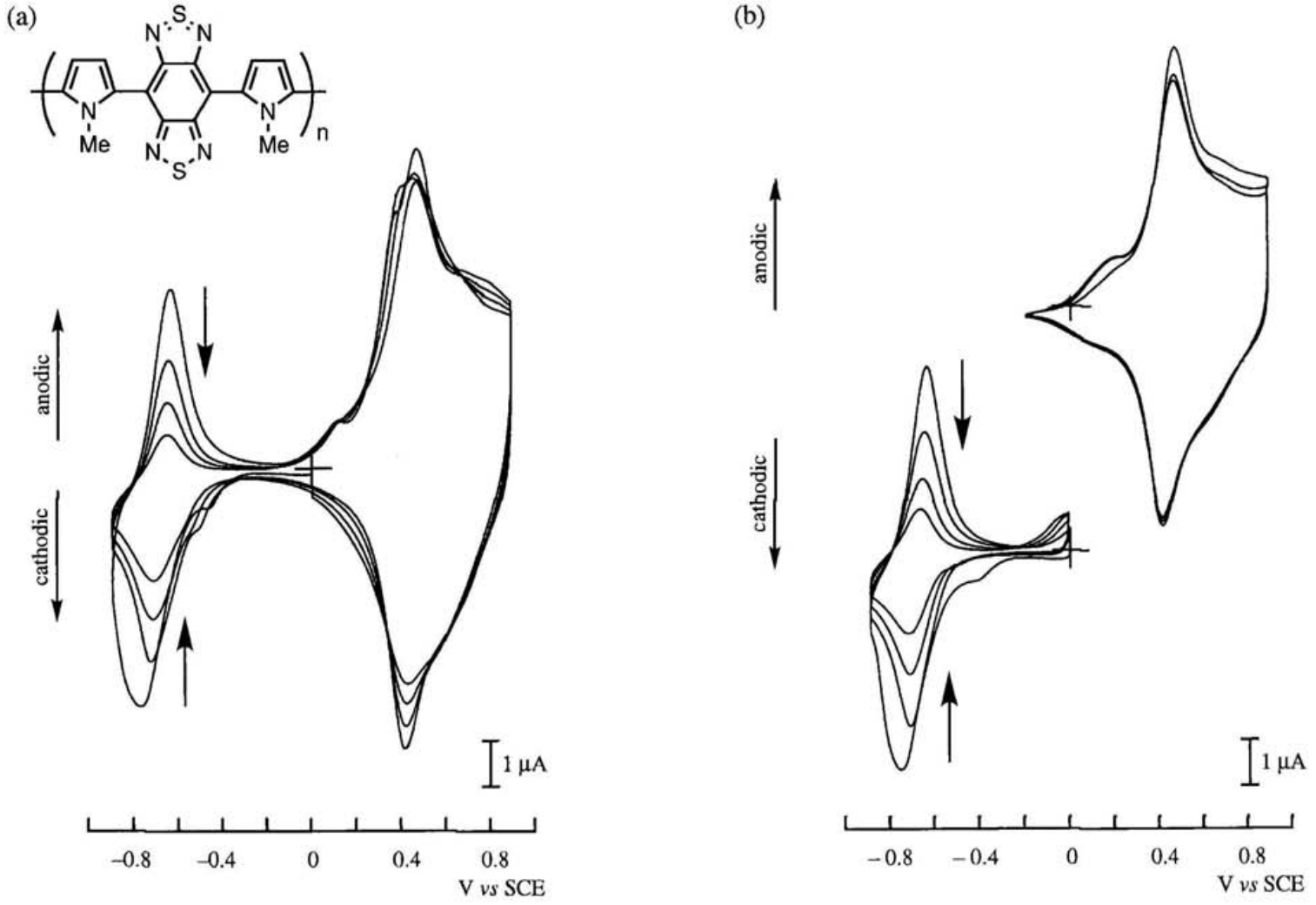


**Figure 18.** Cyclic voltammograms of the polymer of **10** on a Pt disk in PhCN containing 0.1 mol $dm^{-3}$ $Bu_4NClO_4$, scan rate 10 mV $s^{-1}$, showing (a) both p- and n-doping, and (b) p- and n-doping separately.

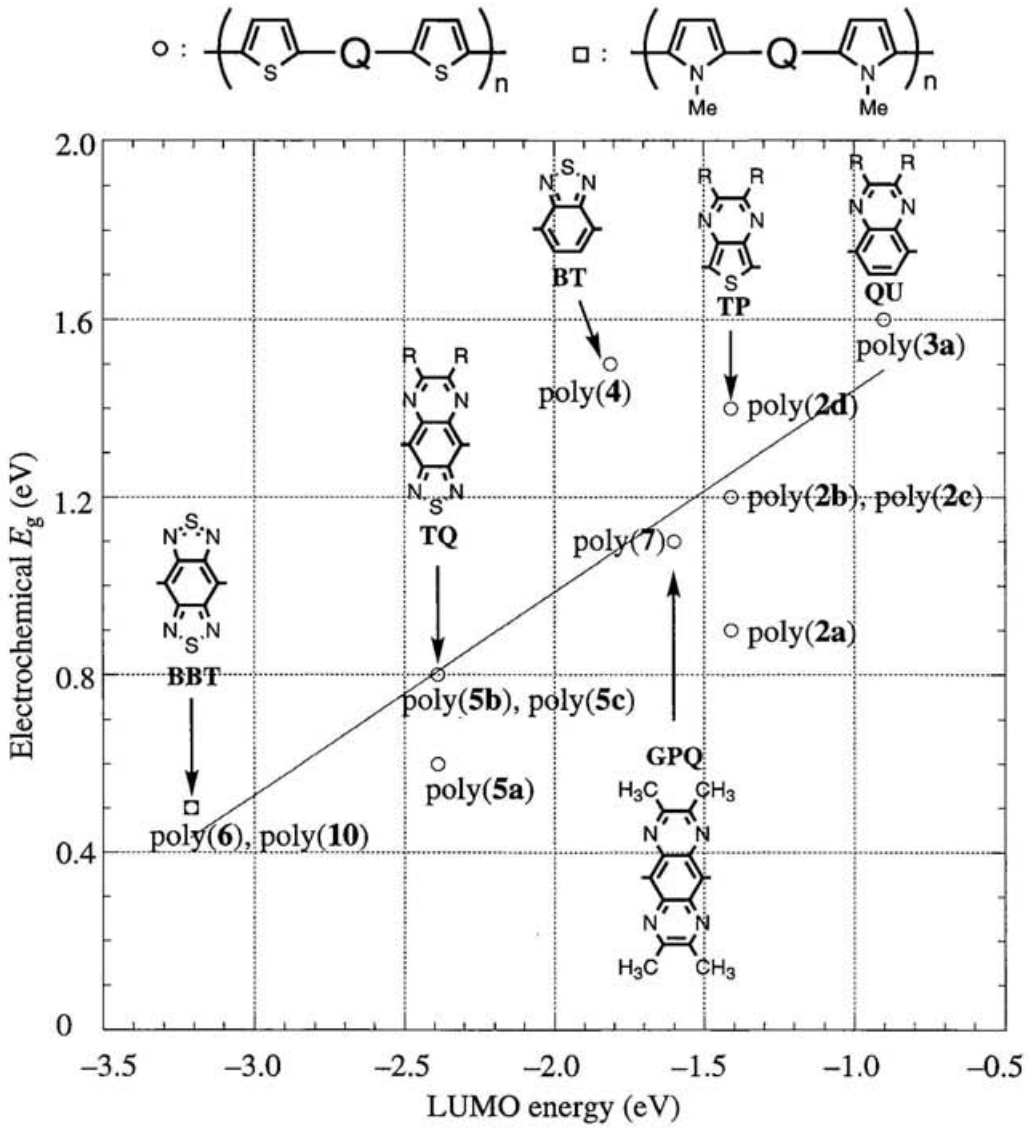


**Figure 19.** Electrochemical bandgaps *vs* LUMO energies of *o*-quinoid-acceptor segments. Inserted line: $y = 0.455x + 1.896$, $r = 0.835$.

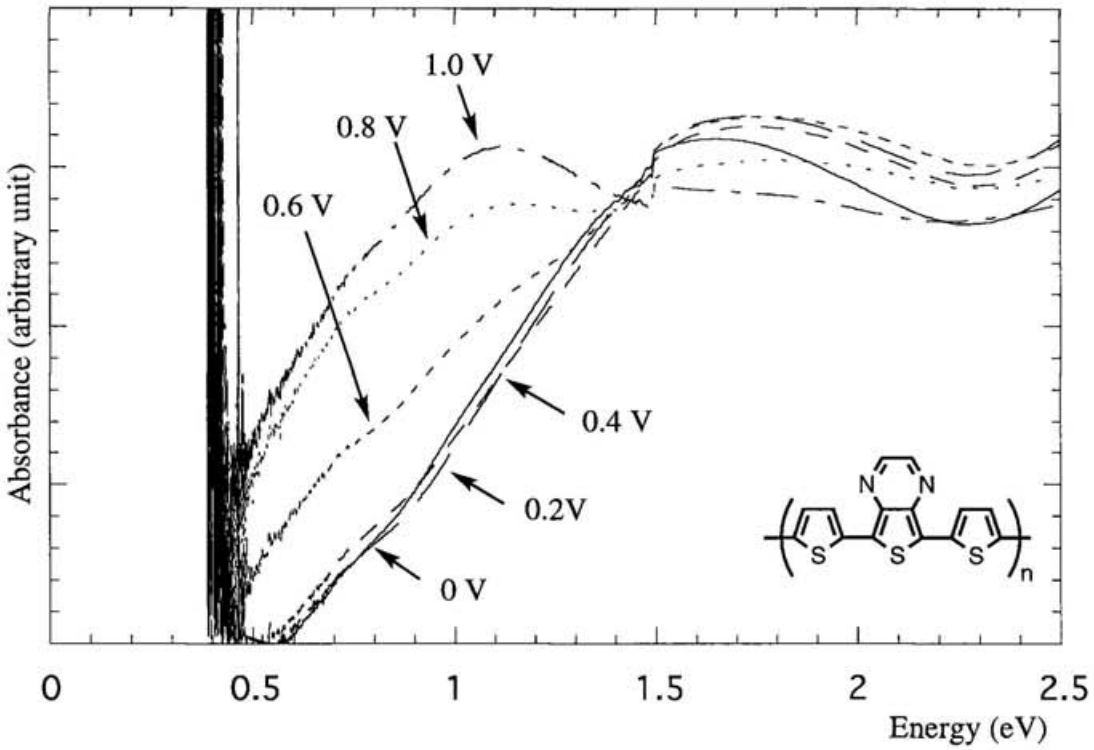


**Figure 20.** Electronic spectra of the polymer of **2a** on ITO, obtained *ex situ* under potential control. Spectra were collected at 0.2 V intervals from 0 to 1.0 V.

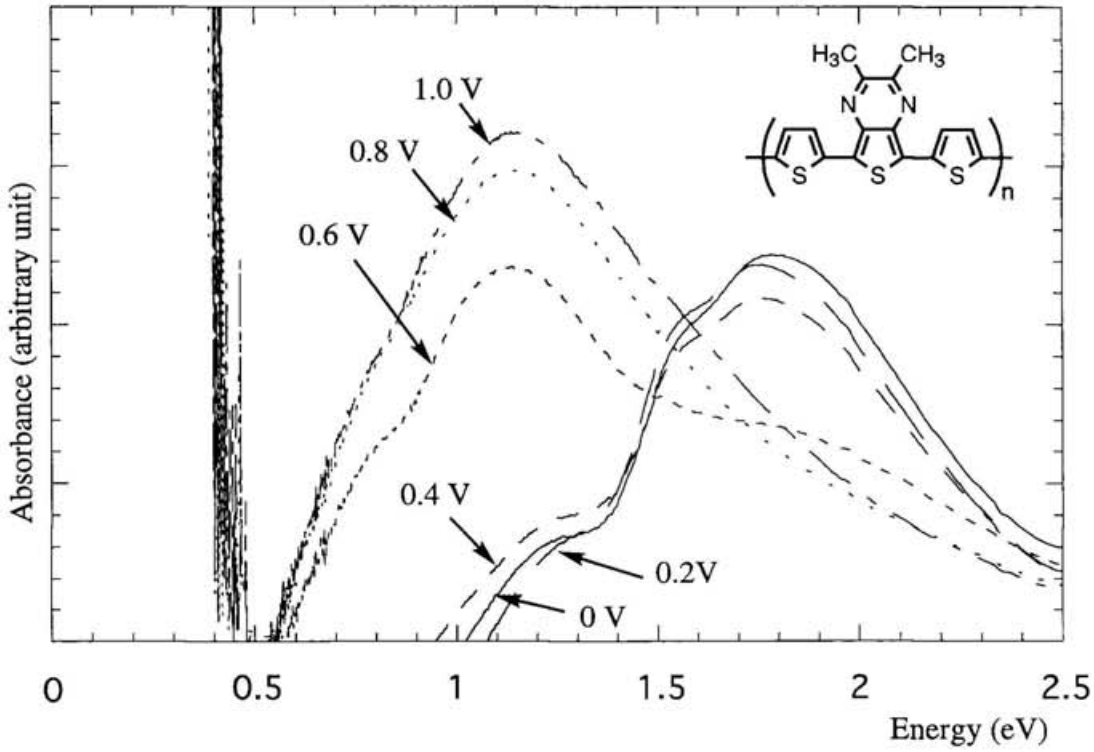


**Figure 21.** Electronic spectra of the polymer of **2b** on ITO, obtained *ex situ* under potential control. Spectra were collected at 0.2 V intervals from 0 to 1.0 V.

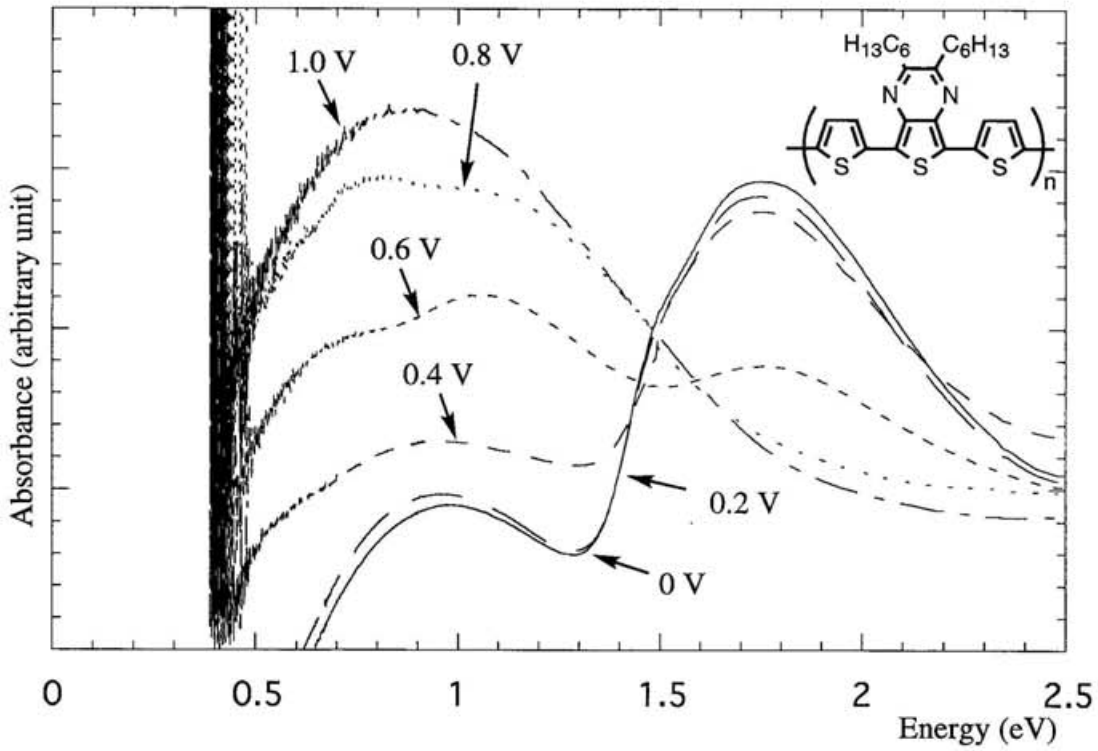


**Figure 22.** Electronic spectra of the polymer of **2c** on ITO, obtained *ex situ* under potential control. Spectra were collected at 0.2 V intervals from 0 to 1.0 V.

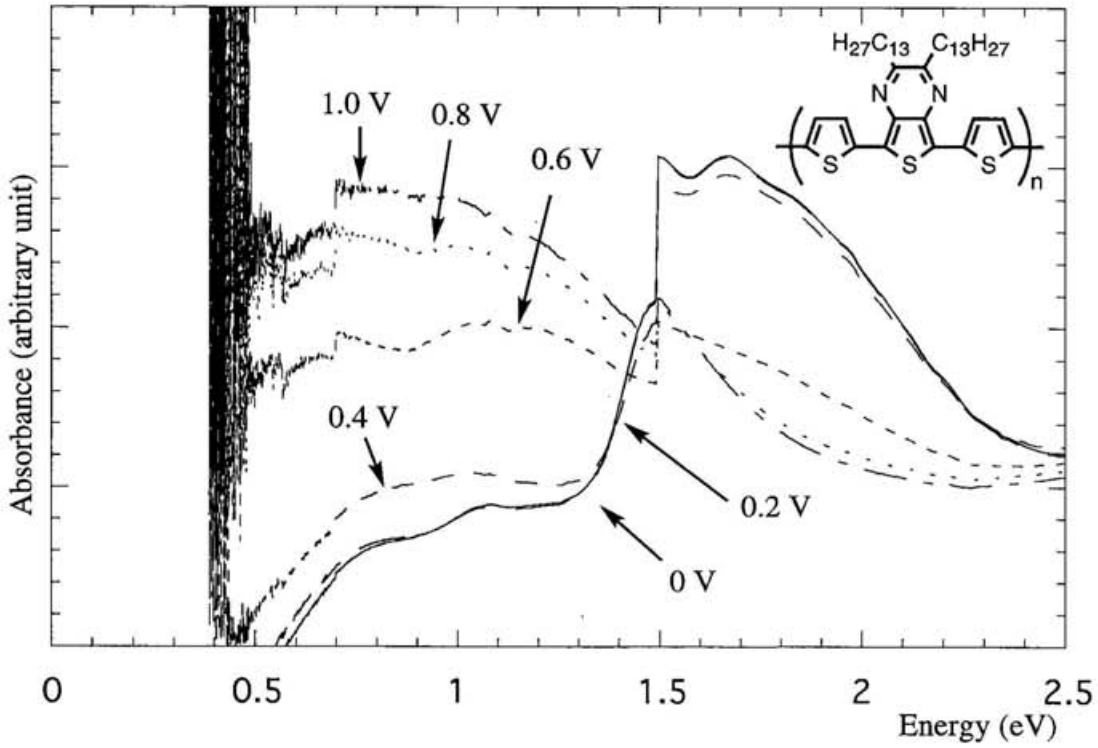


**Figure 23.** Electronic spectra of the polymer of **2d** on ITO, obtained *ex situ* under potential control. Spectra were collected at 0.2 V intervals from 0 to 1.0 V.

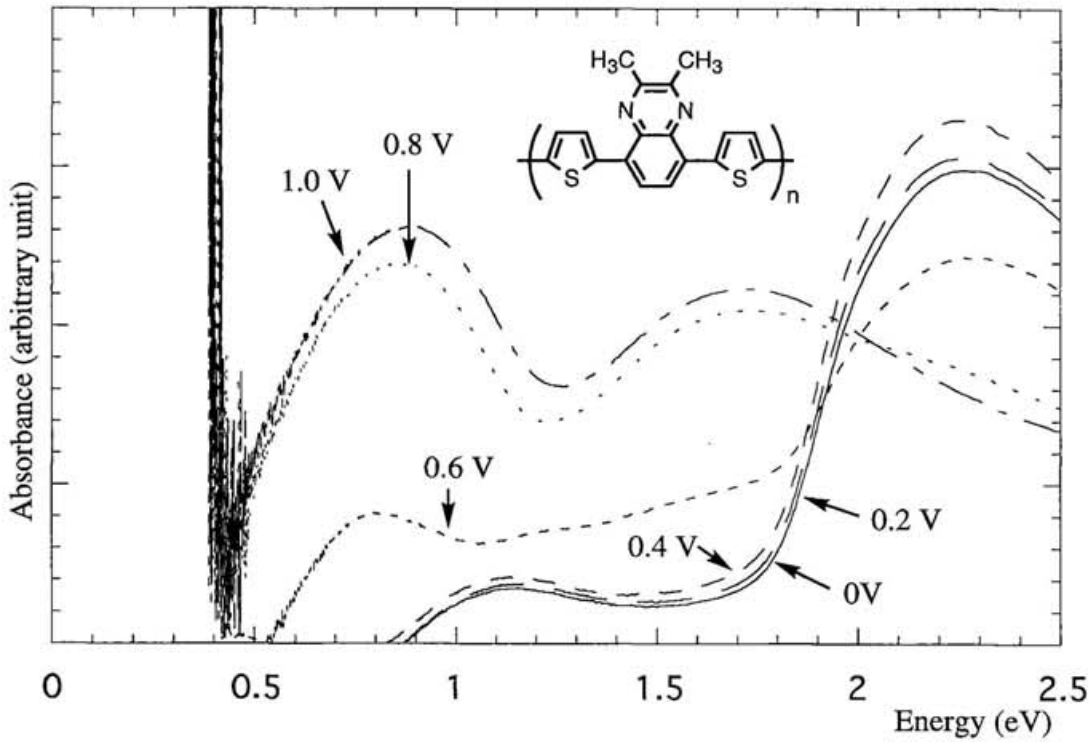


**Figure 24.** Electronic spectra of the polymer of **3a** on ITO, obtained *ex situ* under potential control. Spectra were collected at 0.2 V intervals from 0 to 1.0 V.

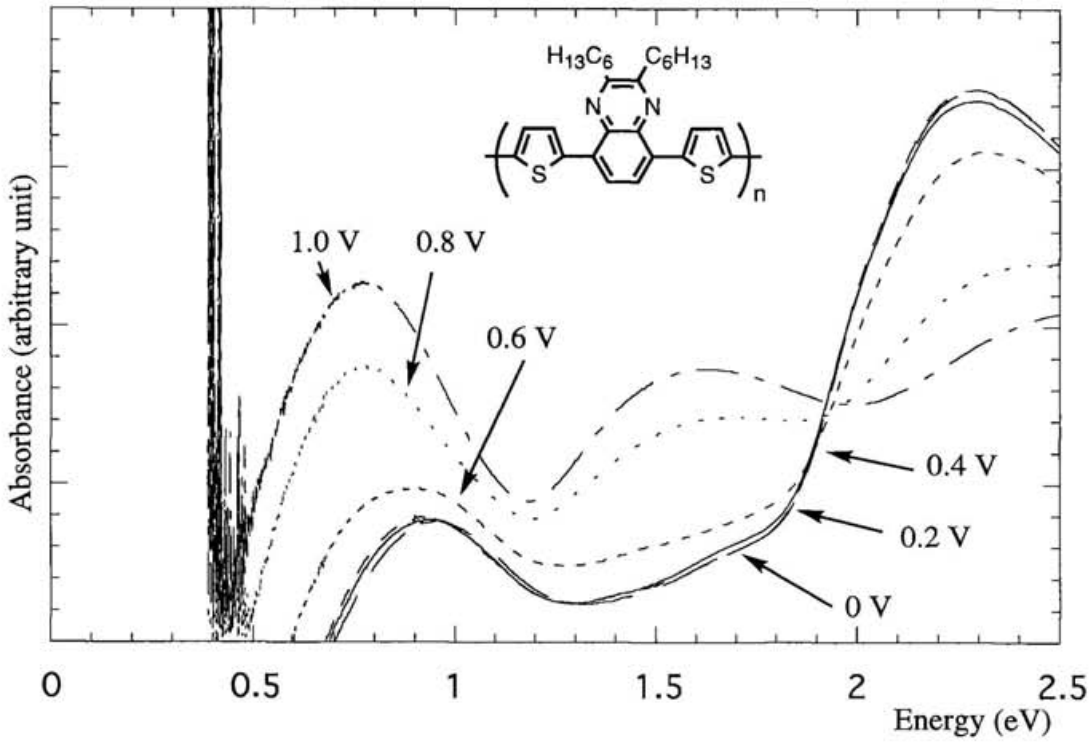


**Figure 25.** Electronic spectra of the polymer of **3b** on ITO, obtained *ex situ* under potential control. Spectra were collected at 0.2 V intervals from 0 to 1.0 V.

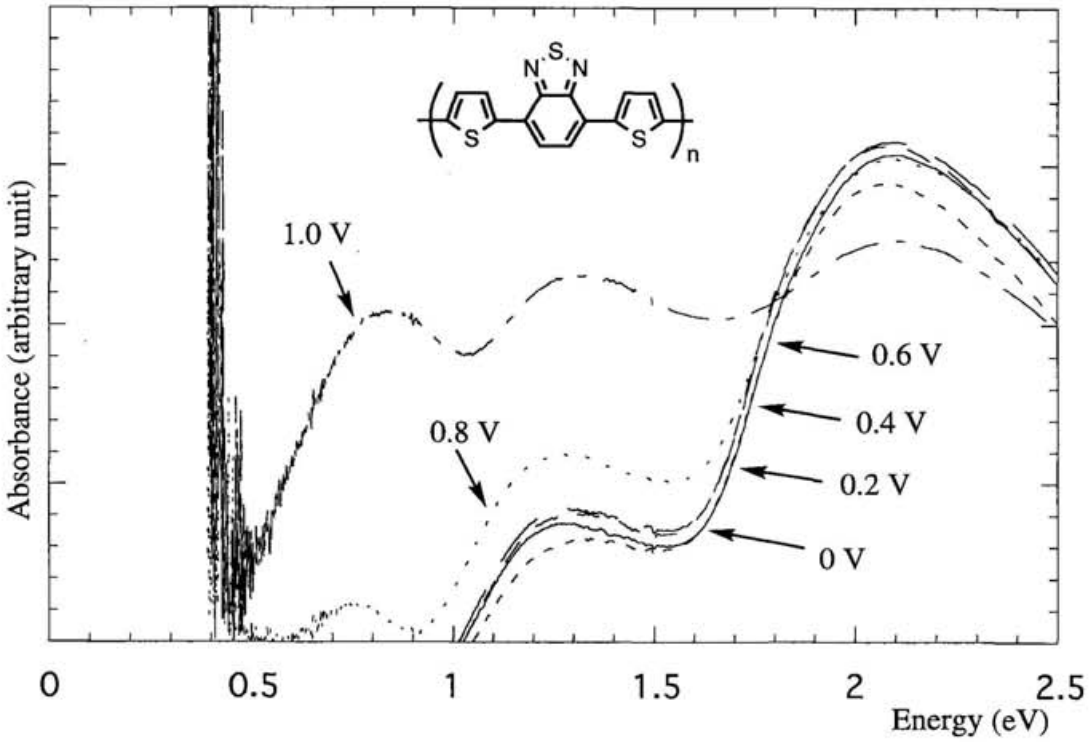


**Figure 26.** Electronic spectra of the polymer of **4** on ITO, obtained *ex situ* under potential control. Spectra were collected at 0.2 V intervals from 0 to 1.0 V.

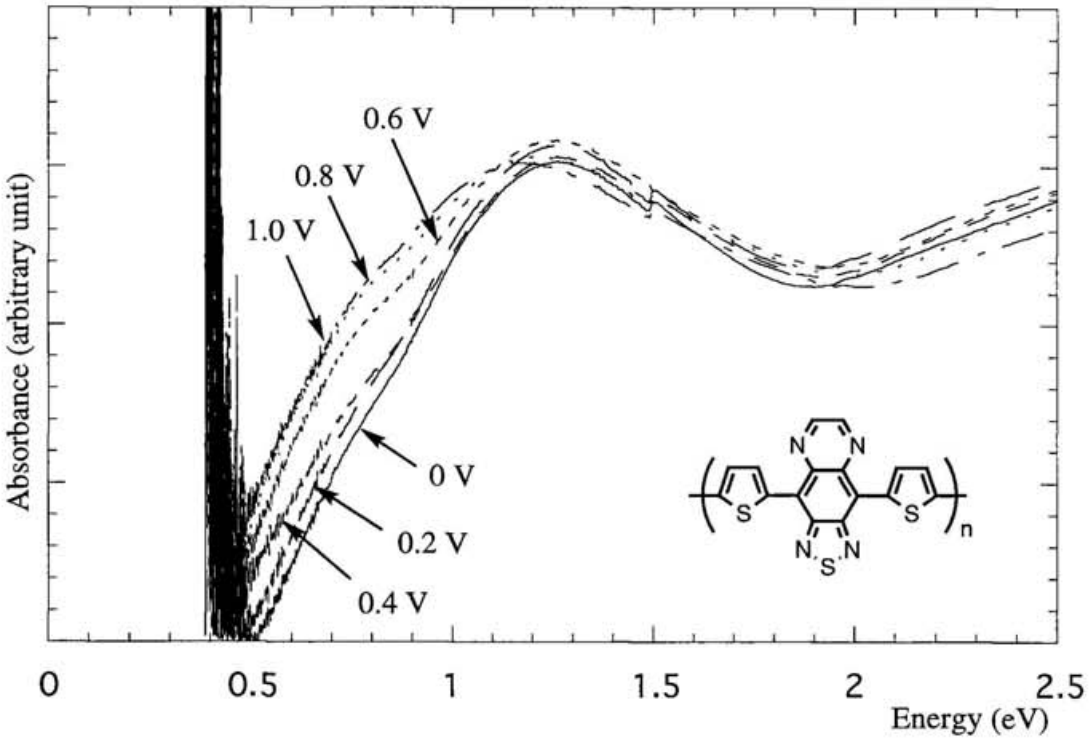


**Figure 27.** Electronic spectra of the polymer of **5a** on ITO, obtained *ex situ* under potential control. Spectra were collected at 0.2 V intervals from 0 to 1.0 V.

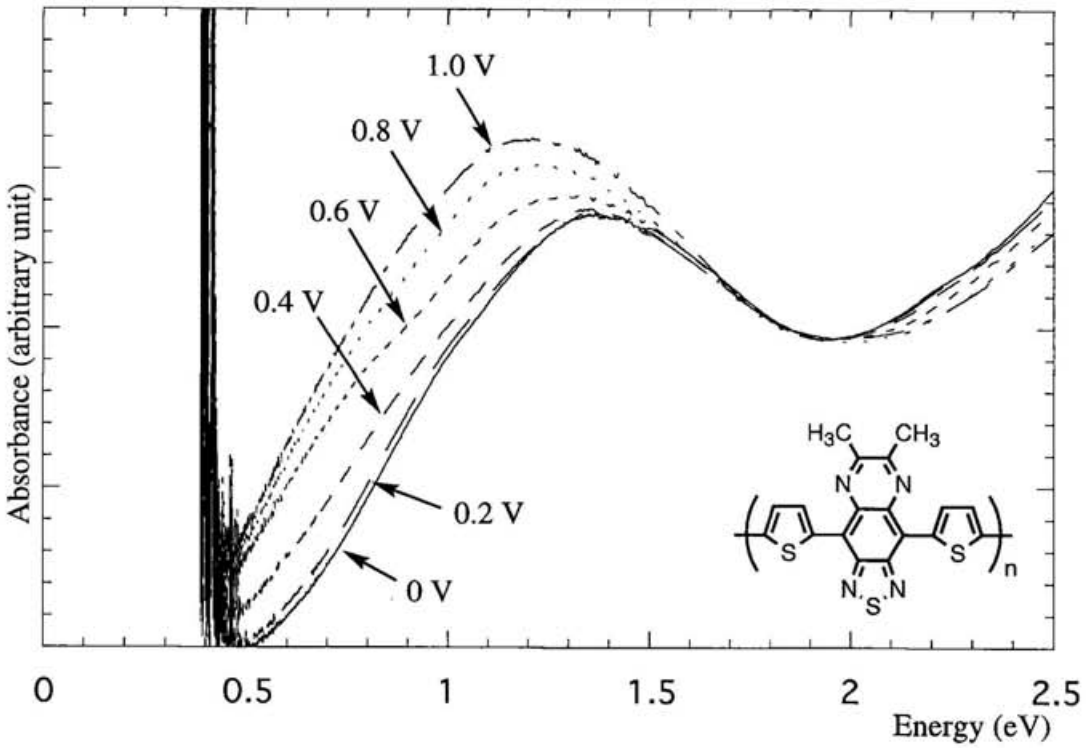


**Figure 28.** Electronic spectra of the polymer of **5b** on ITO, obtained *ex situ* under potential control. Spectra were collected at 0.2 V intervals from 0 to 1.0 V.

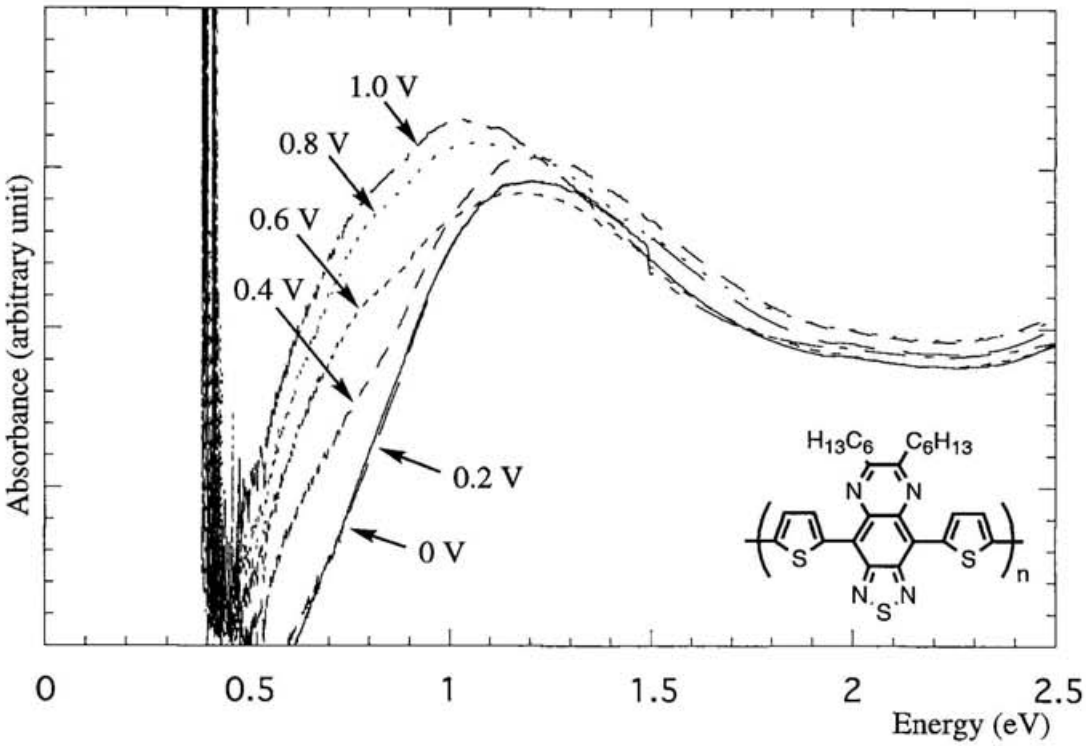


**Figure 29.** Electronic spectra of the polymer of **5c** on ITO, obtained *ex situ* under potential control. Spectra were collected at 0.2 V intervals from 0 to 1.0 V.

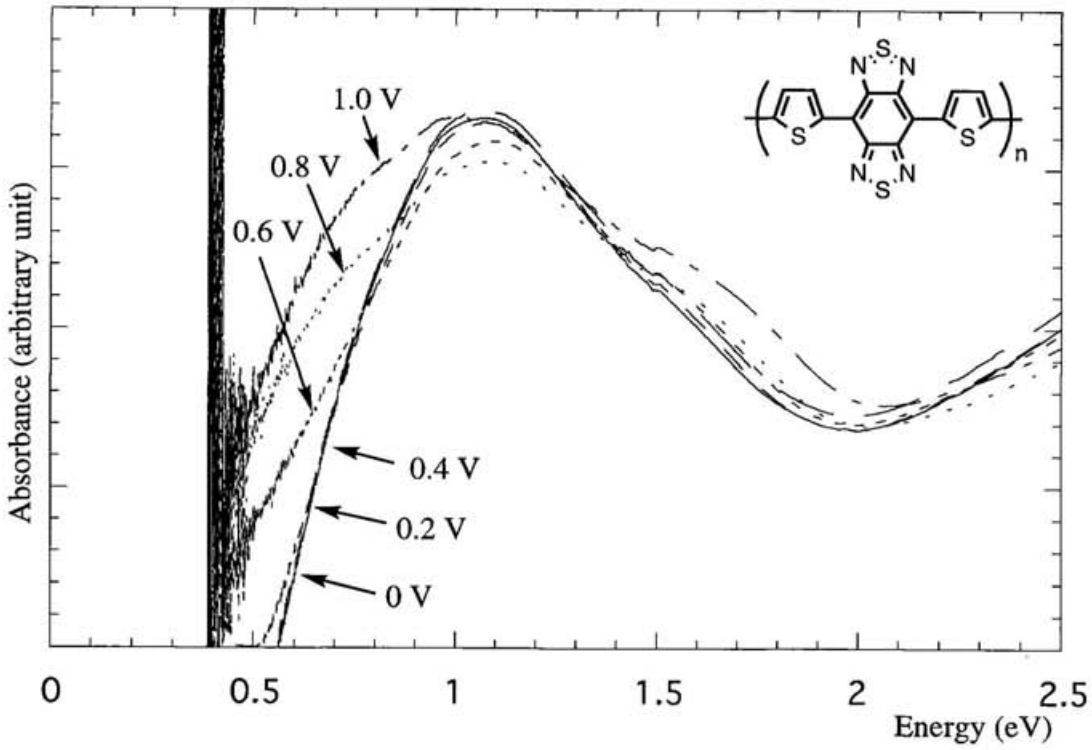


**Figure 30.** Electronic spectra of the polymer of **6** on ITO, obtained *ex situ* under potential control. Spectra were collected at 0.2 V intervals from 0 to 1.0 V.

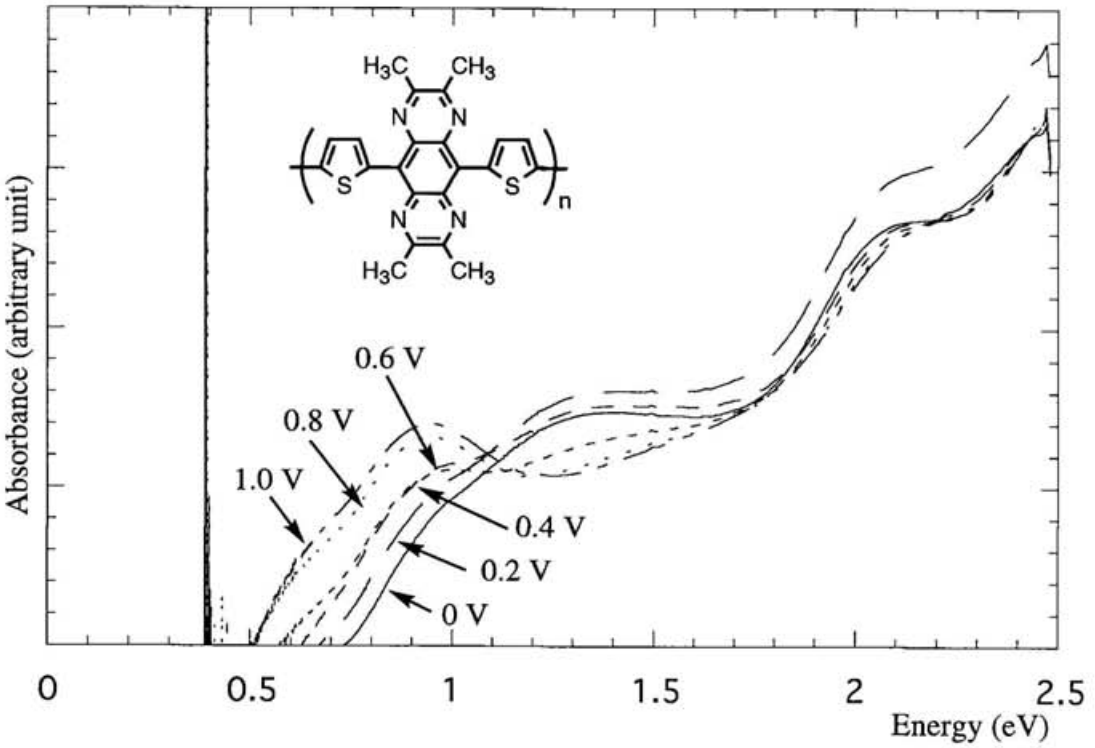


**Figure 31.** Electronic spectra of the polymer of **7** on ITO, obtained *ex situ* under potential control. Spectra were collected at 0.2 V intervals from 0 to 1.0 V.

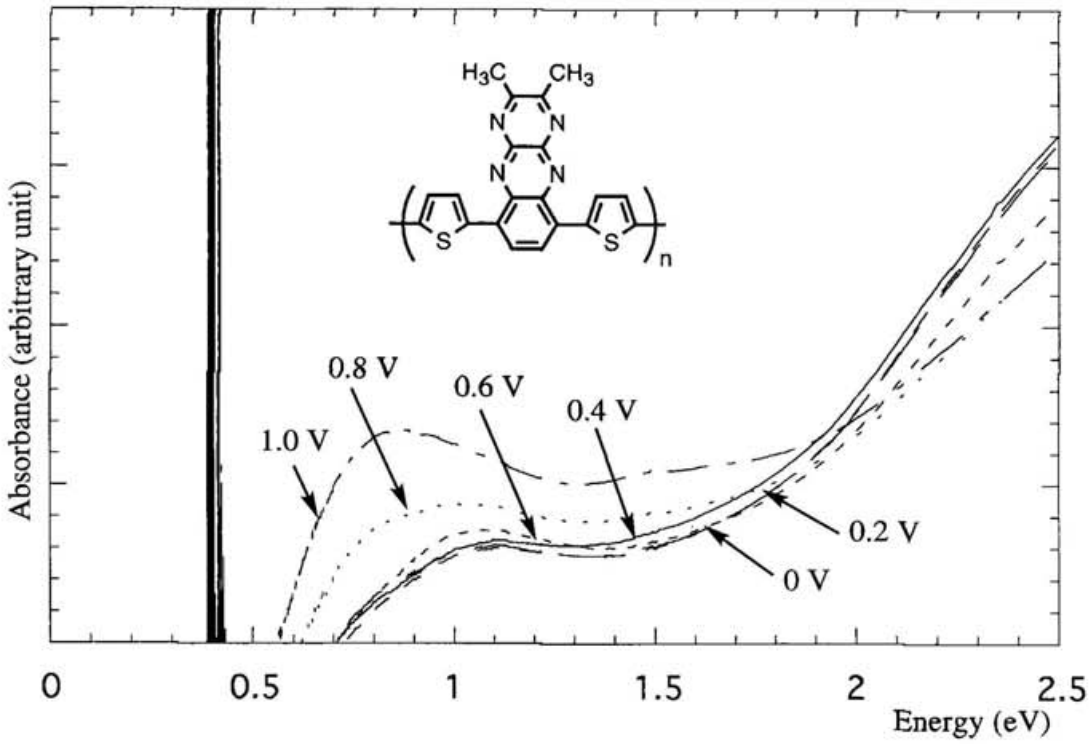


**Figure 32.** Electronic spectra of the polymer of **8** on ITO, obtained *ex situ* under potential control. Spectra were collected at 0.2 V intervals from 0 to 1.0 V.

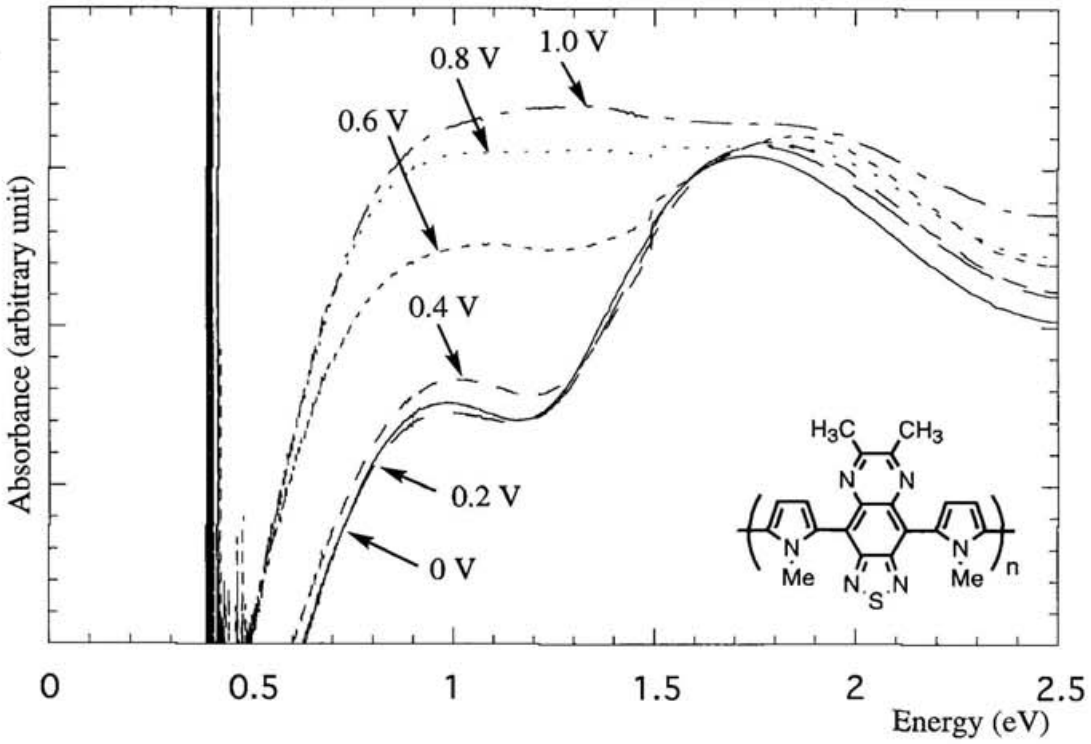


**Figure 33.** Electronic spectra of the polymer of **9a** on ITO, obtained *ex situ* under potential control. Spectra were collected at 0.2 V intervals from 0 to 1.0 V.

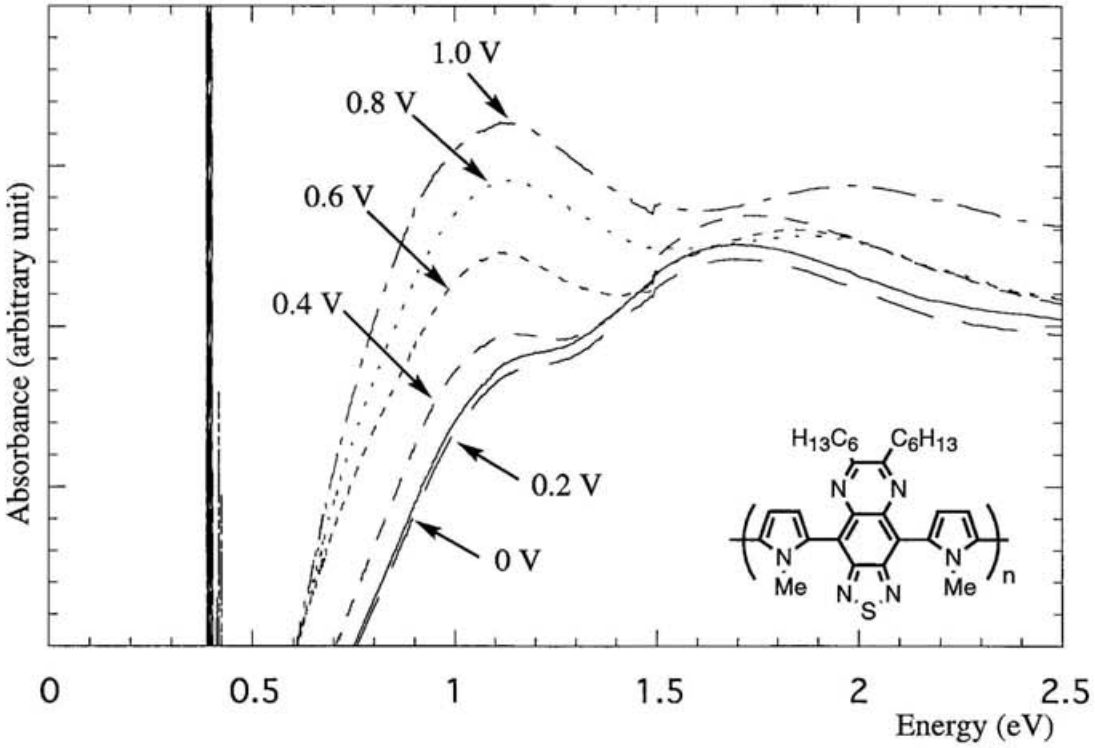


**Figure 34.** Electronic spectra of the polymer of **9b** on ITO, obtained *ex situ* under potential control. Spectra were collected at 0.2 V intervals from 0 to 1.0 V.

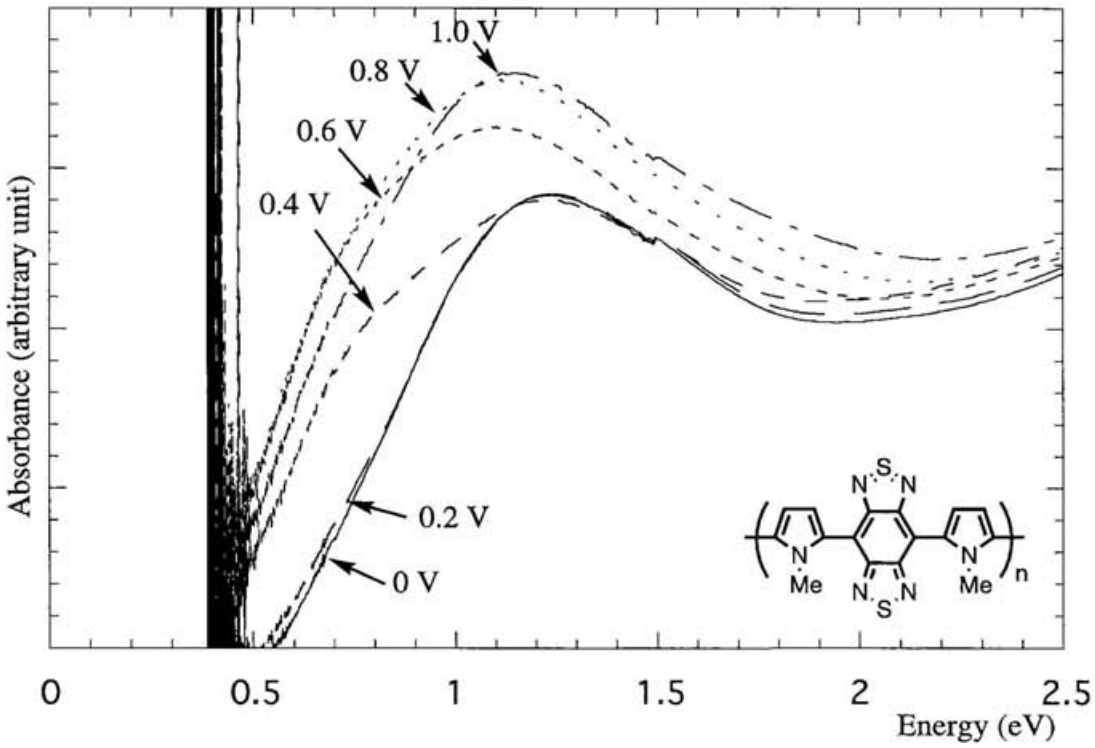


**Figure 35.** Electronic spectra of the polymer of **10** on ITO, obtained *ex situ* under potential control. Spectra were collected at 0.2 V intervals from 0 to 1.0 V.

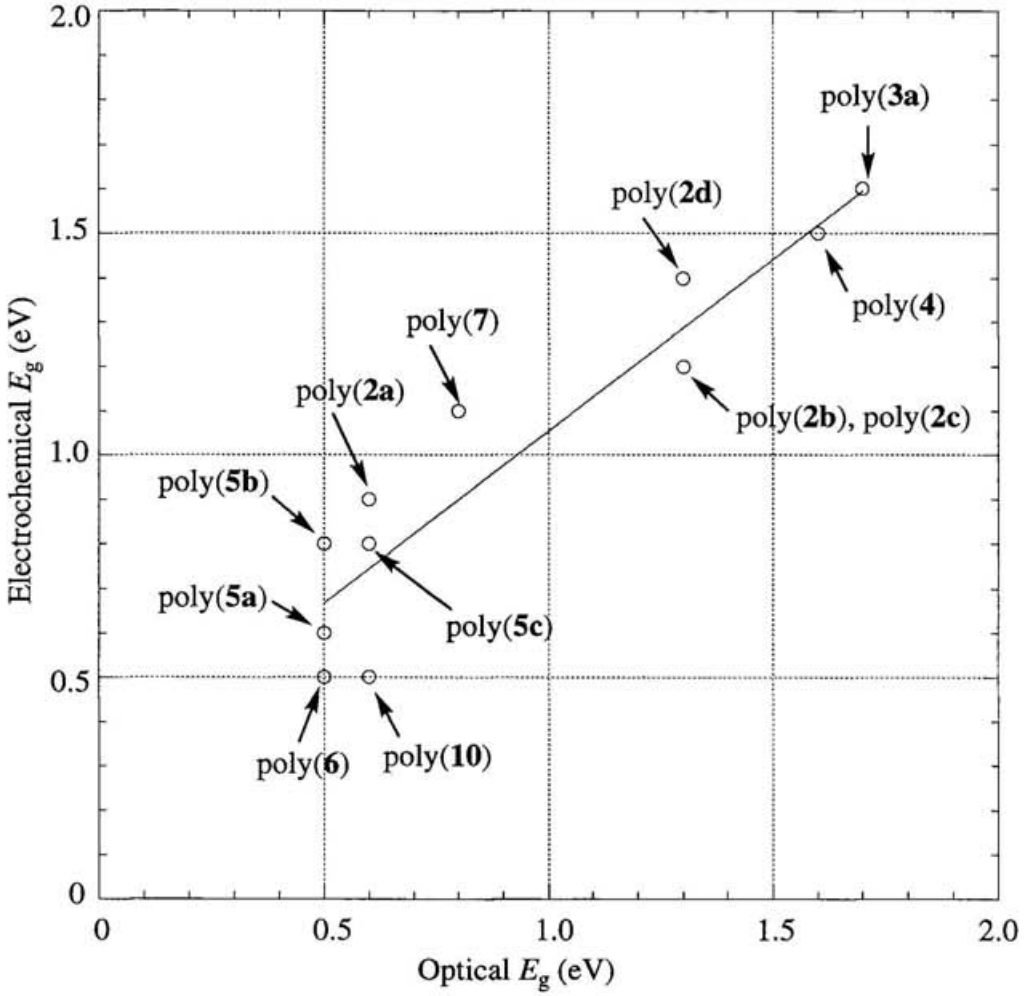


**Figure 36.** Electrochemical bandgaps *vs* optical bandgaps of polymers
Inserted line: $y = 0.773x + 0.280$, $r = 0.934$.

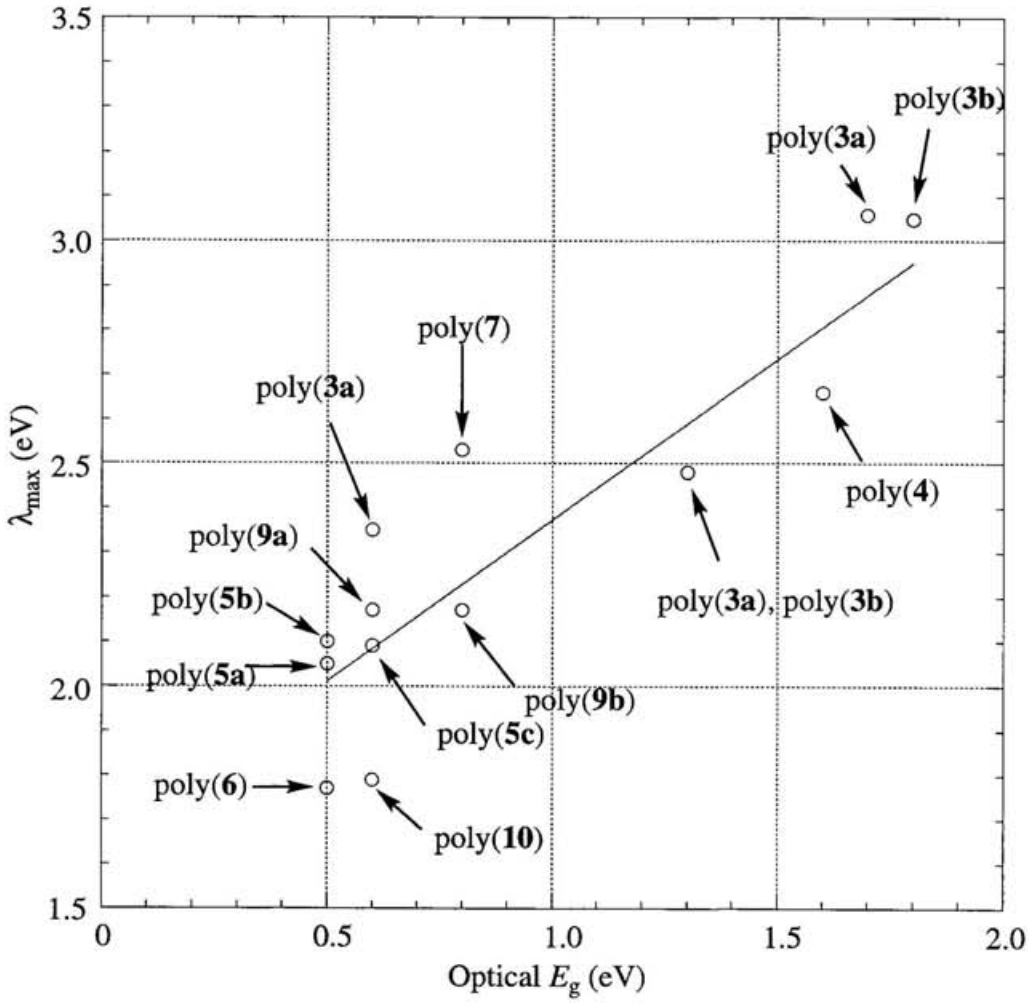


**Figure 37.** Absorption maxima in eV of monomers *vs* optical bandgaps of polymers. Inserted line: $y = 0.691x + 1.612$, $r = 0.849$.

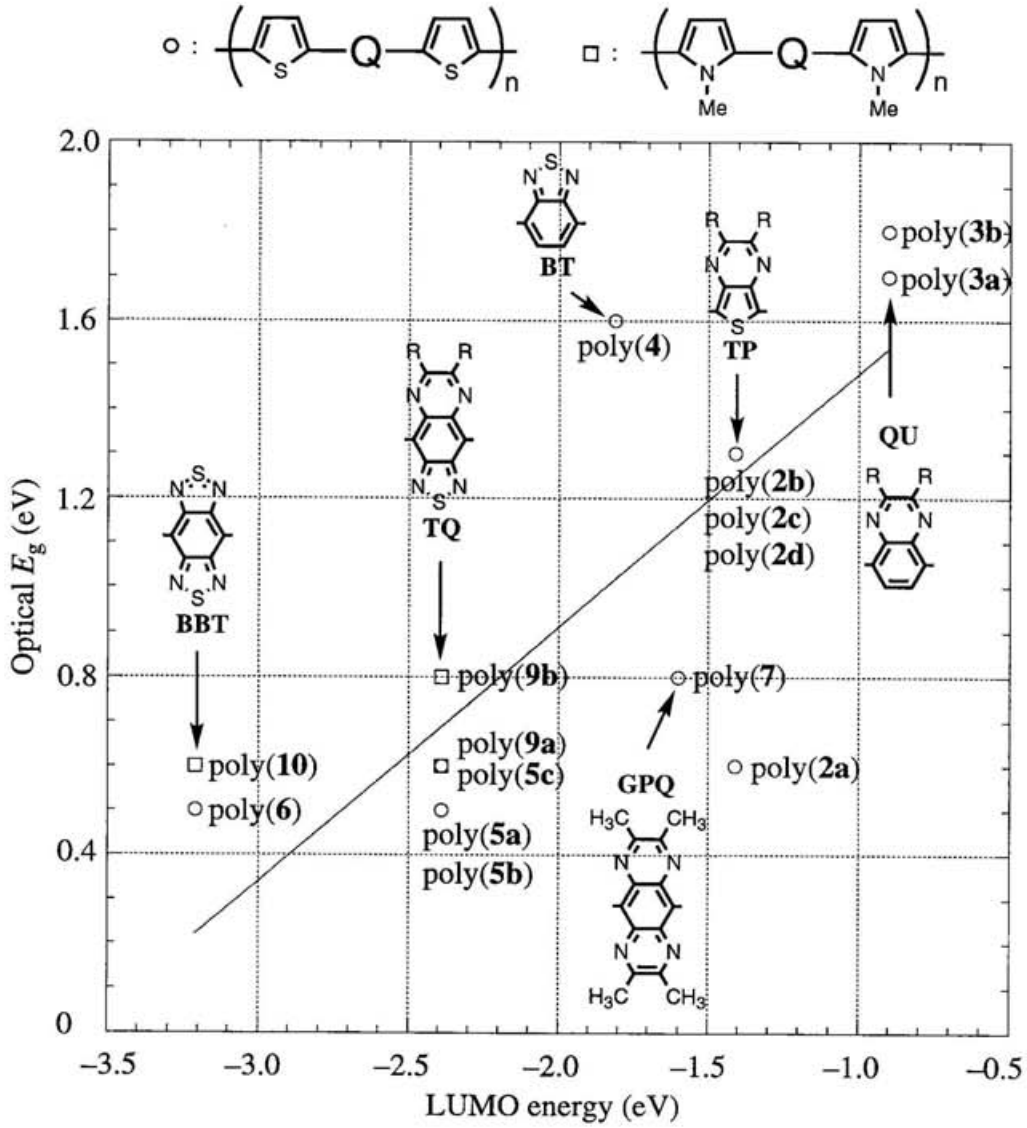


**Figure 38.** Optical bandgaps *vs* LUMO energies of *o*-quinoid-acceptor segments. Inserted line: $y = 0.570x + 2.050$, $r = 0.777$.

## 3.3 Experimental

**General.** UV-vis-NIR spectra were recorded on a Shimadzu UV-3101PC spectrometer. For electropolymerization and cyclic voltammetry, a Toho Technical Research Polarization Unit PS-07 potentiostat/galvanostat was used. Benzonitrile (PhCN) was purified under argon by passing through Merck aluminium oxide 90 (neutral, activity I). Acetonitrile (MeCN) was distilled under argon from $CaH_2$, prior to use. Supporting electrolytes were used without further purification.

**General Procedure for Electrochemical Polymerization.** Polymers were prepared by a cyclic potential sweep technique in a three-compartment cell with $10^{-4} \sim 2 \times 10^{-3}$ mol $dm^{-3}$ monomer solutions containing 0.1 mol $dm^{-3}$ $Bu_4NClO_4$ ($Bu_4NBF_4$ for the monomer **6**) at a scan rate of 100 mV $s^{-1}$. Solutions were degassed by argon bubbling before use, and an argon stream was maintained over the solutions during polymerization. A period of 1-4 h was spent on the polymerization. Pt disk (2.0 $mm^{-2}$), Pt wire, and SCE were used as the working, counter, and reference electrodes, respectively. For measurements of UV-vis-NIR spectra, the polymers were deposited on an ITO-coated glass as the working electrode. Details of experimental conditons have been already shown in Table 1. Neutral polymers were obtained by electrochemical dedoping of self-standing, doped polymer films in monomer-free electrolytes at potentials that do not bring about doping.

**Electrochemistry.** Cyclic voltammetry of the polymers was performed in monomer-free electrolytes at 10 mV $s^{-1}$ under the same conditions as the electrochemical polymerization. Electrochemical oxidation of the polymers on an ITO-coated glass was carried out by a constant potential method in about 2 min at 0.2 V intervals from 0 to 1.0 V.

## 3.4 References and Notes


(1) (a) Wudl, F.; Kobayashi, M.; Heeger, A. J. *J. Org. Chem.* **1984**, *49*, 3382. (b) Kobayashi, M.; Colaneri, N.; Boysel, M.; Wudl, F.; Heeger, A. J. *J. Chem. Phys.* **1985**, *82*, 5717.

(2) For reviews, see: (a) Skotheim, T. A., Ed. *Handbook of Conducting Polymers*; Marcel Dekker: New York, 1986. (b) Patil, A. O.; Heeger, A. J.; Wuld, F. *Chem. Rev.* **1988**, *88*, 183. (c) Scherf, U.; Müllen, K. *Synthesis* **1992**, 23. (d) Brédas, J.-L.; Silbey, R., Eds. *Conjugated Polymers*; Kluwer Academic Publishers: Dordrecht, 1991. (e) Roncali, J. *Chem. Rev.* **1992**, *92*, 711.

(3) (a) Nalwa, H. S. *Adv. Mater.* **1993**, *5*, 341. (b) Brédas, J.-L. *Adv. Mater.* **1995**, *7*, 263.

(4) (a) King, G.; Higgins, S. J. *J. Chem. Soc., Chem. Commun.* **1994**, 825. (b) King, G.; Higgins, S. J.; Garner, S. E.; Hillmann, A. R. *Synth. Met.* **1994**, *67*, 241. (c) King, G.; Higgins, S. J. *J. Mater. Chem.* **1995**, *5*, 447.

(5) Guerrero, D. J.; Ren, X.; Ferraris, J. P. *Chem. Mater.* **1994**, *6*, 1437.

(6) Borjas, R; Buttry, D. A. *Chem. Mater.* **1991**, *3*, 872.

(7) Fincher, C. R., Jr.; Peebles, D. L.; Heeger, A. J., Druy, M. A.; Matsumura, Y.; MacDiarmid, A. G.; Shirakawa, H.; Ikeda, S. *Solid State Commun.* **1978**, *27*, 489.

(8) Keller, S. W.; Mallouk, T. E. *J. Chem. Educ.* **1993**, *70*, 855.

(9) Since many polymers were fragile against negative potentials, the spectra could not be determined.

(10) Because of the intense absorption of the ITO glass itself, the determination of the region below about 0.5 eV was difficult.

(11) (a) Havinga, E. E.; ten Hoeve, W.; Wynberg, H. *Polym. Bull.* **1992**, *29*, 119. (b) Havinga, E. E.; ten Hoeve, W.; Wynberg, H. *Synth. Met.* **1993**, *55-57*, 299.

(12) Tanaka, S.; Yamashita, Y. *Synth. Met.* **1995**, *69*, 599.

## Conclusions

This dissertation deals with syntheses and properties of a new series of triheterocyclic monomers and the corresponding polymers, both of which are composed of aromatic-donor heterocycles (thiophene and *N*-methylpyrrole) and *o*-quinoid-acceptor heterocycles (thieno[3,4-*b*]pyrazine, quinoxaline, 2,1,3-benzothiadiazole, [1,2,5]thiadiazolo[3,4-*g*]-quinoxaline, benzo[1,2-*c*;4,5-*c*']bis[1,2,5]thiadiazole, pyrazino[2,3-*g*]quinoxaline, and pyrazino[2,3-*b*]quinoxaline).

In Chapter 1, the discovery of narrow-bandgap polymers and the pathway of the research are overlooked and connected to a new molecular design. From the analysis of factors of controlling bandgaps, two molecular designs were extracted. On the basis of them, in order to construct new narrow bandgap system, a periodic copolymer composed of aromatic-donor (A) and *o*-quinoid-acceptor (Q) segments was planned. A series of triheterocyclic monomers (A–Q–A) which were expected to polymerize by electrochemical oxidative coupling was designed to examine the structure-property relationship.

In Chapter 2, syntheses and properties of the series of triheterocyclic monomers are described. The monomers were synthesized through the coupling reaction of dihalo-substituted compounds with stannane compounds in the presence of a Pd(II) catalyst. From MO calculations of each segment by the MNDO-PM3 method, the HOMO and LUMO levels were compared each other. Electronic spectra of the monomers with thiophene exhibited a trend that the monomers containing *o*-quinoid-acceptor unit with lower LUMO levels have longer absorption maxima. On the other hand, the absorption bands of the monomers containing *N*-methylpyrrole displayed small blue shifts compared with the corresponding thiophene analogs against the expectation based on the MO calculations. X-ray analyses of some monomers with thiophene and conformational analyses of the other monomers revealed that the molecules containing thiophene have almost coplanar conformations and the molecules containing *N*-methylpyrrole have torsional geometries, which should cause the reduction of effective delocalization. Cyclic voltammograms of the monomers displayed their extension of $\pi$-conjugation and amphoteric redox properties. The difference between

anodic and cathodic peak potentials depended on the LUMO level of *o*-quinoid-acceptor heterocycle.

Chapter 3 describes syntheses and properties of a variety of the corresponding polymers. Electrochemical polymerization of the monomers stated above on Pt and ITO electrodes was attempted by a repetitive potential cycling method. The resulting polymers were relatively stable under ordinary conditions but insoluble in all the organic solvents even when longer alkyl chains were introduced. Most of the polymers containing thiophene units showed both p- and n-doping processes, indicating their amphoteric redox properties similarly to the monomers. On the other hand, the polymers with *N*-methylpyrrole units hardly showed n-doping probably because the special conformations disturbed the ionic transport. The polymers exhibited characteristic electrochromic phenomena. The small difference between the onset potentials of p- and n-doping suggested that the resulting polymers had narrow bandgaps. From the onset of the absorbance of neutral polymers, optical bandgaps were estimated. The bandgaps were a range of 0.5 to 1.8 eV. The value of 0.5 eV is one of the narrowest bandgap reported so far. It was elucidated that the structural variability of *o*-quinoid-acceptor segments play a role in controlling the bandgaps.

Throughout this work, the relationship between the structures and the properties of the monomers and polymers composed of aromatic-donor and *o*-quinoid-acceptor segments was elucidated. The methodology of the combination of two units with different properties proved effective to create new systems. The concept will be a powerful tool to exploit new compounds.

## Acknowledgments

First of all, the author wishes to thank his supervisor, Prof. Dr. Yoshiro Yamashita (The Graduate University for Advanced Studies, and Chemical Materials Center, Institute for Molecular Science), who received the author warmly and lead to the fruitful world of the organic π-conjugated compounds. The author is also indebted to Prof. Yamashita for his right guidance and revising the author's poor English containing this thesis.

The author would like to express his grateful acknowledgment to Dr. Shoji Tanaka (Chemical Materials Center, Institute for Molecular Science) for his help and advice through this work and a gift of a part of X-ray data. The author wishes to thank Dr. Masaaki Tomura (Chemical Materials Center, Institute for Molecular Science) for his useful comments and discussions. The author thanks Miss Sachiyo Nomura (Chemical Materials Center, Institute for Molecular Science) for her fast and confidential service of elemental analyses and high resolution mass determinations. The author is grateful to Dr. Michinori Karikomi (Faculty of Engineering, Utsunomiya University) for the preparation of some compounds. The author wishes to express his thanks to all the member in the Chemical Materials Center, Dr. Masatoshi Kozaki, Dr. Katsuhiko Ono, Mr. Akira Ohta, and Mrs. Takako Ozeki for their valuable suggestions and encouragement.

The author is indebted to the Japan Scholarship Foundation and the Japan Society for the Promotion of Science for Young Scientists for his financial support.

Finally, the author would like to express his hearty gratitude to his parents, Mr. Shoju Kitamura and Mrs. Kazuyo Kitamura for their affectionate encouragement.

November 1995

Chitoshi Kitamura

## List of Publications

1. "Synthesis of New Narrow Bandgap Polymers Based on 5,7-Di(2-thienyl)-thieno[3,4-*b*]pyrazine and its Derivatives"
   Kitamura, C.; Tanaka, S.; Yamashita, Y. *J. Chem. Soc., Chem. Commun.* **1994**, 1585.

2. "New Narrow-Bandgap Polymer Composed of Benzobis(1,2,5-thiadiazole) and Thiophenes"
   Karikomi, M.; Kitamura, C.; Tanaka, S.; Yamashita, Y. *J. Am. Chem. Soc.* **1995**, *117*, 6791.

3. "New Narrow-Bandgap Polymers Composed of [1,2,5]Thiadiazolo[3,4-*g*]-quinoxaline and Aromatic Heterocycles"
   Kitamura, C.; Tanaka, S.; Yamashita, Y. *Chem. Lett.* **1996**, 63.

4. "Design of Narrow-Bandgap Polymers. Syntheses and Properties of Monomers and Polymers Containing Aromatic-Donor and *o*-Quinoid-Acceptor Units"
   Kitamura, C.; Tanaka, S.; Yamashita, Y. *Chem. Mater.* in press.

## Other Publications

1. "Formation of Radical Cation and Dication of 1,3,4,6-Tetrakis(isopropylthio)-2$\lambda^4\delta^2$-thieno[3,4-*c*]thiophene and their Reactions with Nucleophiles"
   Tsubouchi, A.; Kitamura, C.; Matsumura, N.; Inoue, H. *J. Chem. Soc., Perkin Trans. 1* **1991**, 2935.

2. "Oxidation of 1,3,4,6-Tetrakis(alkylthio)thieno[3,4-*c*]thiophenes with Iodine in the Presence of Aniline"
   Tsubouchi, A.; Kitamura, C.; Matsumura, N.; Inoue, H. *J. Heterocycl. Chem.* **1991**, 28, 1643.